AD-A129 710 FREE WAKE AERODYNAMIC ANALYSIS OF HELICOPTER ROTORS(U) 1/2
BOSTON UNIV MA CENTER FOR COMPUTATIONAL AND APPLIED
DYNAMICS.. L MORINO ET AL. 26 MAY 83 CCAD-TR-83-01
UNCLASSIFIED ARO-16294.2-EG DAAG29-80-C-0016 F/G 20/4 NL

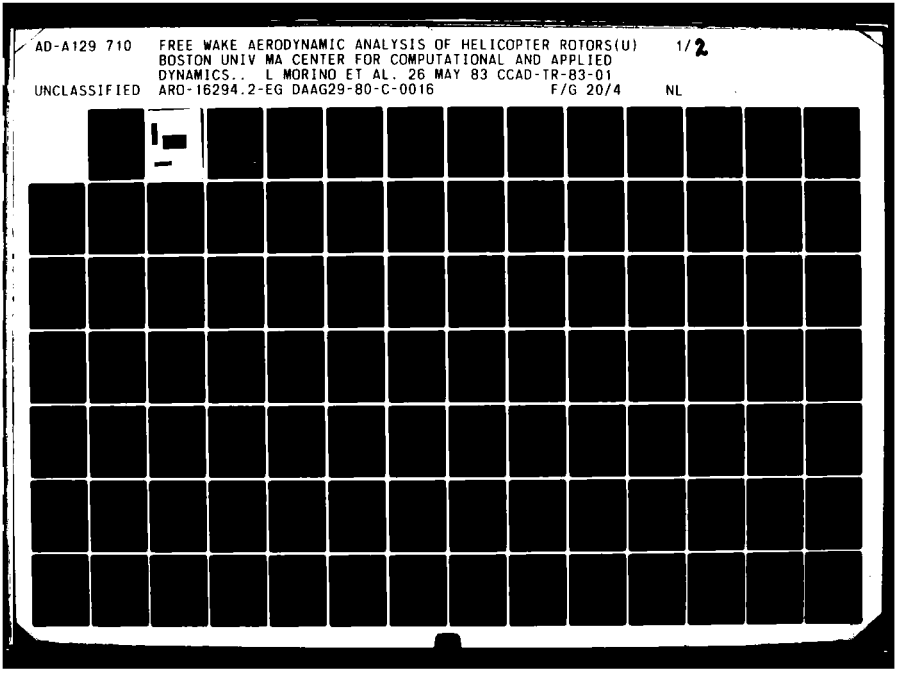

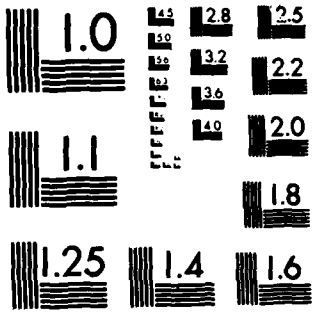

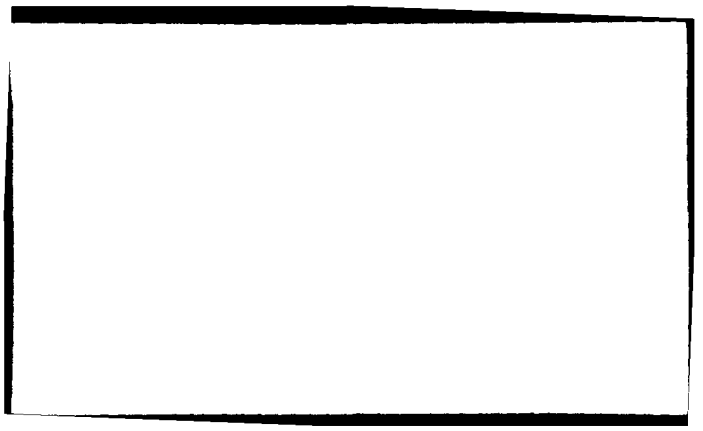

(12)

CCAD-TR-83-01

CENTER FOR COMPUTATIONAL AND APPLIED DYNAMICS

BOSTON UNIVERSITY

BOSTON MASS. 02215

FREE WAKE AERODYNAMIC ANALYSIS OF HELICOPTER ROTORS

Luigi Morino, Zaven Kaprielian, Jr. and Slobodan R. Sipcic

May 1983

Final Report on
U.S. Army Research Office
Contract No. DAAG29-80-C-0016

UNCLASSIFIED

SECURITY CLASSIFICATION OF THIS PAGE (When Data Entered)

REPORT DOCUMENTATION PAGE		READ INSTRUCTIONS BEFORE COMPLETING FORM
1. REPORT NUMBER TR-83-01	2. GOVT ACCESSION NO.	3. RECIPIENT'S CATALOG NUMBER
4. TITLE (and Subtitle) FREE WAKE AERODYNAMIC ANALYSIS OF HELICOPTER ROTORS		5. TYPE OF REPORT & PERIOD COVERED FINAL REPORT (10/17/79 to 5/26/83) 6. PERFORMING ORG. REPORT NUMBER CCAD-TR-83-01
7. AUTHOR(s) Luigi Morino Zaven Kaprielian, Jr. Slobodan R. Sipcic		8. CONTRACT OR GRANT NUMBER(s) DAAG 29-80-C-0016
9. PERFORMING ORGANIZATION NAME AND ADDRESS Boston University Boston, Mass. 02215		10. PROGRAM ELEMENT, PROJECT, TASK AREA & WORK UNIT NUMBERS
11. CONTROLLING OFFICE NAME AND ADDRESS U. S. Army Research Office Post Office Box 12211 Research Triangle Park, NC 27709		12. REPORT DATE May 26, 1983 13. NUMBER OF PAGES
14. MONITORING AGENCY NAME & ADDRESS(if different from Controlling Office)		15. SECURITY CLASS. (of this report) Unclassified 15a. DECLASSIFICATION/DOWNGRADING SCHEDULE

16. DISTRIBUTION STATEMENT (of this Report)

Approved for public release: distribution unlimited.

17. DISTRIBUTION STATEMENT (of the abstract entered in Block 20, if different from Report)

18. SUPPLEMENTARY NOTES

THE VIEW, OPINIONS, AND/OR FINDINGS CONTAINED IN THIS REPORT ARE THOSE OF THE AUTHOR(S) AND SHOULD NOT BE CONSTRUED AS AN OFFICIAL DEPARTMENT OF THE ARMY POSITION, POLICY, OR DECISION, UNLESS SO DESIGNATED BY OTHER DOCUMENTATION.

19. KEY WORDS (Continue on reverse side if necessary and identify by block number)

helicopter, rotor, aerodynamics, wake dynamics, free-wake, trailing-edge conditions

20. ABSTRACT (Continue on reverse side if necessary and identify by block number)

A formulation for the free wake analysis of helicopter rotors in incompressible potential flows is presented here. The formulation encompasses both the theory and its numerical implementation. For the case of a single-bladed rotor in hover, the formulation is validated by numerical results which are in good agreement with the generalized wake of

DD FORM 1 JAN 73 1473 EDITION OF 1 NOV 65 IS OBSOLETE

UNCLASSIFIED

SECURITY CLASSIFICATION OF THIS PAGE (When Data Entered)

Abstract(cont.):

Landgrebe. Extension of the theory to compressible flows is also outlined.

These results indicate that the formulation does not require any empirical assumption (such as the rate of contraction of the radius of the wake) in order to avoid numerical instabilities. To our knowledge, the results presented here are the first ones ever obtained not requiring any ad-hoc assumptions in order to avoid such problems.

A

ACKNOWLEDGEMENTS

This work was supported by ARO contract DAAG29-80-C-0016 by U.S. Army Research Office/Research Triangle Park to Boston University. Dr. Robert E. Singleton acted as technical monitor for this contract.

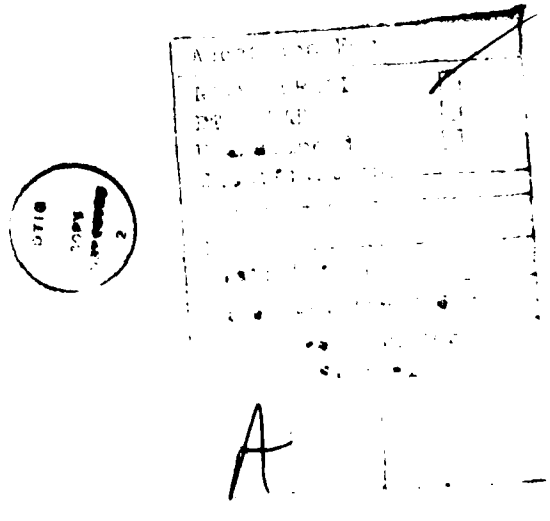

TABLE OF CONTENTS

	Page
ACKNOWLEDGMENTS	ii
LIST OF FIGURES	v
LIST OF SYMBOLS	vii
Section	
1. INTRODUCTION	1-1
1.1 Motivation and Objectives	1-1
1.2 Relation of Work with State of the Art	1-2
1.3 Summary of work	1-7
2. WAKE DYNAMICS IN INCOMPRESSIBLE POTENTIAL FLOWS	2-1
2.1 Incompressible Inviscid Flows	2-1
2.2 Potential Flows, Potential Wakes	2-2
2.3 Potential-Flow Formulation	2-3
2.4 Boundary Conditions on Wake	2-4
2.5 Summary	2-7
3. INTEGRAL FORMULATION	3-1
3.1 Green's Formula for Laplace's Equation	3-1
3.2 Green's Theorem for Incompressible Potential Aerodynamics	3-3
3.3 Wake Contribution	3-4
3.4 Integral Equation	3-5
3.5 Conditions at Infinity	3-8
4. WAKE GENERATION	4-1
4.1 Sudden Start	4-1
4.2 Uniqueness of Solution: Kutta Condition	4-2
4.3 Joukowski Hypothesis	4-3
4.4 Trailing Edge Flow	4-3
4.5 Physical Interpretation	4-7
5. COMPUTATIONAL ALORITHM	5-1
5.1 Theoretical Algorithm	5-1
5.2 Space and Time Discretization: First Time Step	5-2
5.3 Wake Generation During First Time Step	5-3
5.4 Generic Time Step	5-4
5.5 Numerical Stability	5-8
5.6 Finite-Core Vortex	5-10
5.7 Comments: Wake Truncation	5-13

6. NUMERICAL RESULTS 6-1
6.1 Choice of the Test Case 6-1
6.2 Description of Test Case 6-1
6.3 Numerical Results 6-2
6.4 Comments; Numerical Stability 6-32

7. CONCLUDING REMARKS 7-1

REFERENCES

LIST OF FIGURES

Figure		Page
3.1	Geometry for Definition of Solid Angles	3-6
4.1	Vectors $\bar{e}_\tau$ and $\bar{e}_\nu$	4-4
4.2	Wake Geometry at Trailing Edge	4-6
5.1	Wake Generation Between Times $t_0=0$ and $t_1=\Delta t$	5-5
5.2	Wake Generation Between Times $t_1=\Delta t$ and $t_2=2\Delta t$	5-7
5.3	Analysis of Rigid-Body Motion	5-9
5.4	Vortex Geometry	5-11
6.1.(a-p)	Vertical displacement, z, as a function of the azimuth angle,θ, for the vortex-line emanating from the tip point the trailing edge (for case defined in Table A).	6-4
6.2.(a-d)	Vertical displacement, z, as a function of the radius, R, for the vortex-line emanating from the tip point of the trailing edge (for case defined in Table A).	6-20
6.3.a	Convergence analysis: spanwise sectional lift distribution, (lb/ft), as a function of radial distance, r/R, for five spiral wake (for case defined in Table A).	6-25
6.3.b	Convergence analysis: spanwise sectional lift distribution, (lb/ft), as a function of radial distance, r/R,for seven spiral wake (for case defined in Table A).	6-26
6.4	Effect of the number of spirals on the lift distribution: spanwise lift distribution, (lb/ft), as a function of radial distance, r/R, fordifferent numbers of wake spirals (time step 50).	6-27
6.5	Effect of the number of spirals in the wake geometry: vertical displacement, z, as a function of azimuth angle,θ, for different numbers of wake spirals (time step 50).	6-28

6.6 Wake cross-section compared with Landgrebe-wake cross-section at 90 degrees behind trailing edge. 6-29

6.7 Radial coordinate, r, as a function of the azimuth angle, θ, for the vortex-line emanating from the tip point of the trailing edge at timestep 50 (for case defined in Table A), compared to Landgrebe analytical model. 6-30

6.8 Comparison of present results with those of Rao and Schatzle. 6-31

6.9 Geometry of the vortex-line emanating from the tip point of the trailing edge for all the spirals (for the five-spiral case) at the time step, n=45 (for case defined in Table A). 6-33

LIST OF SYMBOLS

c	= chord
$E(P)$	= see Eq. 3.21
$\bar{n}$	= normal to σ
P	= point having coordinates x,y,z
P_e	= control point, (x_e,y_e,z_e)
r	= $\lvert P-P_e \rvert$
t	= time
x,y,z	= space coordinates
$\Delta\varphi$	= discontinuity of φ across the wake, $\varphi_1 - \varphi_2$
σ_{bw}	= surface surrounding body and wake
σ_b	= surface of body in x,y,z space
σ_w	= surface of wake in x,y,z space
φ	= velocity potential
ψ	= normal wash

<u>Subscripts</u>

b	= body
te	= trailing edge
w	= wake

SECTION 1

INTRODUCTION

1.1. Motivation and Objectives

A new methodology for generation of the wake geometry for the computational aerodynamic analysis of a helicopter rotor is presented in this report.

The availability of such a methodology would enhance considerably the present computational capability in this area. This capability is needed for instance for:

(1) performance and structural analysis

(2) evaluation of generalized forces for flutter analysis

(3) evaluation of the outer potential velocity field for the boundary-layer and separated-flow analysis.

In the classical rotor-wake formulation, the wake is described as a spiral (helicoidal) surface which is obtained from the assumption of uniform vertical flow. This method is not sufficiently accurate for the aerodynamic analysis of helicopter rotors. This yields the need for the development of a methodology for fully-automatic or semi-automatic wake generation.

The fully automated wake generation (commonly referred to as 'free wake' analysis) is obtained step-by-step by calculating from the location of a vortex point at a given time step the location at the next timestep: the drawback with this approach is that the free-wake analysis is quite expensive in terms of computer time.

On the other hand, a semi-automatic wake generation (commonly referred to as 'generalized wake') may be obtained by expressing the analytical description of the wake geometry in terms of few parameters which are evaluated by fitting experimental results. The generalized-wake analysis is accurate and not more expensive than the classical-wake analysis, but currently requires the use of expensive wind tunnel experiments for the generation of the generalize-wake model. On the other hand, the free-wake analysis is more expensive than the generalized-wake analysis but less expensive than the wind tunnel experiments.

The objective of work presented here is the development of an efficient and general method for free-wake potential

aerodynamic analysis which then can be used (instead of the more expensive experimental approach) to generate the generalized-wake model for use in a prescribed-wake analysis. The role of the experimental work would then be limited to the validation of the free-wake analysis.

1.2. Relation of Work with State of the Art

An excellent review on aerodynamic technology for advanced rotorcraft was presented by Landgrebe, Moffitt, and Clark in Refs. 1 and 2. Additional reviews are presented in Refs. 3-7. (Compressibility effects in particular are reviewed in Ref. 7.) Therefore only works which are particularly relevant to the objective and the motivation of the proposed work are included in this brief review, which is not to be considered, by any means, complete.

We feel that the unsteady analysis is the main strength of the method presented here over other existing methods (accurate pressure evaluation for compressible unsteady flow is badly needed for flutter analysis, see Ref. 3: a correct and efficient formulation for such a problem is not available at present time even for an isolated rotor). Therefore particular emphasis is given in this review to the unsteady flow analysis. Another important feature of the methodology proposed here is the capability of analyzing rotor-fuselage interaction: this is the main advantage of so-called panel methods over lifting-surface methods (see below). Therefore this aspect is also emphasized in this review. A third advantage of the methodology proposed here is that it can be extended to give an exact integral equation for nonlinear compressible unsteady flows with moving shock waves. The extension of the present formulation to compressible flows is briefly outlined in Appendix A.

It is interesting to examine the Concluding Remarks made in Reference 2 in 1977:

> 'As with any review of a rapidly changing subject, the conclusion that must be drawn from this review is that, although much has been achieved in terms of our understanding the aerodynamics of the rotor, much remains to be accomplished. In recent years, there have been large advances in the capabilities of the helicopter with today's machines flying faster, farther, higher, heavier, smoother and quieter than their predecessors. However, the gains possible with today's advanced technology are becoming smaller as the state of the art approaches goals set using yesterday's ground rules, and the available techniques must be worked harder to achieve even modest improvements. Unfortunately, these techniques,

reflecting with a growing complexity an increased depth of understanding of the rotor behavior, are beginning to strain the capabilities of the computing facilities available. If further advances are to be made, some simplification (without loss of precision) is required. This is especially true if the methods are to be made available to the engineer and the designer at a working, as opposed to a research, level.

More specifically, based on this review, several areas which require more attention as the industry enters another decade of the development of our technology include: the definition of the inflow distribution in forward flight using a generalized wake approach similar to that developed in hover, the combination of the effects of unsteady and skewed flow, a resolution of the limits of applicability of the basic lifting-line assumption, the development of an economic lifting surface analysis, and a representative aerodynamic model of the rotor/airframe interaction. All of these (and other important elements not covered in this review) should be combined in a tractable, well correlated analysis, which will be used in combination with an improved appreciation of the role of the blade aeroelasticity to develop designs for tomorrow's advanced rotorcraft.'

The work presented here addresses most of these issues. As mentioned above, the objective of this work is to develop an efficient and general methodology for free-wake potential aerodynamic analysis of helicopters in hover or forward flight. This methodology may be used to generate a generalized wake which is now obtained from very expensive wind tunnel results. (The availability of such a method and corresponding computer program would enhance considerably the present computational capability for an accurate evaluation of pressure and flow fields for performance and structural analysis. Such evaluation is also required for instance for the problem of drag-reduction as a prerequisite for the boundary-layer analysis.) Also mentioned above is the fact that the possibility of analyzing compressible unsteady flows and rotor-fuselage interference makes the integral method presented here quite unique among the 'integral equation' methods which are well known to be much faster and much simpler to use than finite-difference or finite-element methods.

Three items which are relevant to this report and which need a discussion deeper than the ones presented in Refs. 1 to 7 are advanced computational methods (lifting-surface and panel methods), wake roll-up and compressibility. These items are briefly examined in the following.

Consider first advanced computational methods. Lifting-surface theories are presented in Refs. 6 to 7. Both methods are of interest here. The first (Summa, Ref. 6) introduces an incompressible time-domain analysis (the wake-dynamics analysis of this paper is covered later in this section) while the second one (Rao and Schatzle, Ref. 7) introduces in a simplified form (local Prandtl-Glauert, chordwise transformation) the effect of compressibility for rotors in unsteady flow. This paper is very relevant here because it clearly demonstrates the importance of an accurate evaluation of the wake geometry for the calculation of the section lift distribution acting on the blade. A third lifting- surface method was developed by Suciu, Preuss and Morino (Ref. 8) for windmill rotors and yields results which are in excellent agreement with those of Rao and Schatzle (Ref. 7). An important development which requires special attention is the work by Dat and Costes (Refs. 9-12), who start from the acceleration potential due to a doublet and develop a lifting-surface equation for compressible rotor aerodynamics.

Next consider panel methods, a new methodology recently introduced in aircraft aerodynamics. This methodology (also called boundary-element method) consists of the finite-element solution (over the actual surface of the body) of integral equations for potential aerodynamics. Typically, the surface of the aircraft is covered with source-panels (doublet-, vortex-, and pressure-panels are also used on the surface of the body and of its wake). The intensity of the source distribution is obtained by assuming that the flow does not penetrate the surface of the body. (Note the difference with respect to the lifting-surface formulations, in which the integral equation is over the mean-surface of the rotor blades. By panel methods we indicate only those methods in which the actual surface is used: their main advantage over the lifting-surface methods is the capability of analyzing rotor-fuselage interaction.) An early work on the flow field around three-dimensional bodies by Hess and Smith (Ref. 13) uses constant strength source-elements to solve the problem of steady subsonic flow around nonlifting bodies. This method has been extended to lifting bodies (Refs. 14-18) by including doublet, vortex, and lifting-surface panels. Work in panel method for unsteady flow around complex configurations include extensions of the doublet-lattice method (Refs. 19 and 20) and, more recently, the work of Morino and his collaborators (Refs. 21-28).

This methodology has been recently extended to helicopter aerodynamics. For instance, the work by Dvorak, Maskew and Woodward (Ref. 29) present a method for calculating the complete pressure distribution on a helicopter fuselage with separate flow (the method uses WBAERO for the potential flow solution, the boundary layer is calculated up to the separation line, separated flow is modeled by streamwise panels of uniform vorticity). Additional results are presented in Ref. 30. Straightforward

applications of panel methods to helicopter aerodynamics are also presented by Soohoo, Morino, Noll, and Ham (Refs. 31 and 32: a formulation for compressible flows is presented in Ref. 31).

The above remarks indicate that panel-aerodynamics methods are becoming available for the analysis of the complete configuration. The availability of such methods (and corresponding computer programs) enhances considerably the present computational capability for an accurate evaluation of pressure and flow fields. This evaluation is becoming more and more important because of recent trends in the field of helicopter aerodynamics. Wind tunnel experiments are very costly whereas computers are becoming less and less expensive. Therefore, the use of computers is becoming more attractive for the aerodynamic analysis of helicopter configuration. For instance, items such as higher performance (lower drag, higher speed, higher lift, higher reliability) require more theoretical analysis: in particular, as mentioned above, reduction of drag requires a very accurate evaluation of the potential flow field as a prerequisite for the boundary-layer and flow separation analysis (Ref. 29). Therefore panel-aerodynamics methods deserve further attention and are expected to become a standard design tool for airplane and helicopter aerodynamics within this decade.

Next consider the issue of wake dynamics. An excellent review of the problem of the wake roll-up is given in Refs. 1 and 2 (where additional works not included here are extensively reviewed). The essence of the state of the art in this area is briefly summarized here. The various aerodynamic analysis of the rotor fall into one of the three following types :

A. Classical wake, i.e., a wake geometry described by a helicoidal spiral with pass obtained from uniform flow assumption.

B. Generalized wake, i.e., a wake geometry obtained by interpolating experimental data in terms of few parameters.

C. Free wake, i.e., a wake geometry obtained computationally as an integral part of the solution.

Analytical models for predicting the geometry of the rotor wake were developed from experimental data by Landgrebe (Ref. 33 and 34), Crews, Hohenemser and Ormiston (Ref. 35) and Kocurek (Ref. 36). Landgrebe's model was used by Rao and Schatzle (Ref. 7) in their lifting-surface theory, and shows that a considerable improvement in the comparison with experimental results of Ref. 37 can be made simply by using a generalized wake geometry

instead of the classical wake geometry. Automatic generation of the wake is considered for instance by Scully (Ref. 38), Summa (Ref. 6) ,and Pouradier and Horowitz (Ref. 39). All these works indicate that the algorithms used are unstable unless special constraints (such as specified contraction ratio) are introduced. Another important issue is the one of simplified algorithms which can be used for instance for modeling the far wake: several models are available for the hover case (see e.g., Ref. 40-42). However none of these models is applicable to the case of arbitrary motion considered in this report.

As mentioned above, it is a generally accepted opinion in the helicopter-aerodynamics community that the classical-wake analysis is insufficient (see for instance Ref. 7) to obtain accurate results and that the free-wake analysis is too expensive and that, consequently, all the effort should be devoted to the generalized-wake analysis. While we basically agree with this assessment, we would like to point out again that in generating the generalized-wake geometry it is not necessary to use the costly wind-tunnel results: one can use the free-wake analysis which is more expensive than the generalized-wake analysis but also much less expensive than the experimental approach.

Next consider the issue of compressibility. As mentioned above, the analysis for compressible flows is examined in Appendix A. Hence for completeness, the issue of compressibility is reviewed here. The importance of compressibility was clearly demonstrated by Friedman and Yuan (Ref. 3) for the problem of aeroelastic stability (i.e., flutter and divergence) of rotor blades. The work is based on simple aerodynamic strip-theories (Refs. 43-49). However, the same effect is expected from more sophisticated unsteady three-dimensional compressible theories. As mentioned above, compressibility effects are included in the lifting-line theory by Johansson (Ref. 5), in the lifting-surface method by Rao and Schatzle (Ref. 7 which is based on the work of Rao and Jones, Ref. 50) and in the works of Dat and Costes (Refs. 9-12) and in the work by Morino and Soohoo (Ref. 31). A possible alternative approach is the numerical solution of the differential equation using for instance the finite-difference technique (Caradonna et al., Refs. 51-54): this method however requires considerable amounts of computer time. Therefore the development of a methodology based on the integral equation presented in Appendix A appears to be an attractive alternative to other existing methods for the analysis of unsteady compressible flows around complex configurations (the validation of this integral formulation is limited to the particular case of incompressible flows: the results are presented in Section 6 of this report).

1.3. Summary of Work

The work presented here includes two aspects: (1) the development of a formulation for the time-dependent free-wake aerodynamic analysis of helicopters in hover and forward flight and (2) validation of the formulation, for the particular case of incompressible flows, by developing a computer program and comparing the results against selected existing computational and experimental data.

Regarding the first aspect of the effort, the formulation is very general: the main restriction is the assumption of potential aerodynamics. This implies in particular that viscous (attached and separated) flows are not included here. For the sake of clarity, compressible flows are dealt with in Appendix A: the main body of this report deals with incompressible flows. The formulation is based upon an integral method developed by Morino (Refs. 21 to 23, see also Section 3 and 5) for the exact compressible three-dimensional unsteady velocity-potential equation for lifting bodies having arbitrary shapes and motions. (For incompressible flows with prescribed wake, the formulation has been applied to rotor-fuselage helicopter configurations, Refs. 31-32, and to time-domain analysis of unsteady flows around windmill rotors, Refs. 8.) New theoretical results are included in this report. The formulation for wake dynamics, presented in Section 2, is considerably different from that of our preceding publications (which did not make explicit use of the principles of conservation of mass and momentum across the wake): we believe it is clearer, more convincing and more rigorous than any wake-dynamics formulation of which we are aware. Also new are the results presented in Section 4 which deals with the issues of wake generation, uniqueness of solution, Kutta condition, Joukowski hypothesis and trailing edge condition.

Regarding the second aspect of the effort, the validation of the formulation includes time-domain free-wake analysis of the unsteady velocity-potential equation for flexible rotors in hover or forward flight. The validation involves the implementation of the numerical formulation into a computer program and comparison with existing experimental and numerical results. This validation is limited to an isolated rotor in hover. However, the formulation and the numerical algorithm used in the computer program are time accurate (i.e., they yield a steady state solution via an accurate time-domain analysis) and therefore are in theory applicable to time dependent flows (of course, validation for this application would be required). The computer algorithm is general in that only the geometry and the motion of the surface of the rotor is needed as an input. The issue of the numerical stability for the automatic generation of the wake is also discussed.

SECTION 2

WAKE DYNAMICS IN INCOMPRESSIBLE POTENTIAL FLOWS

A general formulation for the problem of the wake dynamics for potential flows is presented in this section. Fundamental issues related to the wake dynamics have been clarified during the effort reported here. These issues (such as the boundary conditions on the wake and at the trailing edge) are quite subtle and have never been discussed in our preceding publications. Therefore the theoretical foundations of the wake dynamics are presented here (see Sections 2.2 and 2.3), we believe for the first time. (Trailing-edge issues are dealt within Section 4.) For the sake of simplicity, the formulation is presented for incompressible flows (compressible flows are dealt with in Appendix A).

2.1. Incompressible Inviscid Flows

In this report we will assume that the frame of reference is connected with the undisturbed air. We assume the fluid to be inviscid and incompressible. Hence the motion is governed by the Euler equations (conservation of momentum)

$$\frac{D\bar{v}}{Dt} = -\frac{1}{\rho}\,\text{grad}\ p \qquad 2.1$$

and the continuity equation for incompressible fluid (conservation of mass)

$$\text{div}\ \bar{v} = 0 \qquad 2.2$$

where $\bar{v}$ is the velocity vector with respect to a prescribed frame of reference, p is the pressure, ρ is the density (constant for incompressible fluid), t the time, whereas

$$\frac{D}{Dt} = \frac{\partial}{\partial t} + \bar{v}\cdot\text{grad} \qquad 2.3$$

is the material or substantial derivative. Equations 2.1 and 2.2 form a system of four partial differential equations for four unknowns v_x, v_y, v_z, and p.

In order to complete the formulation of the problem, the boundary conditions at infinity, on the body and on the wake must be obtained.

Since the frame of reference has been assumed to be connected with the undisturbed air, the boundary condition at infinity may be written as

$$p = p_\infty \text{ and } \bar{v} = 0 \quad (\text{for P at } \infty) \tag{2.4}$$

On the body (rotor in our case) it is assumed that the surface of the body is impermeable. This implies that the normal components of the velocity $\bar{v}$ of the fluid, and of the velocity $\bar{v}_b$ of the rotor blades coincide at point P on the surface σ_b of the rotor:

$$(\bar{v} - \bar{v}_b)\cdot\bar{n} = 0 \quad (\text{for P on } \sigma_b) \tag{2.5}$$

where $\bar{n}$ is the normal to σ_b at P.

The boundary condition on the wake are discussed in Section 2.4 after introducing the concept of potential wake.

2.2. Potential Flows; Potential Wakes

The basis of the discussion on the wake dynamics is the well known Kelvin's theorem which states that the circulation

$$\Gamma = \oint_C \bar{v}\cdot d\bar{s} \tag{2.6}$$

over a material contour C (i.e., a contour which is made up of material particles) remains constant in time. This theorem is an immediate consequence of the definition of Γ, of Euler equations (Eq. 2.1) and of the fact that the density is constant (or, in general, that the fluid is barotropic).

Next assume that the flow field is irrotational at time 0. Then according to Stokes theorem

$$\oint_C \bar{v}\cdot d\bar{s} = \iint_\sigma \text{curl } \bar{v}\cdot\bar{n}\, d\sigma \tag{2.7}$$

(where C is the contour of σ), Γ is initially equal to zero for any path connected with a surface σ fully inside the fluid volume. Hence, for all these paths, Γ remains identically equal to zero. This implies that

$$\text{curl } \bar{v} = 0 \tag{2.8}$$

for almost all the fluid points at all times: the only points to be excluded are those material points which come in contact with the solid boundaries (since for these points, Kelvin's theorem does not apply). In order to simplify the discussion of this issue, let us focus on the case of an isolated blade with a sharp

trailing edge and consider only those flows such that the fluid leaves the surface of the blade at the trailing edge (this issue is further discussed later in this Section 4). We call these flows attached flows. Hence the points which come in contact with the rotor are only those emanating from the trailing edge and therefore form a surface: such a surface is called wake. Kelvin's theorem does not apply to the points of the wake. [Note that if the trailing edge is fixed with respect to the frame of reference, the wake is a 'streak surface' (Ref. 52). Since the trailing edge in general moves, we say that the wake is a 'generalized streak surface.']

We may conclude that for an inviscid and incompressible fluid, if a flow field is initially irrotational, it remains irrotational at all times except for those points which come in contact with the surface of the body. If the flow is attached (i.e., by definition if the fluid leaves the body only at the points of a line which is called 'trailing edge') then the locus of these points forms a generalized streak surface which is called a wake.

It may be worth emphasizing that as shown above the fact that for attached flows the wake has zero thickness does not require futher assumptions but is a direct consequence of the hypothesis of incompressible (in general, barotropic) inviscid flow and of the definition of attached flows (the assumption if initially irrotational flows is not essential for the presence of zero-thickness wakes).

2.3. Potential-Flow Formulation

Next consider a well known theorem from vector field theory which states that if a vector field $\bar{v}$ is irrotational then there exists a function, φ, called velocity potential such that

$$\bar{v} = \text{grad } \varphi \qquad 2.9$$

Hence our results may be restated as follows: for an inviscid incompressible fluid, a flow field which is attached and initially irrotational is potential at all times and at all points except at the point of the wake.

If the flow is potential, i.e., if $\bar{v}$ is given by Eq. 2.9, Eq. 2.1 may be integrated to yield Bernoulli's theorem

$$\frac{\partial \varphi}{\partial t} + \frac{1}{2}|\text{grad } \varphi|^2 + \frac{p}{\rho} = \frac{1}{\rho}p_\infty \qquad 2.10$$

(The x-derivative of Eq. 2.10 yields the first component of Eq. 2.1: the constant on the right hand side of Eq. 2.10 is obtained from the boundary conditions at infinity.)

Furthermore, Eq. 2.2 may be rewritten as

$$\nabla^2\varphi = 0 \qquad 2.11$$

where ∇^2 is the Laplacian operator.

Similarly, Eq. 2.4 may be rewritten as

$$\varphi = 0 \qquad \text{(for P at } \infty\text{)} \qquad 2.12$$

and Eq. 2.5 becomes

$$\frac{\partial\varphi}{\partial n} = \bar{v}_b \cdot \bar{n} \qquad 2.13$$

2.4. Boundary Conditions on Wake

In order to be able to solve the mathematical problem, we need a boundary condition on the wake. This condition may be obtained from the principles of conservation of mass and momentum across a surface of discontinuity.

Indicating by subscripts 1 and 2 the two sides of the wake, let $\bar{n}$ be the outward normal on side 1 and let

$$\Delta f = f_1 - f_2 \qquad 2.14$$

denote the discontinuity of any function f across the wake surface. (For the classical wing-wake, 1 and 2 correspond to upper and lower sides respectively, $\bar{n}$ is the upper normal and $\Delta f = f_u - f_l$.)

The equation of conservation of mass and momentum across a possible surface of discontinuity (e.g., a shock wave or a wake) are given by (Ref. 58)

$$\Delta[\rho(v_n - v_s)] = 0 \qquad 2.15$$

$$\Delta[\rho(v_n - v_s)\bar{v} + p\bar{n}] = \rho\,(v_n - v_s)\,\Delta\bar{v} + \Delta p\,\bar{n} = 0 \qquad 2.16$$

where $v_n = \bar{v}\cdot\bar{n}$ is the normal component of the velocity $\bar{v}$ whereas v_s is the velocity of the surface (by definition, in direction of the normal $\bar{n}$). In the case of incompressible flows, $\Delta\rho = 0$ and therefore Eq. 2.15 yields

$$\Delta v_n = 0 \qquad 2.17$$

(since v_s is the same for both sides of the wake). Then the

normal component of Eq. 2.16 yields

$$\Delta p = 0 \tag{2.18}$$

Hence using Eq. 2.15, Eq. 2.16 reduces to

$$\rho(v_n - v_s)\Delta\bar{v} = 0 \tag{2.19}$$

which implies either $\Delta\bar{v} = 0$ (that is the surface under consideration is not a surface of discontinuity) or if there is a discontinuity (wake surface)

$$v_n = v_s \tag{2.20}$$

that is the flow does not penetrate the surface of the wake.

Note that Eq. 2.20 implies in particular that only the tangential components of the velocity are discontinuous across the surface of the wake, that is (using a local frame of reference $\bar{i}_1$, $\bar{i}_2$, $\bar{i}_3$ with $\bar{i}_3$ in the direction of the normal $\bar{n}$)

$$\begin{aligned}\Delta\bar{v} &= \Delta(v_1\bar{i}_1 + v_2\bar{i}_2 + v_n\bar{n}) \\ &= \Delta\left(\frac{\partial\varphi}{\partial x_1}\bar{i}_1 + \frac{\partial\varphi}{\partial x_2}\bar{i}_2\right) \\ &= \frac{\partial\Delta\varphi}{\partial x_1}\bar{i}_1 + \frac{\partial\Delta\varphi}{\partial x_2}\bar{i}_2 = \mathrm{grad}_t\Delta\varphi\end{aligned} \tag{2.21}$$

where

$$\mathrm{grad}_t f = \frac{\partial f}{\partial x_1}\bar{i}_1 + \frac{\partial f}{\partial x_2}\bar{i}_2 \tag{2.22}$$

is the 'tangential portion' of the vector grad f. (It is important to note that grad Δf is a meaningless expression since Δf is defined only over the surface of the wake.)

Next consider Bernoulli's theorem Eq. 2.10 with the wake condition, $\Delta p = 0$, Eq. 2.18. This yields

$$\frac{\partial\varphi_1}{\partial t} - \frac{\partial\varphi_2}{\partial t} + \frac{1}{2}(\bar{v}_1\cdot\bar{v}_1 - \bar{v}_2\cdot\bar{v}_2) = 0 \tag{2.23}$$

that is

$$\frac{\partial}{\partial t}(\varphi_1 - \varphi_2) + \frac{1}{2}(\bar{v}_1 + \bar{v}_2)\cdot(\bar{v}_1 - \bar{v}_2)$$

$$= \frac{\partial}{\partial t}\Delta\varphi + \frac{1}{2}(\bar{v}_1 + \bar{v}_2)\cdot\Delta\bar{v} = 0 \qquad 2.24$$

or, introducing the velocity of a wake point, P_w,

$$\bar{v}_w = \frac{1}{2}(\bar{v}_1 + \bar{v}_2) \qquad 2.25$$

and using Eq. 2.17,

$$(\frac{\partial}{\partial t} + \bar{v}_w\cdot\text{grad}_t)\Delta\varphi = 0 \qquad 2.26$$

The above equation is the desired boundary condition on the wake, and may be rewritten as

$$\frac{D_w}{Dt}\Delta\varphi = 0 \qquad 2.27$$

where

$$\frac{D_w}{Dt} = \frac{\partial}{\partial t} + \bar{v}_w\cdot\text{grad}_t = \frac{\partial}{\partial t} + v_{w1}\frac{\partial}{\partial x_1} + v_{w2}\frac{\partial}{\partial x_2} \qquad 2.28$$

is the material time derivative for a function defined only over a surface: in a *frame of reference* moving with (constant) velocity equal to $\bar{v}_w$ at a given time and a given point, the substantial derivative coincides with the partial time derivative. This implies that

$$\Delta\varphi = \text{constant} \qquad 2.29$$

following a point P_w which has velocity $\bar{v}_w$ given by Equation 2.25.

Note that v_{w1} and v_{w2} are the average values of the components 1 and 2 *respectively of* $\bar{v}_1$ and $\bar{v}_2$ (which are discontinuous across the wake), whereas $v_{wn} = v_n = v_s$ (see Equation 2.16) since v_n is continuous across the wake. The above

results can be restated in more physical terms saying that a point of the wake has a velocity $\bar{v}_w$ equal to the average between the velocities, $\bar{v}_1$ and $\bar{v}_2$, on sides 1 and 2 of the wake respectively. The value of $\Delta\varphi(P_w)$ is time independent and equal to the value that it had when the point P_w left the trailing edge.

It may be worth noting that v_{wn} does not appear in Equation 2.24. However the fact that P_w has normal velocity equal to v_{wn} stems from the fact that the points of the surface have velocity equal to $v_n = v_{n1} = v_{n2}$ (Equation 2.20). This is in agreement with the results of Section 2.2 that the wake surface is a generalized streak surface.

2.5. Summary

In summary, if the flow field of an inviscid incompressible fluid is initially irrotational, it remains irrotational at all times and therefore may be given as

$$\bar{v} = \text{grad}\,\varphi \qquad 2.30$$

Then (see 2.11), φ satisfies Laplace equation

$$\nabla^2\varphi = 0 \qquad 2.31$$

with condition at infinity, (Eq. 2.12)

$$\varphi = 0 \quad (\text{for P at } \infty) \qquad 2.32$$

On the other hand (see Eq. 2.13), the boundary condition on the rotor blade is given by

$$\frac{\partial\varphi}{\partial n} = \bar{v}_b \cdot \bar{n} \qquad 2.33$$

whereas on the wake (see Eq. 2.29)

$$\Delta\varphi(P_w) = \text{constant in time} \qquad 2.34$$

Equations 2.30 to 2.34, with the addition of Joukowski's hypothesis (see Section 4), may be used to obtain the solution for φ. Once φ is known, the perturbation velocity may be evaluated using Eq. 2.30. Then the pressure may be evaluated using Bernoulli's theorem

$$\frac{\partial\varphi}{\partial t} + \frac{1}{2}|\bar{v}|^2 + \frac{p}{\rho} = \frac{p_\infty}{\rho} \qquad 2.35$$

SECTION 3

INTEGRAL FORMULATION

The integral equation used in this work is a particular case of that introduced by Morino (Refs. 21-23) for the general case of potential compressible flows for bodies having arbitrary shapes and motions. For the sake of completeness and clarity the derivation of such an equation is briefly outlined here for the specific case of interest, incompressible potential flow around a helicopter rotor having arbitrary shape and motion. The integral equation is based on the classical Green's function method. This requires the use of Green's formula and Green's theorem which are presented first.

3.1 Green's Formula for Laplace's Equation

Consider two arbitrary functions f and g and note that

$$\text{div}(f\ \text{grad}g) = \text{grad}f \cdot \text{grad}g + f\ \nabla^2 g \qquad 3.1$$

and

$$\text{div}(g\ \text{grad}f) = \text{grad}g \cdot \text{grad}f + g\ \nabla^2 f \qquad 3.2$$

or

$$\text{div}(f\ \text{grad}g - g\ \text{grad}f) = f\ \nabla^2 g - g\ \nabla^2 f \qquad 3.3$$

Also, according to Gauss theorem, for any arbitrary vector $\bar{a}$

$$\iiint_{V'} \text{div}\ \bar{a}\ dV = -\oiint_{\sigma} \bar{a}\cdot\bar{n}\ d\sigma \qquad 3.4$$

where σ surrounds V' and $\bar{n}$ is the inward directed normal. Combining Eqs. 3.3 and 3.4 yields

$$-\iiint_{V'} (f\ \nabla^2 g - g\ \nabla^2 f)dV = \oiint_{\sigma} (f\ \text{grad}g - g\ \text{grad}f)\cdot\bar{n}\ d\sigma$$

$$= \oiint_{\sigma} \left(f \frac{\partial g}{\partial n} - g \frac{\partial f}{\partial n}\right) d\sigma \qquad 3.5$$

Next, assume that both f and g satisfy the Laplace equation, that is

$$\nabla^2 f = \nabla^2 g = 0 \quad (\text{in } V). \qquad 3.6$$

Then Equation 3.5 yields

$$\iint_\sigma \left(f \frac{\partial g}{\partial n} - g \frac{\partial f}{\partial n}\right) d\sigma = 0 \qquad 3.7$$

which is the desired Green's formula for the Laplace equation.

Next choose the function g to be the simplest function which satisfies the Laplace equation with the condition

$$g = 0 \qquad \text{at infinity} \qquad 3.8$$

If g is a function of the distance r from a specified point P_*, then the most general function that satisfies the Laplace equation is

$$g = A/r + B \qquad 3.9$$

where

$$r = |P - P_*| \qquad 3.10$$

Using Equation 3.8 yields B = 0. Note that g = A/r represents the velocity potential of a source. It is convenient to choose A such that g represents a unit source, that is, a source with flux equal to one. The flux through a spherical surface of radius R is given by

$$\oiint_\sigma \bar{v}\cdot\bar{n}\, d\sigma = \oiint_\sigma \left.\frac{\partial g}{\partial r}\right|_{r=R} d\sigma = -\frac{A}{R^2}\, 4\pi R^2 = 1 \qquad 3.11$$

which implies $A = -1/4\pi$ and

$$g = -\frac{1}{4\pi r} \qquad 3.12$$

Combining Eq. 3.7 and 3.8 yields the desired Green formula for the Laplace equation

$$\iint_\sigma \left[f \frac{\partial}{\partial n}\left(\frac{-1}{4\pi r}\right) - \frac{\partial f}{\partial n}\left(\frac{-1}{4\pi r}\right)\right] d\sigma = 0 \qquad 3.13$$

Note that P_* must be outside the volume V, otherwise Equation 3.6 is not satisfied at P_*.

3.2. Green's Theorem for Incompressible Potential Aerodynamics

In order to obtain Green's theorem for incompressible aerodynamics, let the function f in Eq. 3.13 be the velocity potential φ. Hence the volume V must exclude the volume V_b of the rotor blades as well as a thin layer, V_w, which includes the wake surface σ_w (because the equation $\nabla^2\varphi = 0$ is not valid in V_b and on σ_w). In addition, the volume V must exclude a small volume around P_* because the equation $\nabla^2 g = 0$ is not valid at P_*. Finally, the volume V must be bound. Hence let the surface σ be the boundary of the volume V. This surface is the sum of three surfaces: the surface σ_{bw} (which surrounds the rotor blade volume, V_b, and the wake volume, V_w: note that the inward normal for σ is outward to σ_{bw}), the surface σ_ε (which is a spherical surface of radius ε and center P_*) and the surface σ_∞ (which is a spherical surface of radius R and center P_*).

Then Eq. 3.13, for $f = \varphi$, reduces to

$$\oiint_{\sigma_{bw}+\sigma_*+\sigma_\infty} \left[\frac{\partial\varphi}{\partial n}\left(\frac{-1}{4\pi r}\right) - \varphi \frac{\partial}{\partial n}\left(\frac{-1}{4\pi r}\right)\right] d\sigma \qquad 3.14$$

Note that, as the radius ε of σ_* goes to zero,

$$\lim_{\varepsilon\to 0} \oiint_{\sigma_*} \left[\frac{\partial\varphi}{\partial n}\left(\frac{-1}{4\pi r}\right) - \varphi \frac{\partial}{\partial n}\left(\frac{-1}{4\pi r}\right)\right] d\sigma$$

$$= -\lim_{\varepsilon\to 0} \left[\varphi_* \frac{1}{4\pi\varepsilon^2}\oiint_{\sigma_*} d\sigma + \frac{1}{4\pi\varepsilon}\oiint_{\sigma_*} \frac{\partial}{\partial n}\, d\sigma\right]$$

$$= -\varphi_* \qquad 3.15$$

whereas, as the radius R of σ_∞ goes to infinity

$$\lim_{R\to\infty} \oiint_{\sigma_\infty} \left[\frac{\partial\varphi}{\partial n}\left(\frac{-1}{4\pi r}\right) - \varphi \frac{\partial}{\partial n}\left(\frac{-1}{4\pi r}\right)\right] d\sigma$$

$$\simeq \lim_{R\to\infty} \left[\varphi + \left(\frac{\partial\varphi}{\partial n}\right) R\right] = 0 \qquad 3.16$$

under the condition

$$\lim_{R\to\infty} \varphi = 0 \qquad 3.17$$

$$\lim_{R\to\infty} \frac{\partial \varphi}{\partial n} R = 0 \qquad 3.18$$

[It is verified a posteriori (Eqs. 3.35-3.36) that these conditions are satisfied.]

Therefore, as ε tends to zero and R tends to infinity, Eq. 3.14 becomes

$$\varphi_* = \oiint_{\sigma_{bw}} [\frac{\partial \varphi}{\partial n} (\frac{-1}{4\pi r}) - \varphi \frac{\partial}{\partial n}(\frac{-1}{4\pi r})] \, d\sigma \qquad 3.19$$

It may be worth noting that if the point P_* is inside σ_b, then there is no need for the surface σ_ε. In this case, Eq. 3.14 yields simply

$$0 = \oiint_{\sigma_{bw}} [\frac{\partial \varphi}{\partial n} (\frac{-1}{4\pi r}) - \varphi \frac{\partial}{\partial n}(\frac{-1}{4\pi r})] \, d\sigma \qquad 3.20$$

Equations 3.19 and 3.20 may be combined by writing

$$E_* \varphi_* = \oiint_{\sigma_{bw}} [\frac{\partial \varphi}{\partial n} (\frac{-1}{4\pi r}) - \varphi \frac{\partial}{\partial n}(\frac{-1}{4\pi r})] \, d\sigma \qquad 3.21$$

where

$$E_* = E(P_*) = 1 \qquad (P_* \text{ outside } \sigma_b)$$
$$= 0 \qquad (P_* \text{ inside } \sigma_b) \qquad 3.22$$

3.3. Wake Contribution

Next let σ_w become infinitesimally close to the surface of the wake. Note that in this process, the closed surface, σ_w, the wake is replaced by the two sides of an open surface σ_w'. Let $\bar{n}$ be the normal on the side 1 of σ_w'. In the limit one obtains

$$\oiint_{\sigma_w} \frac{\partial \varphi}{\partial n} \frac{1}{r} \, d\sigma = \iint_{\sigma_w'} \Delta(\frac{\partial \varphi}{\partial n}) \frac{1}{r} \, d\sigma = 0 \qquad 3.23$$

[since (see Eq. 2.20) $\Delta(\frac{\partial \varphi}{\partial n}) = \Delta v_n = 0$] whereas

$$\oiint_{\sigma_w} \varphi \frac{\partial}{\partial n}\left(\frac{1}{r}\right) d\sigma = \iint_{\sigma_w'} \Delta\varphi \frac{\partial}{\partial n}\left(\frac{1}{r}\right) d\sigma \qquad 3.24$$

Therefore, in the limit, Eq. 3.21 reduces to

$$4\pi E_* \varphi_* = -\oiint_{\sigma_b} \left[\frac{\partial \varphi}{\partial n}\frac{1}{r} - \varphi \frac{\partial}{\partial n}\left(\frac{1}{r}\right)\right] d\sigma + \iint_{\sigma_w'} \Delta\varphi \frac{\partial}{\partial n}\left(\frac{1}{r}\right) d\sigma \qquad 3.25$$

where σ_b is the (closed) surface of the rotor blade and σ_w' is the (open) surface of the wake of the rotor blade. Furthermore (see Eq. 2.14), $\Delta\varphi = \varphi_1 - \varphi_2$, whereas $\bar{n}$ is the normal on the side 1 of the wake. Note that $\Delta\varphi$ on σ_w is evaluated from Eq. 2.34. Note also that the vortex-layer wake of the rotor is represented as a doublet layer. The proof of the equivalence of doublet layers and vortex layers is given, for instance, in Reference 57.

3.4. Integral Equation

Equation 3.25 may be used to obtain the value of φ at any point in the field if the value of φ and $\partial\varphi/\partial n$ on the surface of the rotor and the value of $\Delta\varphi$ on its wake are known. Note that $\partial\varphi/\partial n$ is known from the boundary condition on the rotor, Eq. 2.33, whereas $\Delta\varphi$ may be calculated from the boundary condition on the surface of the wake, Eq. 2.34.

Hence, in order to be able to use Eq. 3.25 one must have an equation to evaluate φ on the surface: such an equation is obtained by noting that if P_* approaches a point on the surface of the rotor, then the value of φ_* approaches the value of φ on the surface of the rotor. In order to perform this limit, it is convenient to interpret the doublet integral in terms of solid angles. Note that (see Figure 3.1)

$$\iint_\sigma \varphi \frac{\partial}{\partial n}\left(\frac{-1}{4\pi r}\right) d\sigma = \frac{1}{4\pi}\iint_\sigma \varphi \bar{n}\cdot\frac{\bar{r}}{r}\frac{d\sigma}{r^2}$$

$$= \frac{1}{4\pi}\iint_\sigma \varphi \cos\alpha \frac{d\sigma}{r^2}$$

$$= \frac{1}{4\pi}\iint_\Omega \varphi \, d\Omega \qquad 3.26$$

In particular, for a closed surface and $\varphi = 1$, Eq. 3.26 becomes

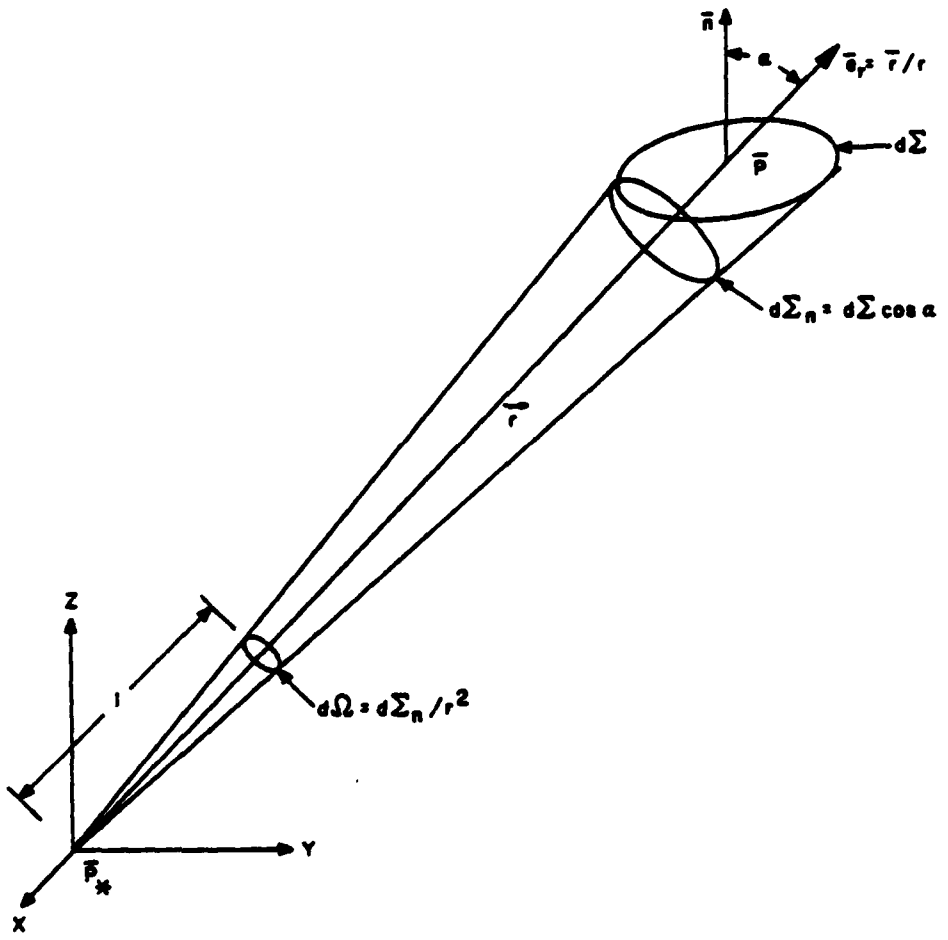

Figure 3.1. Geometry for Definition of Solid Angles

$$\oiint_{\sigma} \frac{\partial}{\partial n}\left(\frac{-1}{4\pi r}\right) d\sigma = \frac{1}{4\pi}\oiint_{\Omega} d\Omega = \frac{1}{4\pi}\,\Omega_* \qquad 3.27$$

Note that, as is well known

$$\Omega_* = 1 \quad \text{for } P_* \text{ inside } \sigma_b \qquad 3.28$$

$$= 0 \quad \text{for } P_* \text{ outside } \sigma_b$$

Comparing Equation 3.22 and 3.28 yields

$$E_* = 1 - \Omega_*/4\pi \quad (P_* \text{ inside and outside } \sigma_b) \qquad 3.29$$

Using Equations 3.29, Equation 3.25 may be rewritten as

$$4\pi\varphi_* = -\oiint_{\sigma_b} \frac{\partial \varphi}{\partial n}\left(\frac{1}{r}\right) d\sigma$$

$$+ \oiint_{\sigma_b} (\varphi - \varphi_*)\frac{\partial}{\partial n}\left(\frac{1}{r}\right) d\sigma + \iint_{\sigma'_w} \Delta\varphi \frac{\partial}{\partial n}\left(\frac{1}{r}\right) d\sigma \qquad 3.30$$

The advantage of Equation 3.30 over Equation 3.25 is that each term is continuous (as P_* crosses σ_b) and therefore is valid in particular even if P_* is on σ_b.

Having established this, one can now go back to Equation 3.25 with E_* given by Equation 3.29 which is valid also for P_* on σ_b (and coincides with Equation 3.22 if P_* is not on σ_b). In particular if P_* is a regular point of σ_b (i.e., a point where σ_b has a unique tangent plane) then $\Omega_* = 2\pi$ and $E_* = 1/2$. Equation 3.22 may thus be generalized as

$$\begin{aligned} E_* = 1 - \Omega_*/2\pi &= 1 \quad && P_* \text{ outside } \sigma_b \\ &= 1/2 && P_* \text{ on } \sigma_b \text{ (regular point)} \\ &= 0 && P_* \text{ inside } \sigma_b \end{aligned} \qquad 3.31$$

In any event, for P_* on σ_b, Equation 3.25 (with E_* given by Equation 3.29, or Equation 3.31 if P_* is a regular point of σ_b) is an integral equation relating the unknown values of the velocity potential on the surface of the rotor, to the values of $\partial\varphi/\partial n$ (prescribed by the boundary condition on the surface of the blade) and the values of the potential discontinuity on the wake (known from the preceding time history).

The time evolution described by Equation 3.25 and its interpretation in physical terms is presented in Section 4 along with a discussion of the trailing edge condition.

3.5 Conditions at Infinity

In this subsection Equations 3.17 and 3.18 are verified. Note as r goes to infinity, Equation 3.43 yields

$$\varphi_e \simeq \oiint_{\sigma_{bw}} \left[\frac{\partial \varphi}{\partial n}\left(\frac{-1}{4\pi r}\right) - \varphi \frac{\partial}{\partial n}\left(\frac{-1}{4\pi r}\right)\right] d\sigma$$

$$\simeq \left[\frac{1}{4\pi r}\oiint_{\sigma_{bw}} \frac{\partial \varphi}{\partial n}\, d\sigma - \frac{1}{4\pi r^2}\oiint_{\sigma_{bw}} \varphi \frac{\bar{r}\cdot\bar{n}}{r}\, d\sigma\right] \qquad 3.32$$

Since the flux through σ_{bw} is equal to zero, i.e.,

$$\oiint_{\sigma_{bw}} \frac{\partial \varphi}{\partial n}\, d\sigma = 0 \qquad 3.33$$

(this condition must be satisfied by $\frac{\partial \varphi}{\partial n}$ and is obtained by using $g = 1$ in Equation 3.7), whereas

$$\lim_{P_s \to \infty} \iint_{\sigma_{bw}} \varphi \frac{\bar{r}\cdot\bar{n}}{r}\, d\sigma = \text{finite}, \qquad 3.34$$

Equation 3.32 implies

$$\varphi = O(r^{-2}) \quad \text{at } \infty \qquad 3.35$$

and

$$\frac{\partial \varphi}{\partial n} = O(r^{-3}) \quad \text{at } \infty \qquad 3.36$$

SECTION 4

WAKE GENERATION

In this section the issue of the wake generation is analyzed. First the analytical results of Section 3 are interpreted from a physical point of view. Next Joukowski hypothesis (of smooth flow at the trailing edge) is introduced and then the wake generation and the trailing edge condition are discussed.

We believe in particular that the issue of the trailing edge condition (i.e., Kutta condition, Joukowski hypothesis) is not well understood and quite confusing in the existing literature (and it may be a source of error in the numerical formulation). Whereas this issue is discussed in greater details in Reference 55, the major conclusions reached there are summarized here in the hope of shedding some light on this aspect of the foundations of potential flows.

4.1 Sudden Start

In order to discuss the problem of wake generation it is convenient to consider the problem of a rotor subject to sudden start, that is the case of a rotor which for $t < 0$ is at rest and is surrounded by a fluid which is also at rest. At time 0^+ the rotor is subject to a motion (which for simplicity we will assume to be of rigid-body type) with finite velocity.

Since for time $t < 0$ the fluid was at rest, the wake has not yet had time to form. Therefore $\Delta\varphi = 0$ everywhere in the field and the solution to the problem at time 0^+ is obtained by solving Equation 3.25 with $\Delta\varphi = 0$, that is

$$4\pi E_* \varphi_* = - \iint_{\sigma_b} [\frac{\partial \varphi}{\partial n} \frac{1}{r} - \varphi \frac{\partial}{\partial n}(\frac{1}{r})] \, d\sigma \qquad 4.1$$

with $E_* = 1 - \Omega_*/4\pi$ ($E_* = 1/2$ on regular points of σ_b, see Eq. 3.31). This corresponds to the solution of Laplace equation without wake contribution and, as well known (for instance from conformal mapping solution in two dimensional flows), this yields a separation point which is different from the trailing edge and hence infinite velocity at the trailing edge. In turn this indicates the presence of a vortex at the trailing which is manifested by the fact that

$$\Delta \varphi_{te} = 0 \qquad 4.2$$

[This can be seen from the fact that according to Stokes theorem

$$\Delta\varphi_{te} = \oint_C \bar{v}\cdot d\bar{s} = \Gamma \qquad 4.3$$

where C is a contour around the trailing edge whereas Γ is the intensity of the vortex at the trailing edge.]

4,2 Uniqueness of Solution: Kutta Condition

Perhaps less well known is the fact that the solution for the problem is unique (the proof of uniqueness is given for instance in Batchelor, Ref.57). More precisely it may be shown that if the solution to exterior Neumann problem for Laplace equation is single-valued then it is also unique. Multi-valued solutions cannot occur in simply connected regions. This is in sharp conflict with the classical two dimensional results in which an arbitrary vortex can be added inside an airfoil to obtain smooth flow at the trailing edge. The mathematical reason for the difference is that the flow region around an airfoil is doubly connected, whereas that around a rotor (as well as most three dimensional shapes of aerodynamic interest) is simply connected. From a physical point of view we can say that it is possible to add a vortex of arbitrary intensity inside an airfoil (or inside a doughnut-shaped object, which also yields a doubly connected flow-region): then, adding a suitable single-valued solution one obtains a nontrivial solution to the homogeneous Neumann exterior problem for Laplace equation. This solution can always be added to the solution of the airfoil problem, which is therefore nonunique. (From a mathematical point of view it may be noted that the field caused by the vortex is multivalued and the proof of uniqueness fails for multivalued potential functions).

In the case of a rotor it is possible to add a vortex inside the rotor-surface: however it is not possible to have a contour which is 'interlocked' with the vortex without penetrating the rotor surface (this is true, by definition, for any simply connected region). The potential flow is then single-valued and is impossible to generate a nontrivial solution. The solution to the rotor problem is thus unique.

In order to clarify the issue of the trailing edge conditions we will call Kutta condition as that trailing edge condition which is used to eliminate the issue of a nonunique solution. This condition is required for two-dimensional flows, but not in three-dimensional flows (unless the region is multiply connected) in which the wake is responsible for the elimination of singularities at the trailing edge. From a mathematical point of view the Kutta condition requires that the vorticity

distribution over the airfoil does not go to infinity at the trailing edge. This is different from the condition that discrete vortices cannot remain at the trailing edge: such a condition is a consequence of Joukowski hypothesis discussed in Section 4.3.

4.3 Joukowski Hypothesis

The assumption introduced here is that the physical behavior of the fluid is such that the 'flow is smooth at the trailing edge.' Such an assumption is connected with the works of Joukowski (Ref. 59) and Kutta (Ref. 60). In order to avoid confusion with the Kutta condition discussed in Section 4.2, we will refer to the above assumption as Joukowski hypothesis (for a historical account on the works of Kutta and Joukowski *see Refs.* 57 and 61).

In particular we assume that if concentrated vortices form at the trailing edge (this may happen because of a sudden start, as discussed in Section 4.1, as well as any other time-discontinuity in the velocity distribution on the surface of the rotor), then these vortices are immediately shed. At any other time there are no concentrated vortices at the trailing edge: the implication of this assumption is that the value of $\Delta\varphi$ is continuous at the trailing edge, i.e., if P_w is a point on the wake and P_{te} is a point on the trailing edge,

$$\lim_{P_w \to P_{te}} \Delta\varphi(P_w) = \Delta\varphi_{te} \qquad 4.4$$

where $\Delta\varphi_{te}$ is the difference of the values of the potential as the points on upper and lower two sides of the rotor blade approach a point of the trailing edge.

4.4 Trailing Edge Flow

In order to appreciate the Joukowski hypothesis as it relates to the issue of uniqueness of the solution, let us examine in detail the flow at the trailing edge. In particular we want to examine the limiting case of the wake boundary condition, Eq. 2.16, as a wake point approaches the trailing edge. This analysis is an extension to unsteady flows of the work by Mangler and Smith, Ref. 62, but the interpretation of the results is quite different from theirs. Let $\bar{e}_\tau$ be a unit vector tangent to the trailing edge and $\bar{e}_\nu$ be a unit vector in the plane of the wake and normal to $\bar{e}_\tau$(see Figure 4.1). Let v_τ and v_ν be the components of $\bar{v}_w$ in direction $\bar{e}_\tau$ and $\bar{e}_\nu$

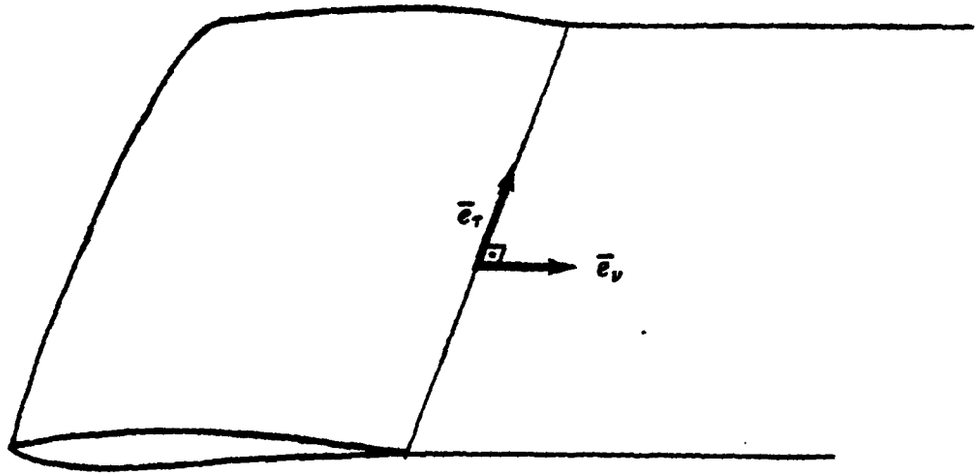

Figure 4.1. Vectors $\bar{e}_\tau$ and $\bar{e}_\nu$

$$\bar{v}_w = \frac{1}{2}(\bar{v}_1 + \bar{v}_2) = v_\tau \bar{e}_\tau + v_\nu \bar{e}_\nu \qquad 4.5$$

The sense of $\bar{e}_\tau$ is arbitrary, but the sense of $\bar{e}_\nu$ is away from the rotor, so that

$$v_\nu \geq 0 \qquad 4.6$$

Also let δ_τ and δ_ν be the components of

$$\Delta\bar{v} = \bar{v}_1 - \bar{v}_2 = \delta_\tau \bar{e}_\tau + \delta_\nu \bar{e}_\nu \qquad 4.7$$

With these definitions, Eq. 2.26 may be written as

$$\Delta\dot{\varphi} + v_\tau \delta_\tau + v_\nu \delta_\nu = 0 \qquad 4.8$$

It may be worth noting that Eq. 4.6 is the limiting case of Eq. 2.26 which may be integrated to yield Eq. 2.29, which describes the fact that $\Delta\varphi$ is convected by the flow. Therefore we believe that Eq. 4.6 is not an additional condition to be imposed but is a relationship that is satisfied since the solution satisfies Eq. 2.29. However such a relationship has interesting properties that help clarify the issue of Joukowski hypothesis.

The case of interest here is that of a rotor with a finite trailing-edge angle. Considering Figure 4.2, there are five cases of interest here. In the first two cases (a and b) the velocity is infinite at the trailing edge: according to Joukowski hypothesis, a concentrated vortex, located at the trailing edge, is immediately shed. Therefore this case occurs only at a discrete number of times and thus the other three cases are the only ones which need further discussion. Consider first the case (c): the velocity on both sides of the rotor must have zero components at the trailing edge (in a frame of reference having the velocity of the trailing edge point 0) along the normal to the rotor, because of the body boundary conditions, Eq. 2.5 (this is obtained automatically with the integral representation given by Eq. 2.25) and must also have zero components (in that same frame of reference) in direction normal to the wake (which is a generalized streak surface). If two components are equal to zero then the whole vector of the cross-flow velocity (velocity of the flow yield in the plane of the figure, i.e., normal to the trailing edge) is equal to zero. Hence

$$v_{1\nu} = 0 \qquad 4.9$$

whereas $v_{2\nu} > 0$. Note that according to Eq. 4.4,

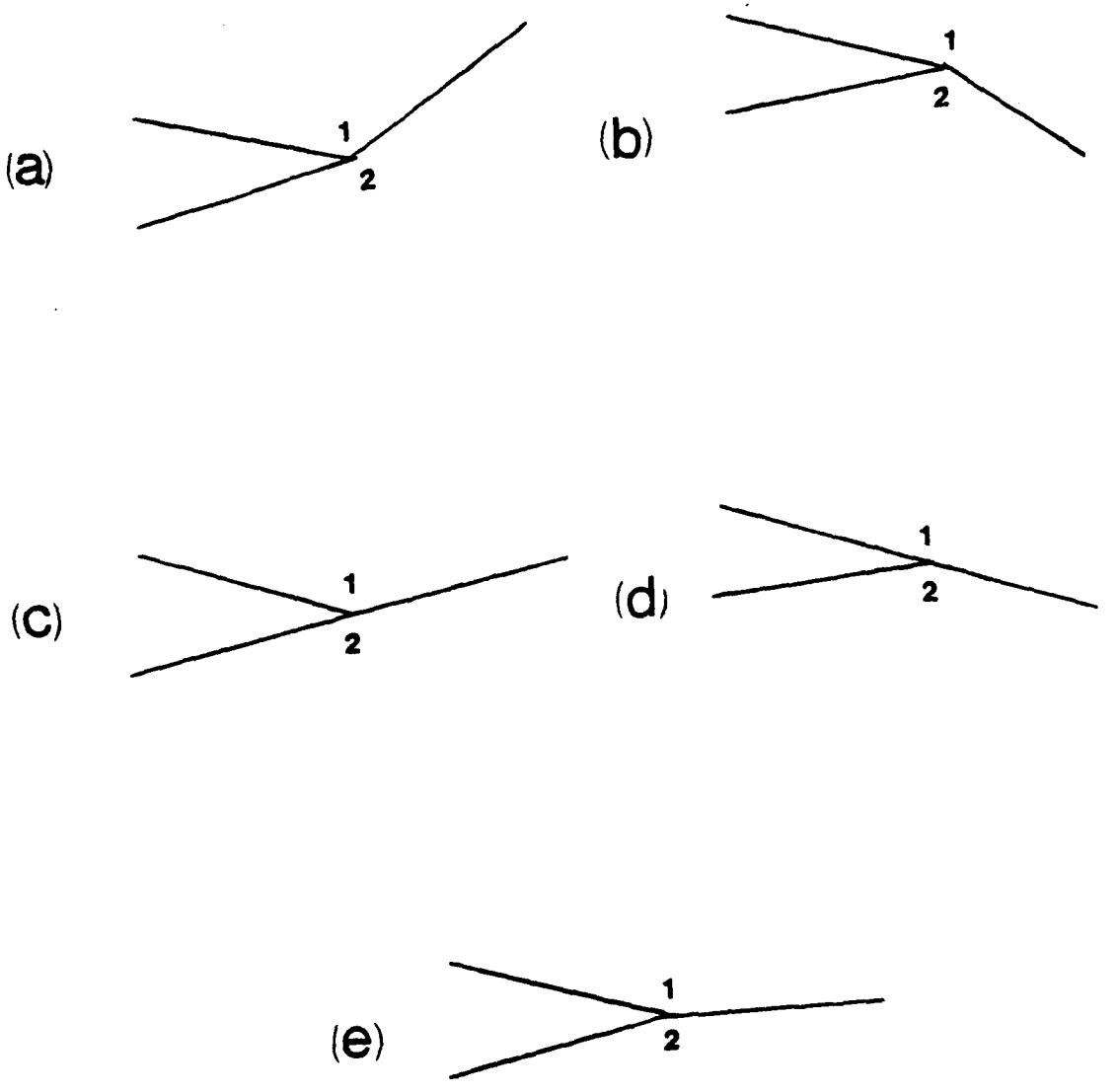

Figure 4.2. Wake Geometry at Trailing Edge

$$v_\nu = \frac{1}{2}(v_{1\nu} + v_{2\nu}) = \frac{1}{2} v_{2\nu} > 0 \qquad 4.10$$

whereas

$$\delta_\nu = v_{1\nu} - v_{2\nu} = -v_{1\nu} < 0 \qquad 4.11$$

Therefore case (c) can occur if and only if

$$\Delta\dot{\varphi} + v_\tau \delta_\tau > 0 \qquad 4.12$$

Similarly, case (d) implies $v_{1\nu} > 0$, $v_{2\nu} = 0$, and hence

$$v_\nu = \frac{1}{2} v_{1\nu} > 0$$

$$\delta_\nu = v_{1\nu} > 0 \qquad 4.13$$

and therefore such case is possible if and only if

$$\Delta\dot{\varphi} + v_\tau \delta_\tau < 0 \qquad 4.14$$

Finally consider case (e): in this case v_1 and v_2 are both zero. Hence both v_ν and δ_ν are equal to zero and Eq. 4.6 reduces to

$$\Delta\dot{\varphi} + v_\tau \delta_\tau = 0 \qquad 4.15$$

The flow moves parallel to the trailing edge, and the vorticity is perpendicular to the trailing edge. [Note that for two-dimensional flows $v_\tau = \delta_\tau = 0$ which implies $\Delta\dot{\varphi} = 0$: hence for two-dimensional flows, case (e) occurs if and only if $\Delta\dot{\varphi} = 0$ (e.g., steady state). Case (c) occurs if $\Delta\dot{\varphi} > 0$ and case (d) occurs if $\Delta\dot{\varphi} < 0$.]

4.5 Physical Interpretation

Let us go back to the case of impulsive start. A vortex is generated at the trailing edge and immediately shed. Then the wake is continuously shed from the trailing edge and convected with velocity $\bar{v}_w = (\bar{v}_1 + \bar{v}_2)/2$. The wake is typically tangent to one of the two sides of the rotor. This causes a cross-flow stagnation point (high pressure) on one side and a low pressure point on the other side.

It may be worth emphasizing that in deriving the above formulation we have used only the principles of conservation of mass and momentum, plus the assumptions of inviscid, incompressible and initially irrotational flows and the Joukowski hypothesis. The correct 'amount and distribution' of vorticity

(as doublet layers) is predicted by these basic assumptions. It may be said as the viscosity goes to zero the solution to the Navier Stokes equations is that of Euler equation with the addition of Joukowski hypothesis. (As mentioned above, Kutta condition of finite vorticity distribution at the trailing edge is needed to insure the uniqueness of the solution only for two-dimensional flows: the nonuniqueness arises only for multiply-connected regions, as the one of a two-dimensional airfoil.)

SECTION 5

COMPUTATIONAL ALGORITHM

The computational algorithm used to obtain an approximate solution of Eq. 3.25 is presented in this section. The surfaces of the rotor and of its wake are divided into small surface elements, σ_j. The potential and the normalwash are assumed to be constant with each element. This yields a set of equations relating the values of the potential φ_j at the centroids of the elements, σ_j, to the values of the normalwash at the centroids of the elements, σ_j and to the values of $\Delta\varphi_n$ at the centroids of the wake elements, σ'_n. The wake geometry is evaluated step-by-step as follows: the velocity of the fluid at the corners of each element is evaluated and from this the location of the element at the new time step is obtained.

5.1. Theoretical Algorithm

The results of the preceding sections may be summarized as follows: assume that at time $t = t_*$ the wake geometry and the potential-discontinuity distributions are known, then the value of the potential is obtained by solving Eq. 3.25

$$E_*\varphi_* = \iint_{\sigma_b} \left[\psi \frac{-1}{4\pi r} - \varphi \frac{\partial}{\partial n}\left(\frac{-1}{4\pi r}\right)\right] d\sigma$$

$$- \iint_{\sigma'_w} \Delta\varphi \frac{\partial}{\partial n}\left(\frac{-1}{4\pi r}\right) d\sigma \qquad 5.1$$

with

$$\psi = \frac{\partial\varphi}{\partial n} \qquad 5.2$$

and E_* given by Eq. 3.29. Once φ_* is known, Eq. 5.1 may be used to calculate the velocity at any point in the fields as $\bar{v}_* = \text{grad}_* \varphi_*$ (where grad_* indicates differentiation with respect to P_*). Noting that

$$\text{grad}_*\left(\frac{1}{r}\right) = \frac{\bar{r}}{r^3}, \qquad 5.3$$

where

$$\bar{r} = P - P_* \qquad 5.4$$

one obtains

$$\bar{v}_* = -\iint_{\sigma_b} [\psi \frac{\bar{r}}{4\pi r^3} - \varphi \frac{\partial}{\partial n}(\frac{\bar{r}}{4\pi r^3})] d\sigma$$

$$+ \iint_{\sigma_w} \Delta\varphi \frac{\partial}{\partial n}(\frac{\bar{r}}{4\pi r^3}) \, d\sigma \qquad 5.5$$

This equation may also be used to calculate the velocity of the points of the wake if the contribution of the wake integral in an infinitesimal neighborhood of the wake point is excluded from the calculation (such a contribution is responsible for the velocity discontinuity across the wake and its exclusion automatically yields the semi-sum between the two values on the two sides of the wakes).

Once the velocity $\bar{v}_w$ (of a wake point P_w) is evaluated, the new position of the wake-point P_w may be evaluated as

$$P_w(t_* + dt) = P_w(t_*) + \bar{v}_w(P_w, t_*) \, dt \qquad 5.6$$

Note that a new infinitesimal strip of wake surface has been added (between the trailing edge and the locus of the points which were on the trailing edge at time t_*). Note also that, according to Eq. 2.34, $\Delta\varphi(P_w)$ does not change in time (i.e., $\Delta\varphi$ is 'convected' with the wake point P_w) and therefore $\Delta\varphi$ does not require any additional calculation.

Now the wake geometry and the potential discontinuity are known at time $t_* + dt$ and the process may be repeated.

5.2 Space and Time Discretization: First Time Step

For the sake of clarity, consider first the case of impulsive start, i.e., assume that for $t < 0$ the rotor was at rest in a fluid also at rest. Hence at time $t = 0$ there is no wake surface (the potential is continuous throughout the fluid region). Equation 5.1 (without wake integral) may be discretized by dividing the surface of the rotor into N_b surface panels σ_j and assuming that ψ and φ are constant within each panel.

$$2E(P_*,0) \, \varphi(P_*,0) = \sum_{n=1}^{N_b} B_j(P_*,0) \, \psi_j$$

$$+ \sum_{n=1}^{N_b} C_j(P_*,0) \, \varphi_j \qquad 5.7$$

where ψ_j and φ_j are the values of ψ and φ on the j-th panel at time $t = 0$, whereas

$$B_j(P_e,t) = \iint_{\sigma_j} \frac{-1}{2\pi r}\, d\sigma$$

$$C_j(P_e,t) = \iint_{\sigma_j} \frac{\partial}{\partial n}\left(\frac{1}{2\pi r}\right) d\sigma \qquad 5.8$$

By imposing the condition that Eq. 5.7 be satisfied at the centroids P_k of the elements σ_k, one obtains (note that according to Eq. 2.29 $E(P_k) = 1/2$, since P_k is a regular point of σ_b)

$$\varphi_k = \sum_{j=1}^{N_b} B_{kj}(0)\ \psi_j + \sum_{j=1}^{N_b} C_{kj}(0)\ \varphi_j \quad (k = 1,\ldots,N_b) \qquad 5.9$$

where

$$B_{kj}(t) = B_j(P_k,t)$$

$$C_{kj}(t) = C_j(P_k,t) \qquad 5.10$$

It should be emphasized that if the rotor moves with rigid body motion, the coefficients B_{kj} and C_{kj} are time independent.* Equation 5.9 is a system of N_b algebraic equations with N_b unknowns φ_j (the values of ψ_j are known from the boundary conditions).

5.3. Wake Generation During First Time Step

As mentioned above, the frame of reference is assumed to be connected with the air. This is particularly convenient to discuss the wake generation. (The actual formulation used in the computer program is for a frame of reference connected with the blade: the two are related through a rigid body rotation. This point is discussed later in this section where it is indicated that unstable results may be obtained if this issue is not handled carefully.)

Between time $t = 0$ and time $t = \Delta t$, the fluid points which were at the trailing edge at time $t = 0$ move into a new position, which (in our frame of reference, i.e., a frame of reference connected with the undisturbed air) is given by (see Eq. 5.6)

$$P_w(\Delta t) = P_{te}(0) + \int_0^{\Delta t} \bar{v}(P_w(t),t)\, dt \qquad 5.11$$

---

*An analytic expression for the coefficients is given in Ref. 25.

From a discrete (i.e., finite element) point of view, the new geometry is defined by the location of the wake point emanating from the trailing edge nodes as shown in Figure 5.1. The location of these points may be is obtained by approximating the above equation as

$$P_w(\Delta t) = P_{te}(0) + \bar{v}(P_w(0),0)\ \Delta t \qquad 5.12$$

However, the calculation of $\bar{v}(P_w(0),0)$ cannot be based on the use of Eq. 5.5. The reason being that because of the time discretization, the motion history is actually replaced by a sequence of sudden starts (see Section 4.1). This implies that in the time-discretized formulation a discrete vortex is formed at each time step and therefore the velocity as given by Eq. 5.5 goes to infinity at the trailing edge. In order to circumvent this problem, we made use of the results of Section 4.4 and impose that the relative velocity is tangent either to the upper or the lower side of the rotor blade depending upon the sign of the expression in Eqs. 4.12 and 4.14. Then we used standard finite-difference expressions to determine the components of the perturbation velocity along the trailing edge (central-difference) and over the appropriate side of the blade (e.g., the two-point backward difference approximation of $\partial\varphi_u/\partial x$ if the wake is tangent to the upper side of the blade).

It should be noted that as mentioned above, the new locations of the wake points are within a frame of reference connected with the undisturbed air. Therefore while the wake points move, the blade also moves into its new position. Hence a row of wake elements, σ_n, has been generated (see Figure 5.1): these elements have two corners on the trailing-edge points A and B whereas the other two corners coincide with the location at time $t = \Delta t$ of the fluid points that coincided with the blade points A and B at time $t = 0$. Hence, at time $t = \Delta t$, we have a row of wake elements: the value of $\Delta\varphi_n$ assigned to the elements σ_n is the difference of the values (evaluated at time $t = 0$) of the potential φ at the centers of the upper and lower blade elements that are in contact with σ_n.

5.4. Generic Time Step

Now, at time $t = \Delta t$, the wake geometry and the values of $\Delta\varphi$ on the wake are known. The values of ψ_j are also known. Hence, Eq. 5.1, discretized as (see Eq. 5.7)

$$\sum_{j=1}^{N_b} (\delta_{kj} - C_{kj})\ \varphi_j = \sum_{j=1}^{N_b} B_{kj}\psi_j + \sum_{n=1}^{N_w} F_{kn}\Delta\varphi_n \qquad 5.13$$

may be used to evaluate φ_j at time Δt. In Eq. 5.13, B_{kj} and C_{kj}

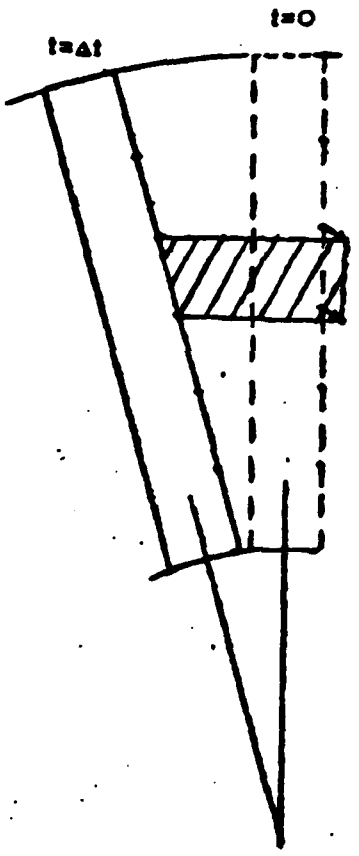

Figure 5.1. Wake Generation Between Times $t_0 = 0$ and $t_1 = \Delta t$

are given by Eq. 5.10 whereas

$$F_{kn}(t) = \iint_{\sigma_n'} \frac{\partial}{\partial n}\left(\frac{1}{2\pi r}\right) d\sigma \Big|_{P_* = P_k} \qquad 5.14$$

is a constant-doublet integral over the wake element σ_n'.

Once the values of φ_j are known, the same procedure described in Section 5.3 may be repeated to calculate the geometry of new wake elements (and corresponding values for $\Delta\varphi_n$) generated between Δt and $2\Delta t$. In addition, the new location of the old row of elements (those generated between 0 and Δt) is obtained as follows: evaluate the velocity at the wake points which are not on the trailing edge using Eq. 5.5 which is discretized as

$$\bar{v}_q = \sum_{j=1}^{N_b} \bar{b}_{qj} \psi_j + \sum_{j=1}^{N_b} \bar{c}_{qj} \varphi_j + \sum_{n=1}^{N_w} \bar{f}_{qn} \Delta\varphi_n \qquad 5.15$$

where q spans over all the nodes of the wake surface which are not on the trailing edge, whereas

$$\bar{b}_{qj} = \frac{1}{4\pi} \iint_{\sigma_j} \frac{\bar{r}}{r^3} \, d\sigma \Big|_{P_* = P_q}$$

$$\bar{c}_{qj} = \frac{-1}{4\pi} \iint_{\sigma_j} \frac{\partial}{\partial n}\left(\frac{\bar{r}}{r^3}\right) d\sigma \Big|_{P_* = P_q}$$

$$\bar{f}_{qj} = \frac{-1}{4\pi} \iint_{\sigma_j} \frac{\partial}{\partial n}\left(\frac{\bar{r}}{r^3}\right) d\sigma \Big|_{P_* = P_q} \qquad 5.16$$

Then calculate the new locations as

$$P_q(t + \Delta t) = P_q(t) + \bar{v}_q(t)\Delta t \qquad 5.17$$

Now all the nodes of the wake surface are known. Note that if the node numbering of the wake elements is not changed from time Δt to time $2\Delta t$ then, according to Eq. 2.34

$$\Delta\varphi_n = \text{constant in time} \qquad 5.18$$

Hence, the new wake geometry and the corresponding values for $\Delta\varphi_n$ are known at time $2\Delta t$ (as mentioned above, the geometry and the values for $\Delta\varphi$ for the row of elements generated between Δt and $2\Delta t$ is determined using the procedure presented in Section

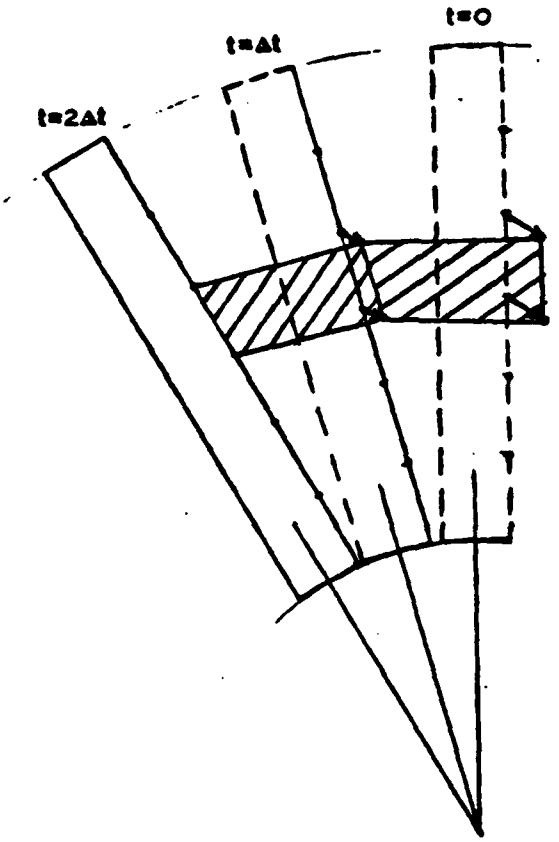

Figure 5.2. Wake Generation Between Times $t_1 = \Delta t$ and $t_2 = 2\Delta t$

5.3) and the process may be repeated: the same procedure used in the time step between Δt and $2\Delta t$ may be used for the time step between $t_n = n\Delta t$ and $t_{n+1} = t_n + \Delta t$.

5.5. Numerical Stability

Issues related to numerical instability are discussed in this section. A large portion of this research effort was completely devoted to this issue: after the formulation had been completed and incorporated into a computer program, the results consistently indicated the presence of numerical instability. It was not clear at that time whether the instability correctly represented a physical instability (experimental results indicate that the wake of a helicopter rotor in hover oscillates and eventually the tip vortex breaks down), or was caused by the numerical algorithm (or even more trivial, a bug in the program). In order to examine the possibility of a bug in the program, a second code was written using a different frame of reference, i.e., a frame of reference connected with the undisturbed air (in the first code the frame of reference is connected with the rotor). In spite of the equivalence of the two formulations, the two codes gave different results. The source for the difference was traced to the fact that in the first code the new location of the wake point was evaluated as

$$\bar{P}_w(t + \Delta t) = \bar{P}_w(t) + (\bar{V}_o + \bar{v}_w)\Delta t \qquad 5.19$$

where $\bar{v}_w$ is the perturbation velocity whereas $\bar{V}_o$ is the velocity of the undisturbed fluid

$$\bar{V}_o = \bar{\Omega} \times \bar{r}$$

Unfortunately,

$$\Delta \bar{P}_w = \bar{\Omega} \times \bar{r}\, \Delta t \qquad 5.20$$

does not correspond to the correct rigid-body displacement (see Figure 5.3). This error (which goes to zero as Δt goes to zero) seems to have been the origin of the instability: the results obtained with the second code have been consistently stable. For the hover case, it is actually convenient to use a frame of reference connected with the blade. The original code was therefore modified as follows: the displacement caused by the perturbation velocity is calculated then the whole wake geometry is rigidly rotated (around a vertical axis, i.e., $\bar{\Omega} = \Omega\bar{k}$) as

$$\begin{aligned} x &= x_o \cos \Delta\theta - y_o \sin \Delta\theta \\ y &= x_o \sin \Delta\theta + y_o \cos \Delta\theta \\ z &= z_o \end{aligned} \qquad 5.21$$

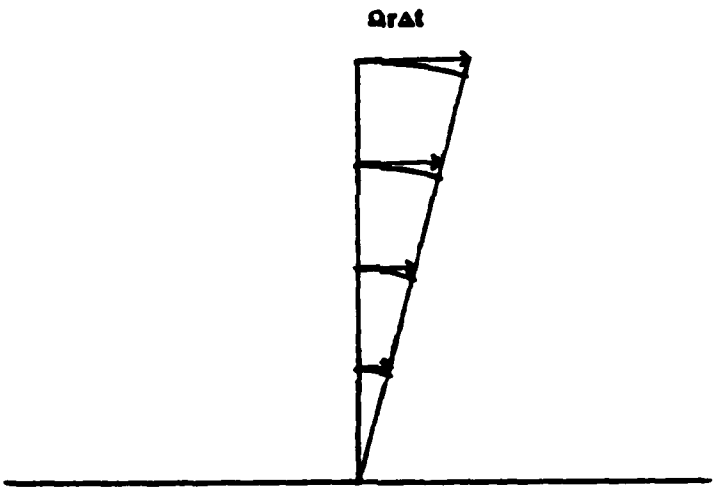

Figure 5.3. Analysis of Rigid-Body Motion

where $\Delta\theta = \Omega\Delta t$ whereas, x_0, y_0, z_0 are the coordinates before rotation.

5.6. Finite-Core Vortex

Before the cause of the instability had been traced to the issue discussed in Section 5.5, the concept of finite-core vortex was introduced in an attempt to eliminate the instability. (This concept is often referred to as artificial viscosity: we believe that this name is misleading and prefer the name finite-core vortex.)

The essence of the idea is that concentrated vortices are introduced in the process of spatial discretization of the formulation. The integral formulation describes the wake as a doublet layer which is fully equivalent to a vortex layer. When the wake integral is divided into quadrilateral panels and $\Delta\varphi$ is assumed to be constant within the element, we are in effect replacing a continuous distribution of vorticity with concentrated vortices located at the edges of the panels. Such an approximation therefore introduces infinite induced velocities in the vicinity of the panels edges. If the wake spirals come too close to each other, this may be a cause for instability.

In order to avoid this problem, the velocity distribution induced by constant-doublet panels (i.e., concentrated vortices) is replaced with those induced by a finite-core vortex. Note that we considered this only as a convenient expedient to eliminate instabilities, not an effort to improve the model by making it closer to physical reality (in order to get closer to physical reality we would rather introduce a higher-order finite-element representation for the distribution of the potential discontinuity in place of the constant-doublet approximation).

In order to accomplish that, the following scheme was used in our computer code. The velocity induced by the edge P_1P_2 of a constant doublet panel is

$$\bar{v} = \frac{1}{2\pi} \frac{\bar{q}_1 \times \bar{q}_2}{|\bar{q}_1 \times \bar{q}_2|^2} \left(\frac{\bar{q}_1 \cdot \bar{q}_1 - \bar{q}_1 \cdot \bar{q}_2}{|\bar{q}_1|} - \frac{\bar{q}_2 \cdot \bar{q}_2 - \bar{q}_1 \cdot \bar{q}_2}{|\bar{q}_2|} \right) \qquad 5.22$$

where $\bar{q}_i = P_i - P_*$ (see Figure 5.4).

$$\bar{q}_1 = -x\,\bar{i} + z_1\bar{k}$$

$$\bar{q}_2 = -x\,\bar{i} + z_2\bar{k}$$

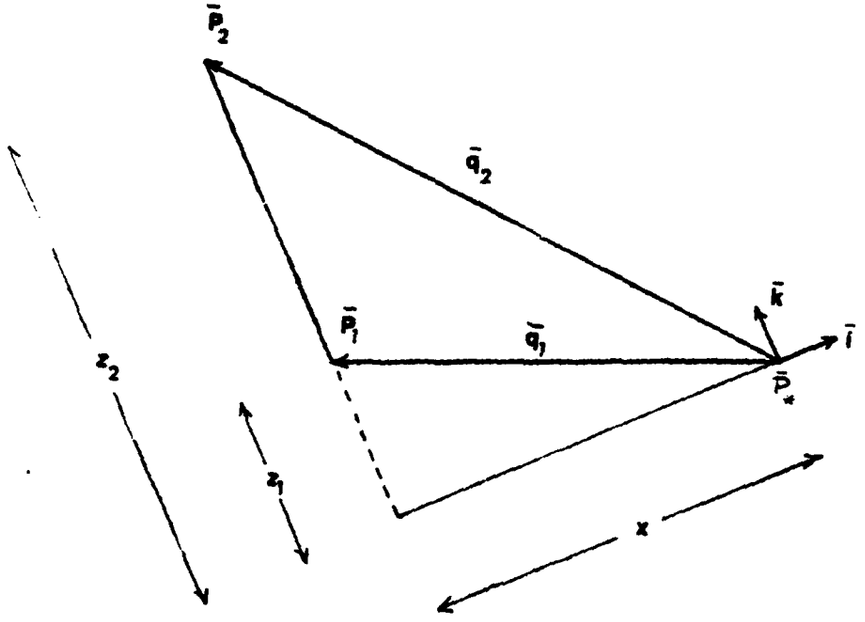

Figure 5.4. Vortex Geometry

This is exactly equal to the expression obtained from the Biot and Savart law for the velocity 'induced' by a vortex line. Introducing a frame of reference such that the vortex-line coincides with the z-axis and that the x-axis goes through P_e, Eq. 5.22 yields (*see Figure 5.2*)

$$\bar{v}_v = \frac{1}{2\pi x} \left[z_1 (x^2 + z_1^2)^{-1/2} + z_2 (x^2 + z_2^2)^{-1/2} \right] \bar{j} \qquad 5.23$$

As P_e approaches the vortex line (i.e., as x tends to zero), this expression yields

$$\bar{v}_v = \frac{1}{2\pi x} \bar{j} \qquad 5.24$$

(which is the velocity induced by an infinite vortex) if P_e approaches a point between P_1 and P_2 (i.e., $z_1 < 0$ and $z_2 > 0$) and

$$\bar{v} = 0 \qquad 5.25$$

if P_e approaches a point of the line P_1P_2 outside the segment P_1P_2 (i.e., if $z_1 < z_2 < 0$ or $z_2 > z_1 > 0$). An infinite vortex with a finite core of radius ε yields a velocity

$$\bar{v}_v = \alpha \frac{1}{2\pi x} \bar{j} \qquad 5.26$$

where

$$\alpha = 1 \qquad x > \varepsilon$$

$$= x^2/\varepsilon^2 \qquad x < \varepsilon \qquad 5.27$$

Hence, going back to vector notations, Equation 5.26 may be rewritten as

$$\bar{v}_v = \frac{1}{2\pi} \frac{\bar{q}_1 x \bar{q}_2}{|\bar{q}_1 x \bar{q}_2|^2} \left(\frac{\bar{q}_1 \cdot \bar{q}_1 - \bar{q}_1 \cdot \bar{q}_2}{|\bar{q}_1|} - \frac{\bar{q}_2 \cdot \bar{q}_2 - \bar{q}_1 \cdot \bar{q}_2}{|\bar{q}_2|} \right) \qquad 5.28$$

if $x > \varepsilon$ and

$$\bar{v}_v = \frac{1}{2\pi} \frac{1}{\varepsilon^2} \frac{\bar{q}_1 x \bar{q}_2}{|\bar{q}_1 - \bar{q}_2|^2} \left(\frac{\bar{q}_1 \cdot \bar{q}_1 - \bar{q}_1 \cdot \bar{q}_2}{|\bar{q}_1|} - \frac{\bar{q}_2 \cdot \bar{q}_2 - \bar{q}_1 \cdot \bar{q}_2}{|\bar{q}_2|} \right) \qquad 5.29$$

if $x < \varepsilon$, where

$$x = \frac{|\bar{q}_1 \times \bar{q}_2|}{|\bar{q}_1 - \bar{q}_2|} \qquad 5.30$$

5.7. Comments: Wake Truncation

For the sake of clarity, the formulation has been presented for the case of start from rest, that is, for time $t < 0$, the rotor has been assumed to be at rest and surrounded by fluid also at rest.

It should be apparent at this point that such an assumption is not essential to the formulation. The method of solution requires only that the geometry wake surface and the potential-discontinuity distribution over the surface of the wake to be known at time t_n. Then, the potential distribution may be evaluated using Eq. 5.13. Once the potential distribution is known, Eq. 5.15 may be used to calculate the velocity of the nodes of the wake and hence their new location (the row of the new wake elements generated between t_n and $t_n + \Delta t$ is obtained with the procedure given in Section 5.3).

As mentioned above, the frame of reference connected with the undisturbed air is more convenient from a conceptual point of view even though the calculations are more conveniently presented in a frame of reference connected with the rotor. Also, the issue of artificial viscosity discussed in Section 5.6 does not appear to be essential to the formulation: small values of ε give the same results as $\varepsilon=0$.

The last major issue to be discussed is that of the wake truncation: as the number of time steps grows, the length of the wake also grows. This implies that the computer time per time step also grows. In order to keep computer time within reasonable bounds, it is necessary to obtain a simplified model for the remote element of the wake. While sophisticated intermediate-and far-wake models have been introduced for the hover case (Refs. 40 and 41), these models require ad-hoc assumptions based on empirical data. Since the objective of the present work is to develop a method which may be used to study problems for which such data does not exist (such as maneuvering), it would have been inappropriate to introduce any of the above far-wake models or, for that matter, any model based on experimental data. For this reason in the results presented here, the wake is simply truncated after a certain number of spirals. The implication of this procedure is that the last few spirals are to be considered as modelling of the far wake effects. As indicated by the results presented in Section 6, this is an expensive approach to the problem (the case presented in Section 6 requires approximately eight hours of CPU time on an IBM 370/168). There is need to develop a less expensive approach to the far wake modelling. However, such a model should be based on first principle rather than empirical data, if the methodology proposed here is to be used independently of the experimental analysis.

SECTION 6

NUMERICAL RESULTS

In order to validate the theory presented above, the numerical algorithm was implemented in a computer program. The results obtained with this program and the comparison with existing data are presented in this section.

6.1. Choice of the Test Case

It is a generally accepted opinion in helicopter-rotor aerodynamics that the wake roll-up problem is harder to solve for hover than for forward flight: this is because the wake spirals are closer to each other in the hover case. Also the hover case seems to be the only one for which satisfactory results exist. Therefore, in order to test our formulation we have started by studying a hover case. In order to validate the time-domain algorithm the hover case was studied through a time-accurate transient response analysis. These steady state results are the only ones presented here. We believe that the validation of the formulation will be satisfactory only if more extensive results, (including forward flight results now under consideration) will confirm the results presented here.

In particular, we chose the case studied by Rao and Schatzle (Ref. 7) for several reasons, the most important of which is that their formulation (lifting surface with prescribed wake) is based on first principles (no ad-hoc assumption is used except for the wake geometry and zero-thickness blade) and yields results which are in excellent agreement with the experimental ones of Bartsch (Ref. 37). Also important in Ref.7 is the comparison between classical- and Landgrebe-wake analysis: the latter shows a marked spike near the tip in the section lift distribution, in full agreement with experimental results (the spike is absent in the classical wake results). These results not only demonstrate the importance of the wake geometry for the prediction of the section lift distribution, but also are important in the interpretation of our convergence scheme.

6.2. Description of Test Case

As mentioned above, all the results presented in this report for a case considered by Rao and Schatzle: an isolated rotor, with tip radius $R_T = 17.5'$, cut-out radius $Y_{CO} = 2.33'$, chord $c = 1.083'$, collective pitch angle $\theta_c = 10.61^\circ$ and twist angle $\theta_1 = -5^\circ$. The angular speed is $\Omega = 355$ r.p.m.

For all the results, the initial wake geometry is a classical wake

$$x = x_0 \cos\theta - y_0 \sin\theta$$

$$y = y_0 \sin\theta + x_0 \sin\theta$$

$$z = z_0 + kR\theta$$

where $k = \sqrt{C_T/2}$ and $C_T = 0.00186$ (this is the value obtained by Rao and Schatzle).

All the results were obtained using three elements in the chord directions and seven in the span directions for a total of twenty-one elements on each side of the blade. A convergence analysis presented in Ref. 32 indicates that this is sufficient to obtain relatively converged results. For the classical wake analysis the time step is $\Delta t = T/12$ where T is the period: this yields twelve elements in the 'circumferential' direction per each wake spiral (there are seven elements in the radial directions because that is the number of elements on the blade in the spanwise direction).

These data are summarized in Table A.

6.3 Numerical Results

In order to illustrate the type of problems encountered in the effort presented here, consider Figures 6.1.a to 6.1.p which depicts the vertical displacement, z, as a function of the azimuth angle θ_x (for different time steps, more precisely for $t_n/\Delta t = 15$ and 21 through 35) for the last vortex line, i.e., the vortex-line emanating from the tip point of the trailing edge (as clarified later it would be misleading to refer to this vortex as the tip vortex).

It may be noted that at time-step 15 the vortex line appears to have the expected behavior. However at time step 20, the vortex line shows a hump which becomes more marked as in the following time steps but it seems to be pushed downward in time. The phenomenon is more clearly illustrated in Figure 6.2.a to 6.2.d which depicts the vertical displacement, z, as a function of the radial position (for different time steps, $t_n/\Delta t = 15$, 22, 23, 25) also for the last vortex line. It is apparent that the last spirals tend to move outward. This is caused by the fact that the wake is truncated (the 'following' spiral would have a 'restraining' effect on the last spiral: in its absence the last spiral tends to move outward, this point is clearer after discussion of Figure 6.5).

Table A

Single Rotor Blade

Geometry and Flight Conditions of Rotor:

Number of Spirals 5 or 7 as indicated in captions

Number of Elements on Blade (3 x 7)(one side)

Number of Elements per Spiral (12)

R = 17.5 ft. (span)

c = 1.083 ft. (chord)

Y_{co} = 2.33 ft. (root cut-out)

θ_r = 10.61° (collective pitch angle)

θ_1 = -5° (twist angle)

C_t = 0.00186 (thrust coefficient)

Ω = 355 r.p.m.

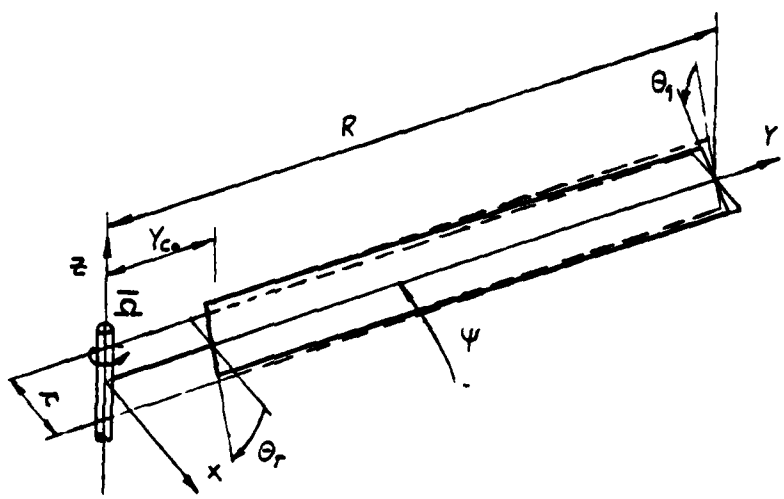

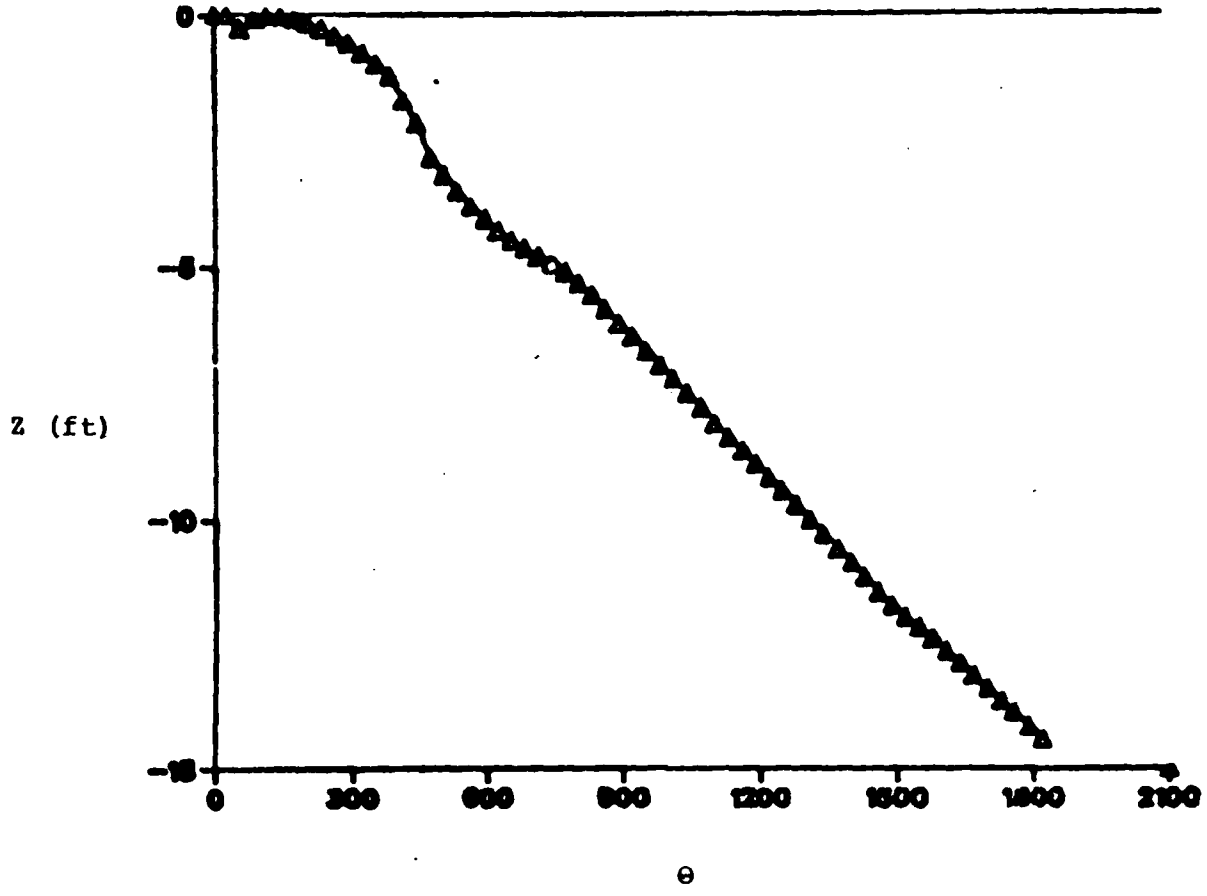

Figure 6.1.a. Vertical displacement, Z, as a function of the azimuth angle, Θ, for the vortex-line emanating from the tip point of the trailing edge at timestep #15(for case defined in Table A).

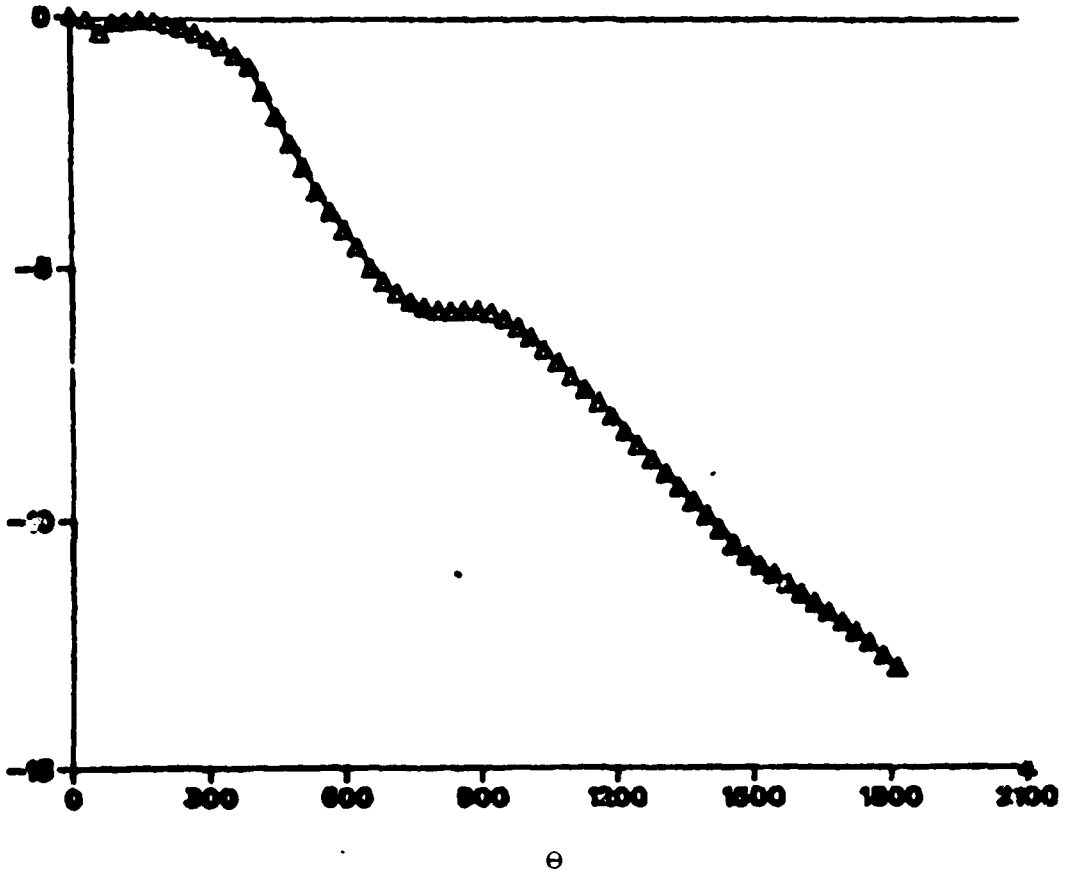

Figure 6.1.b. Vertical displacement, Z, as a function of the azimuth angle, Θ, for the vortex-line emanating from the tip point of the trailing edge at timestep #21(for case defined in Table A).

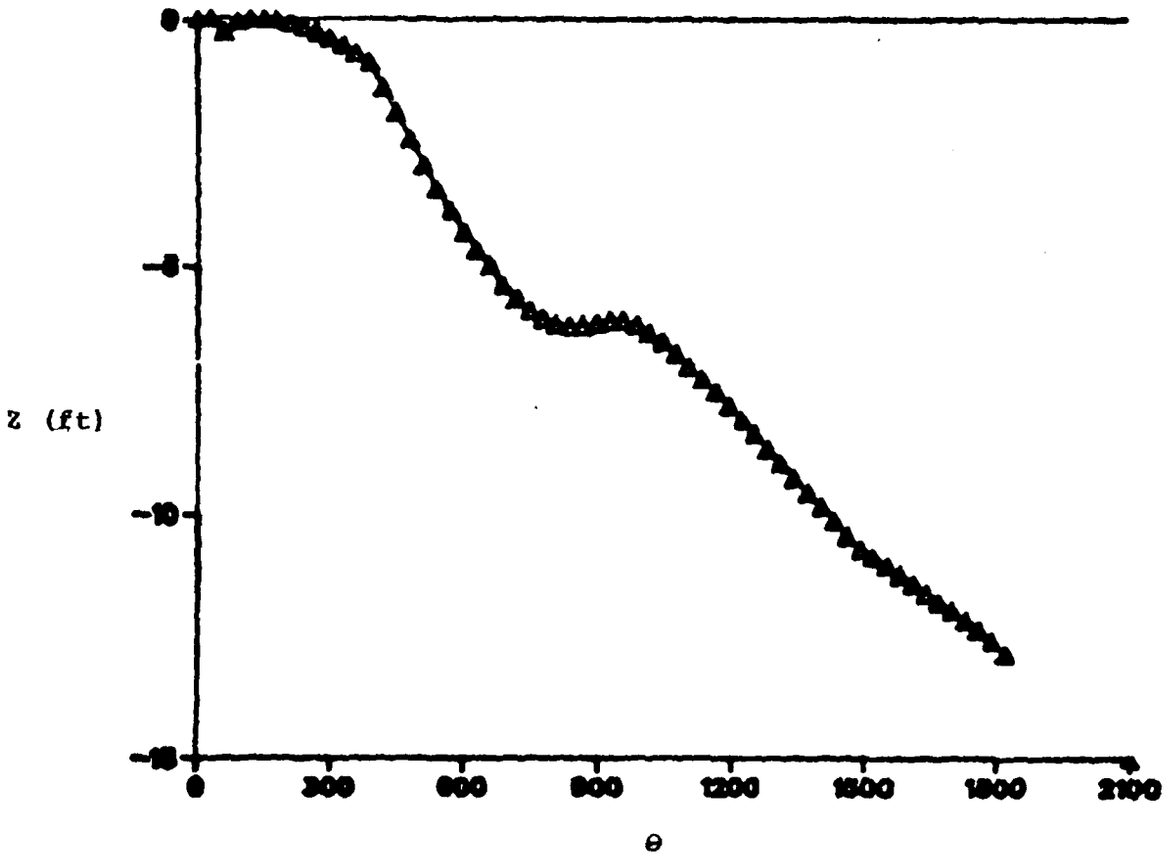

Figure 6.1.e. Vertical displacement, Z, as a function of the azimuth angle, θ, for the vorter-line emanating from the tip point of the trailing edge at timestep #22(for case defined in Table A).

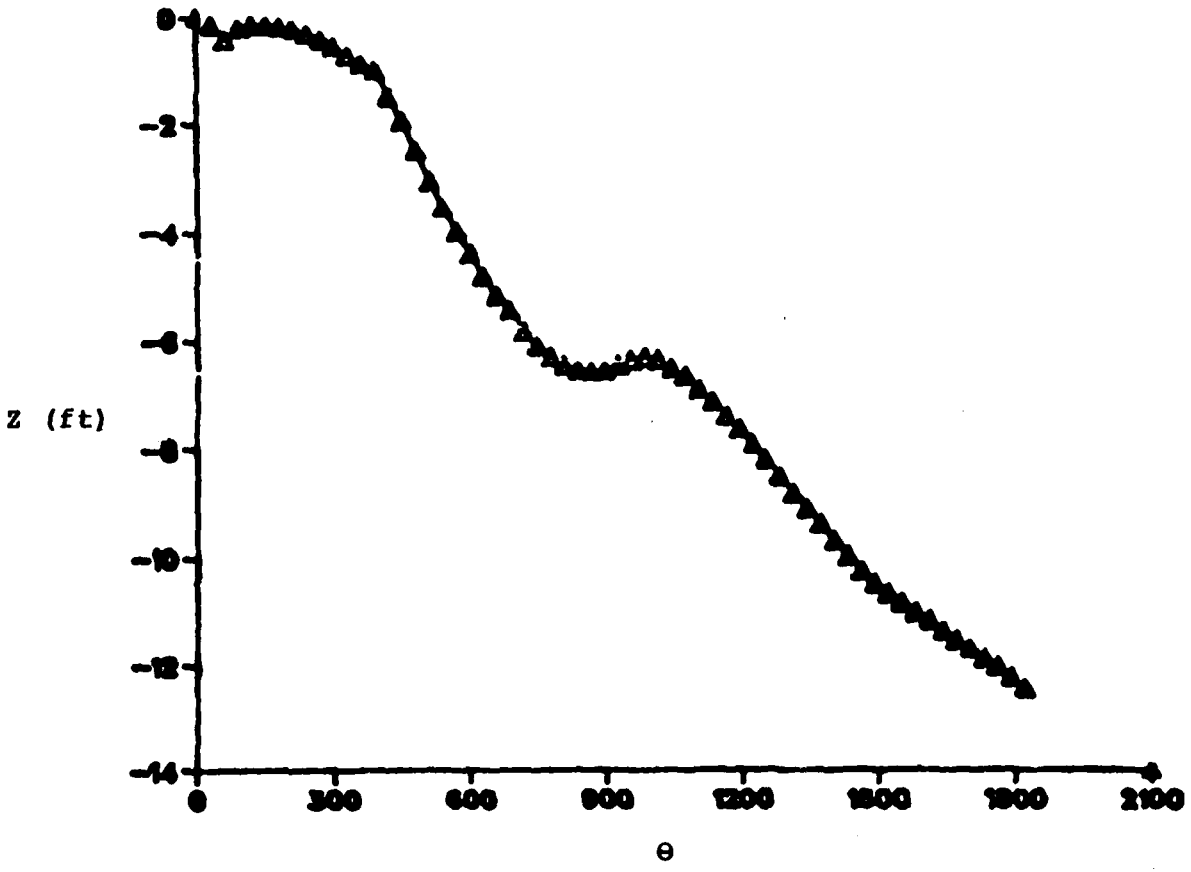

Figure 6.1.d. Vertical displacement, Z, as a function of the azimuth angle, θ, for the vorter-line emanating from the tip point of the trailing edge at timestep #23(for case defined in Table A).

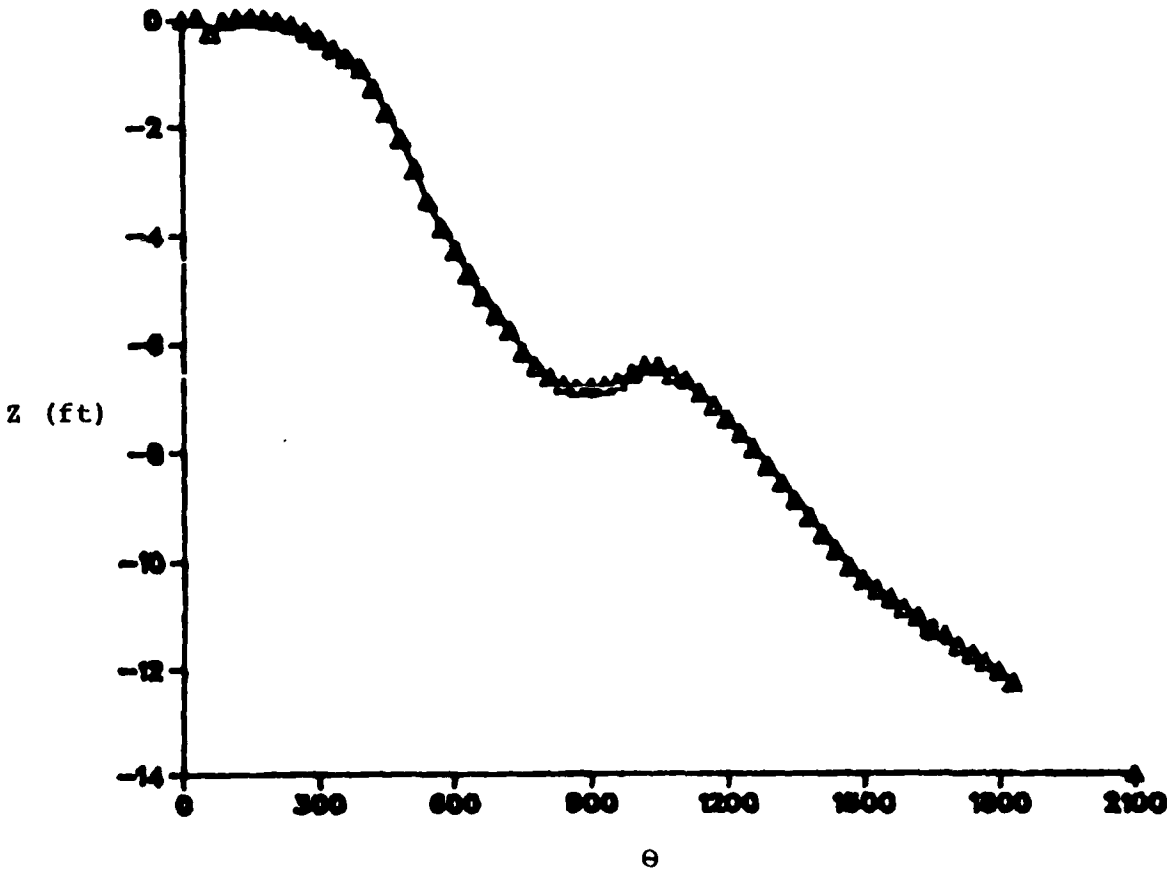

Figure 6.1.e. Vertical displacement, Z, as a function of the azimuth angle, Θ, for the vortex-line emanating from the tip point of the trailing edge at timestep #24(for case defined in Table A).

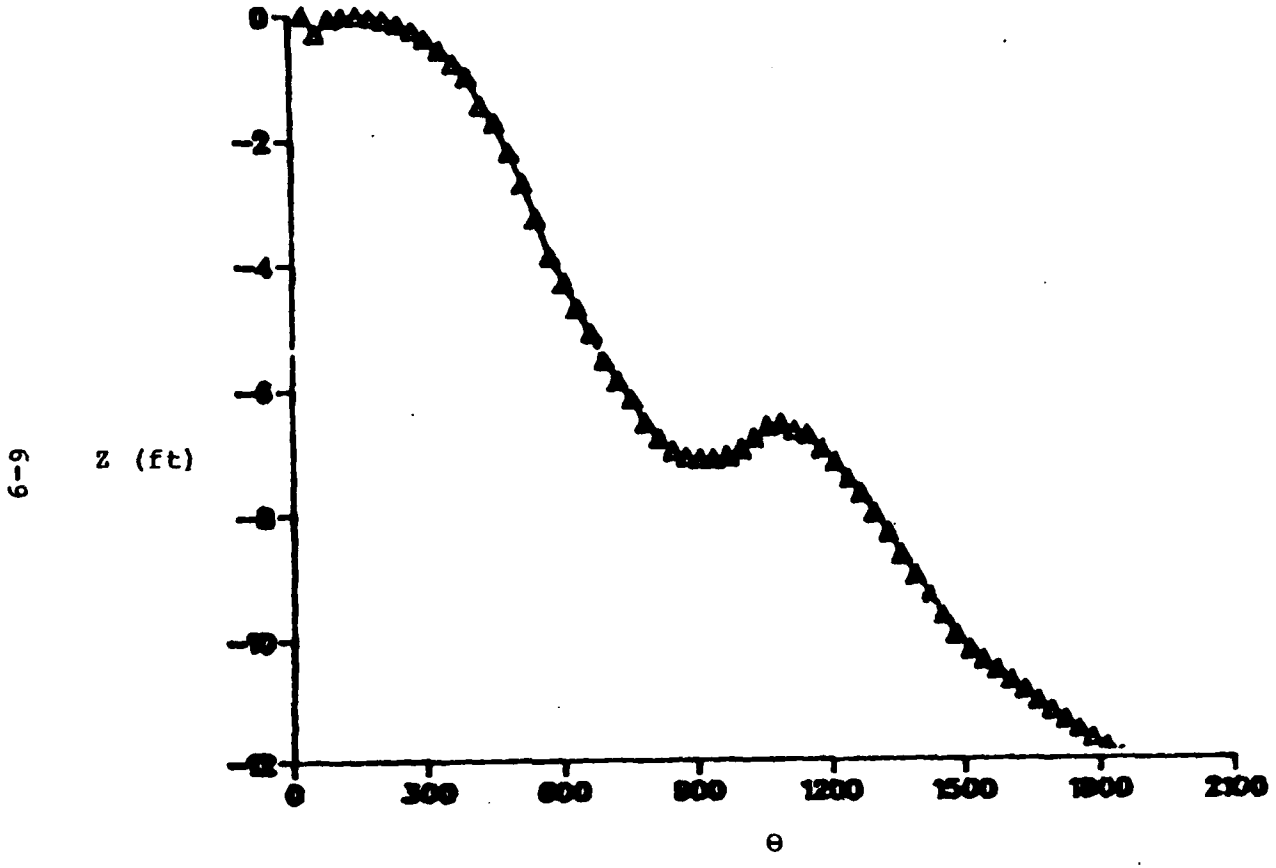

Figure 6.1.f. Vertical displacement, Z, as a function of the azimuth angle, Θ, for the vortex-line emanating from the tip point of the trailing edge at timestep #25(for case defined in Table A).

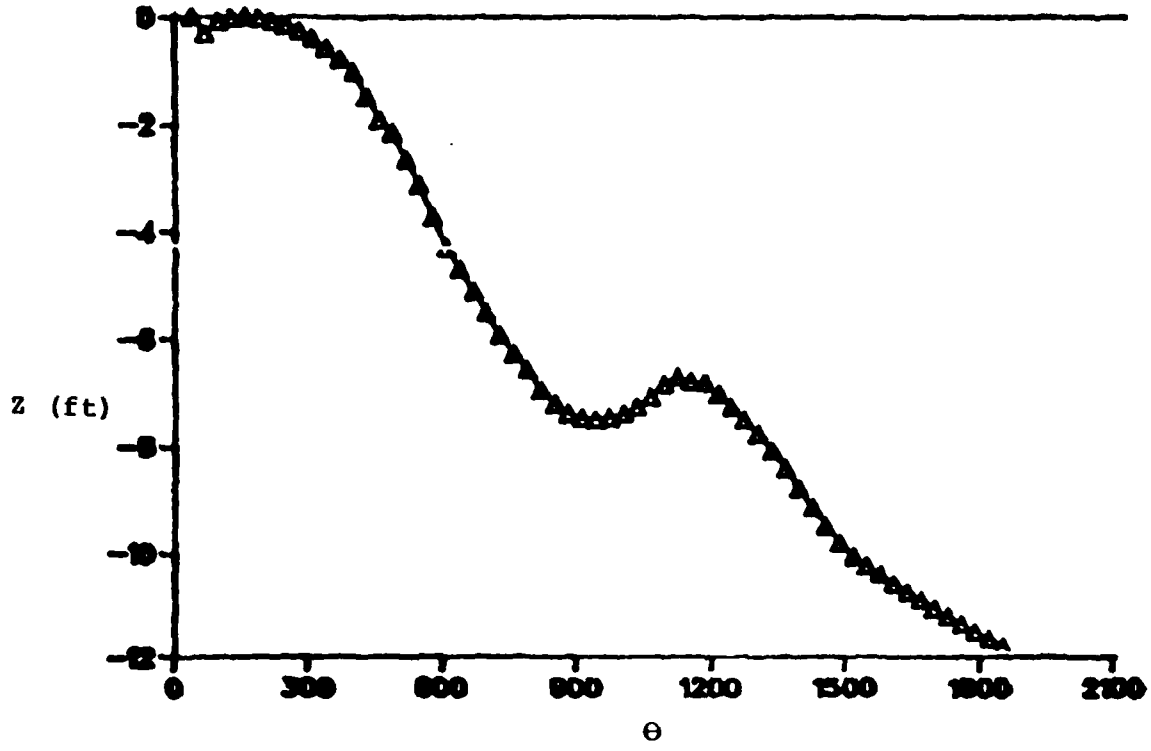

Figure 6.1.g. Vertical displacement, Z, as a function of the azimuth angle, Θ, for the vortex-line emanating from the tip point of the trailing edge at timestep #26(for case defined in Table A).

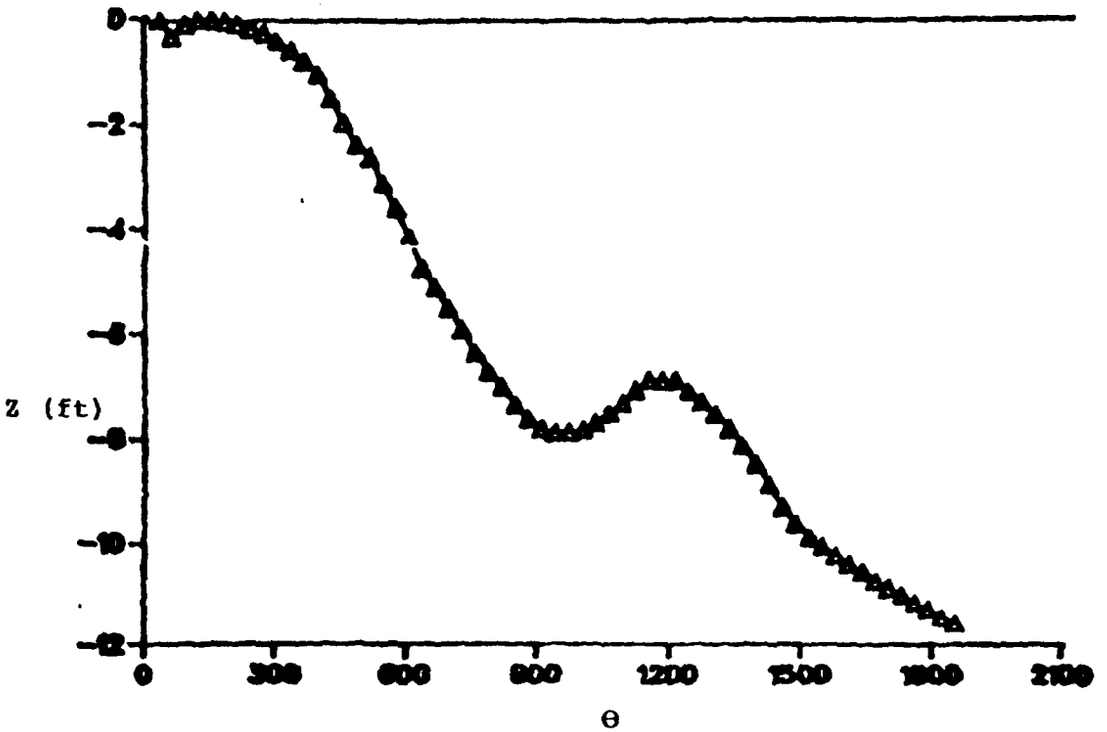

Figure 6.1.h. Vertical displacement, Z, as a function of the azimuth angle, Θ, for the vortex-line emanating from the tip point of the trailing edge at timestep #27(for case defined in Table A).

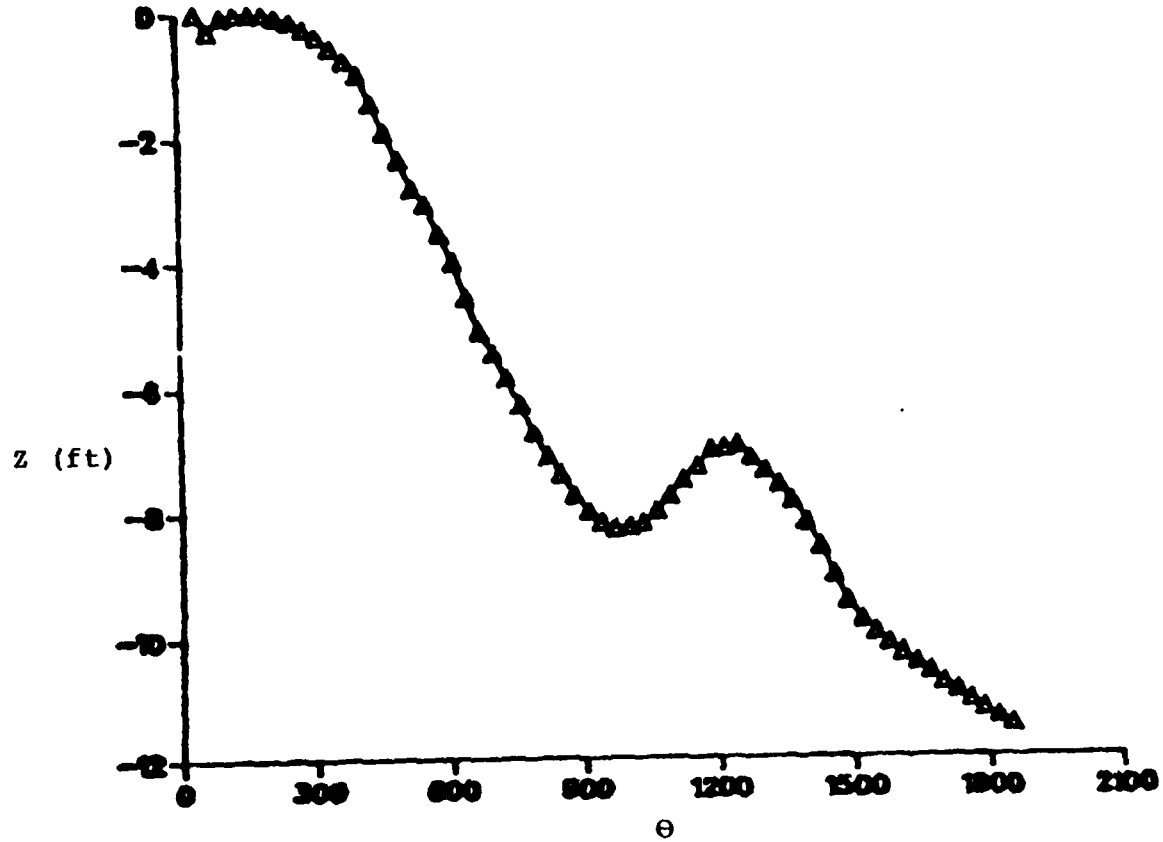

Figure 6.1.1. Vertical displacement, Z, as a function of the azimuth angle, Θ, for the vortex-line emanating from the tip point of the trailing edge at timestep #28(for case defined in Table A).

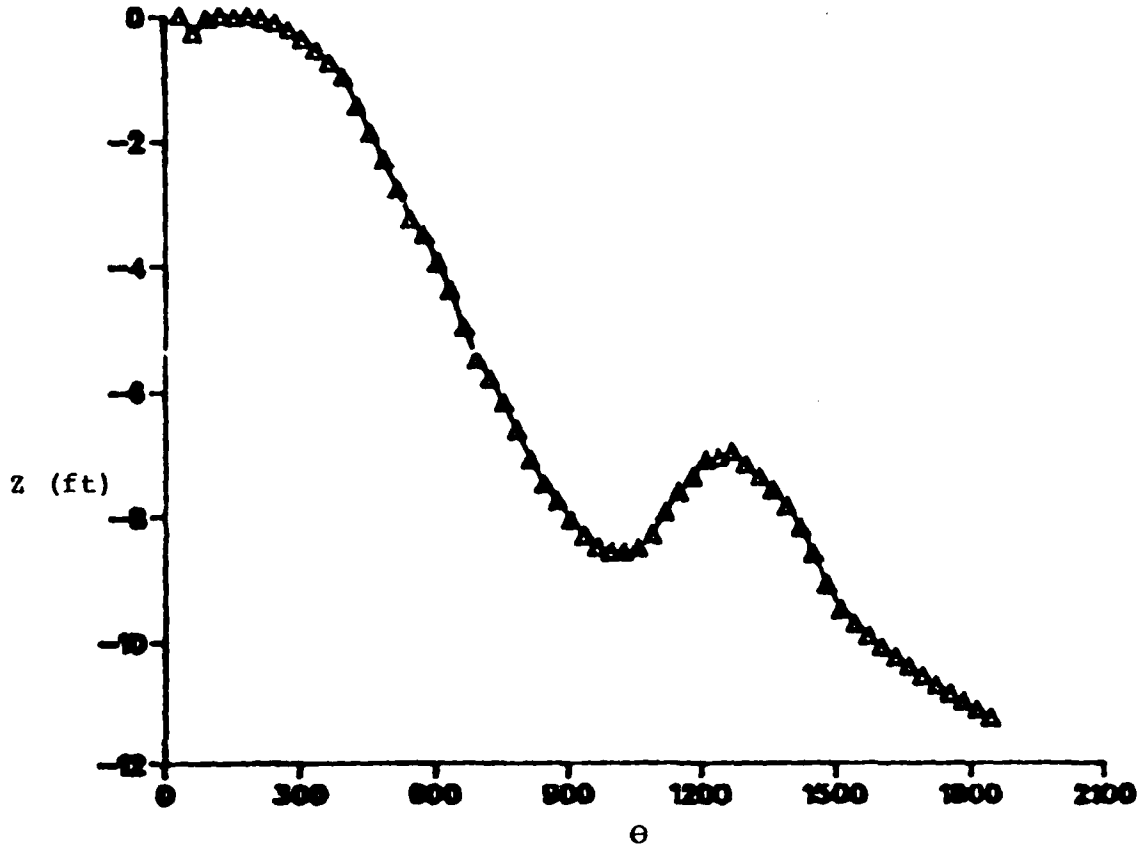

Figure 6.1.j. Vertical displacement, Z, as a function of the azimuth angle, Θ, for the vortex-line emanating from the tip point of the trailing edge at timestep # 29(for case defined in Table A).

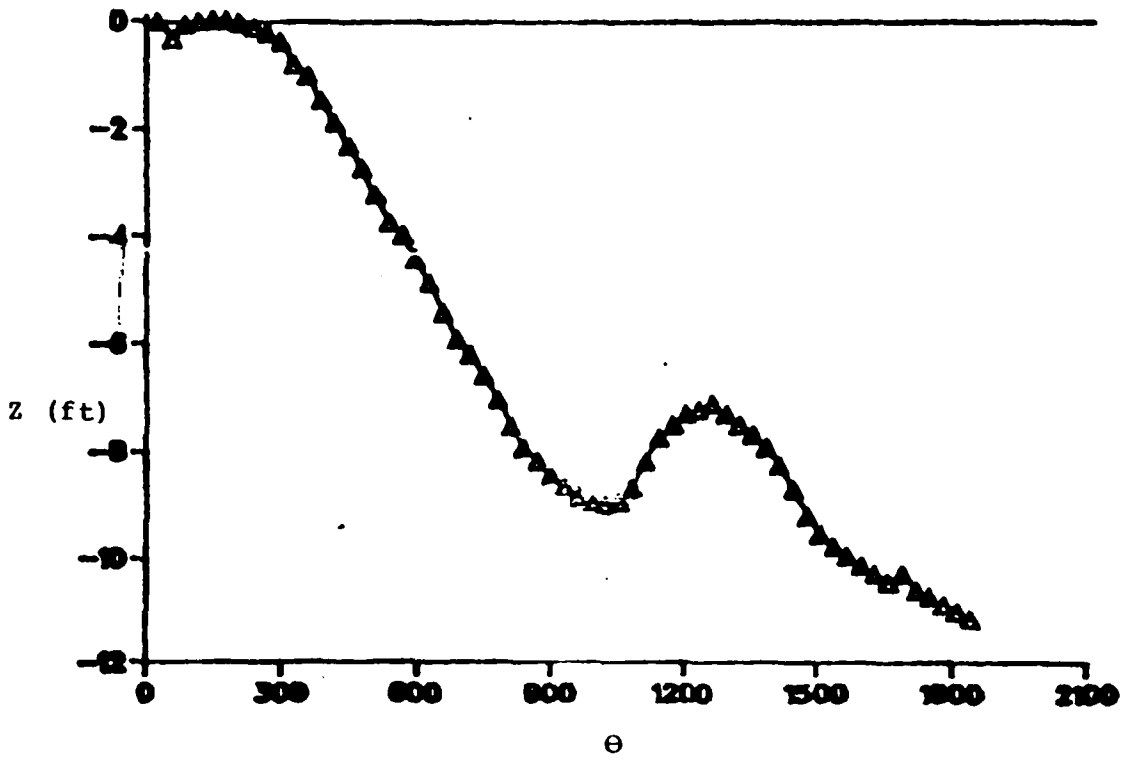

Figure 6.1.k. Vertical displacement, Z, as a function of the azimuth angle, Θ, for the vortex-line emanating from the tip point of the trailing edge at timestep # 30(for case defined in Table A).

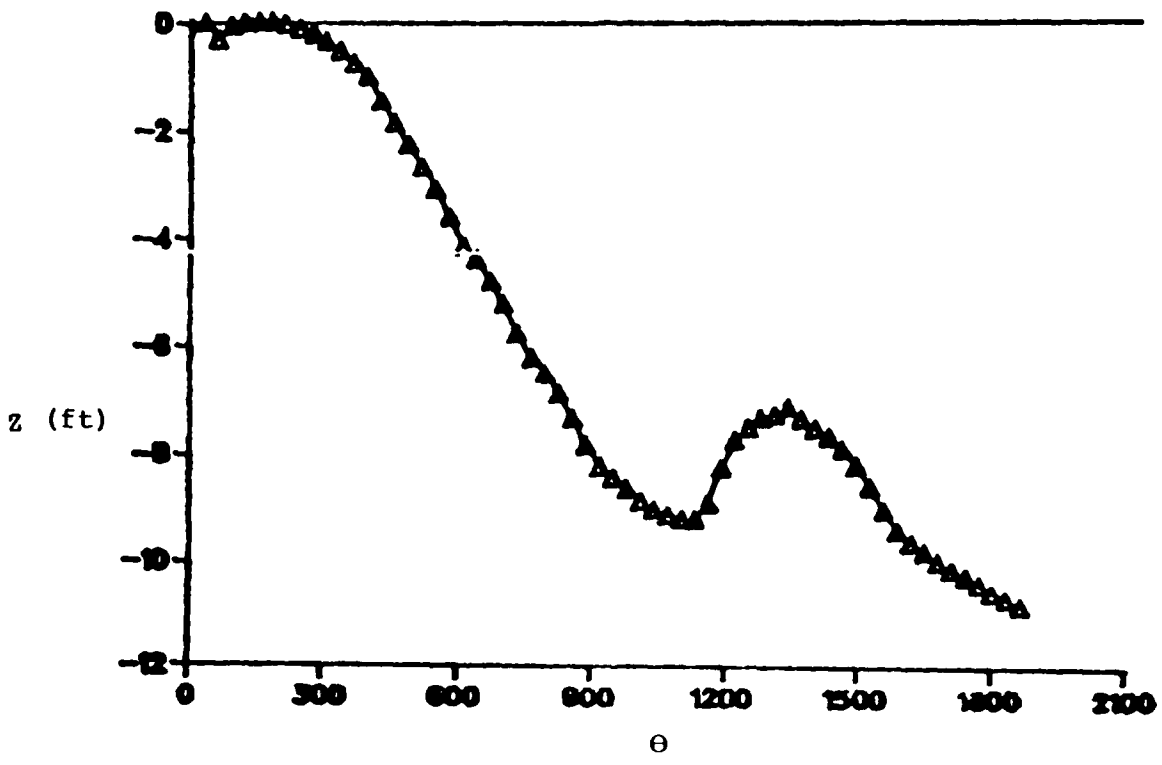

Figure 6.1.1. Vertical displacement, Z, as a function of the azimuth angle, Θ, for the vortex-line emanating from the tip point of the trailing edge at timestep # 31(for case defined in Table A).

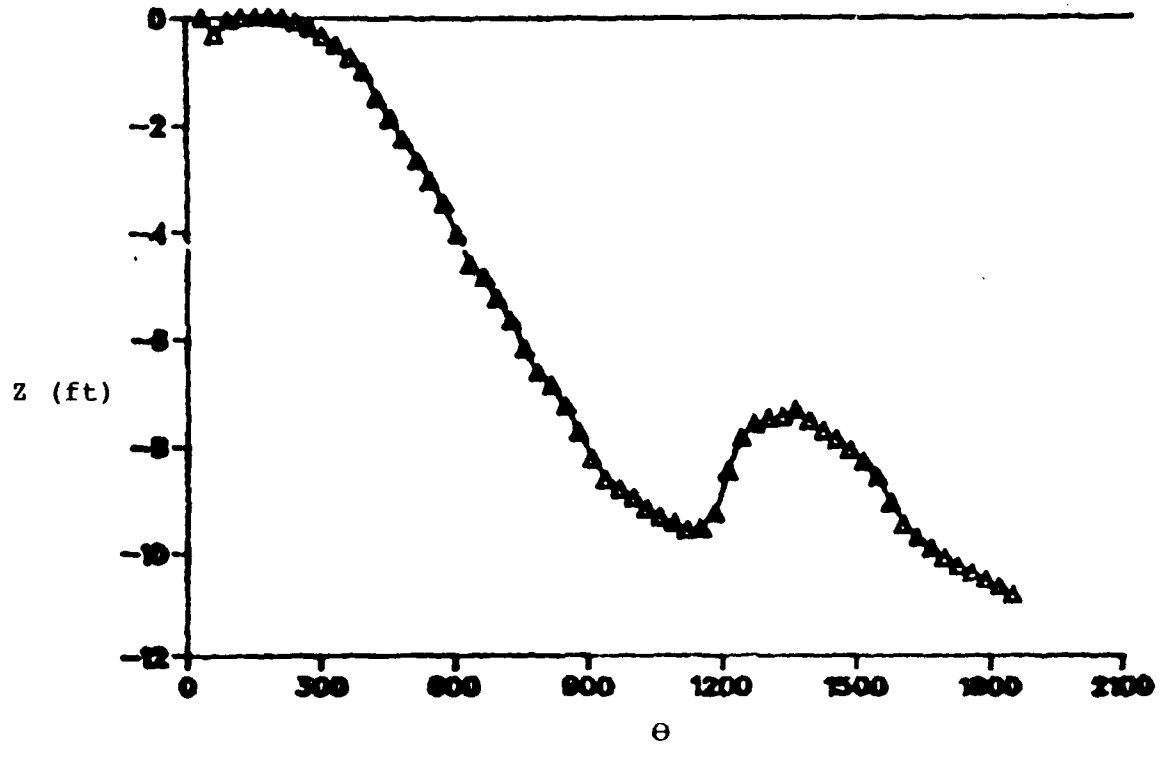

Figure 6.1.m. Vertical displacement, Z, as a function of the azimuth angle, Θ, for the vortex-line emanating from the tip point of the trailing edge at timestep # 32(for case defined in Table A).

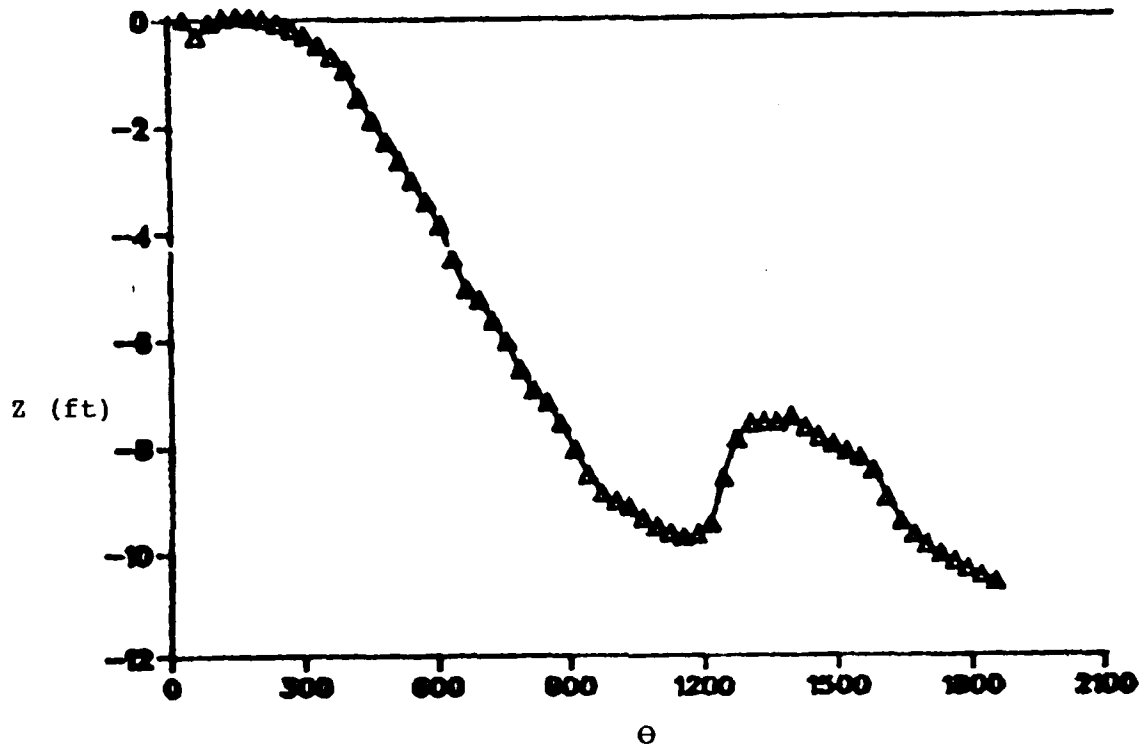

Figure 6.1.n. Vertical displacement, Z, as a function of the azimuth angle, Θ, for the vortex-line emanating from the tip point of the trailing edge at timestep # 33(for case defined in Table A).

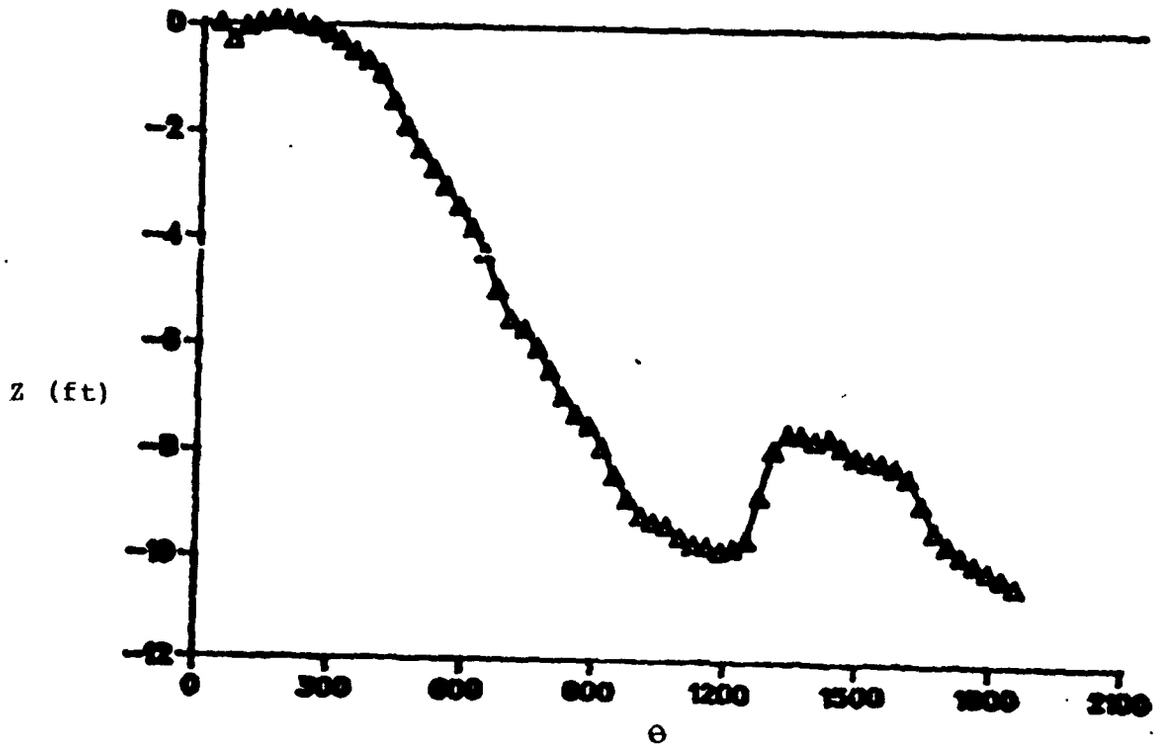

Figure 6.1.o. Vertical displacement, Z, as a function of the azimuth angle, θ, for the vortex-line emanating from the tip point of the trailing edge at timestep # 34(for case defined in Table A).

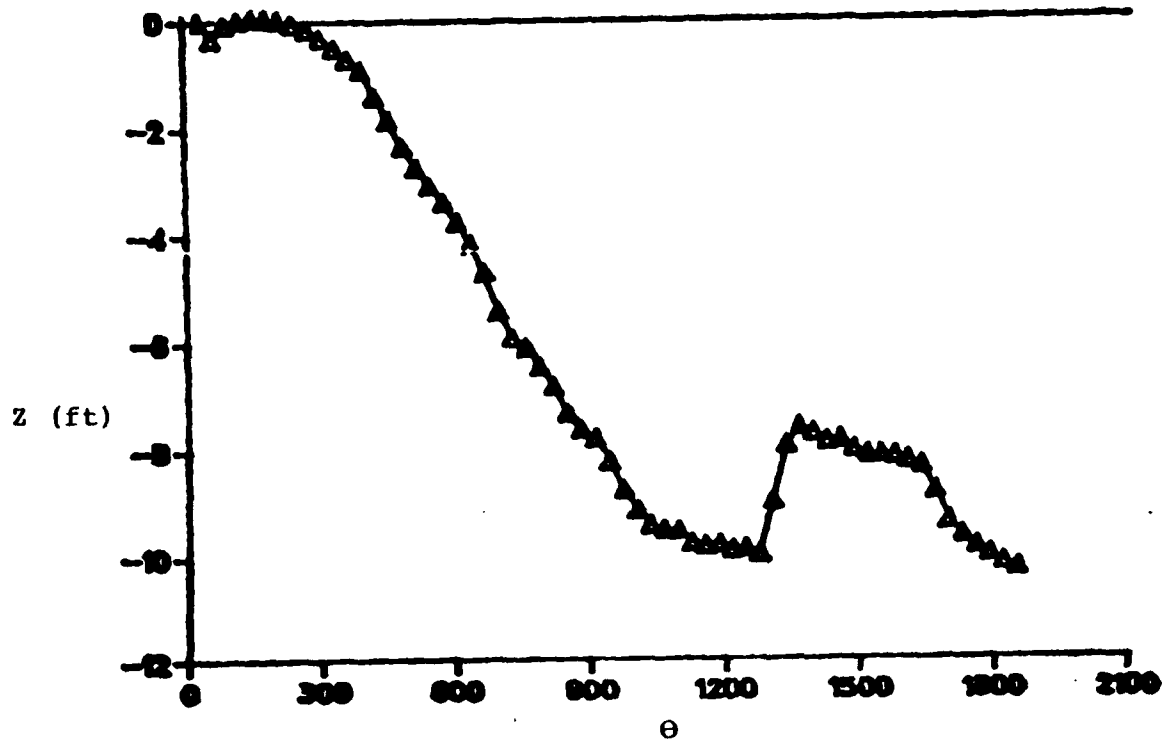

Figure 6.1.p. Vertical displacement, Z, as a function of the azimuth angle, Θ, for the vortex-line emanating from the tip point of the trailing edge at timestep # 35(for case defined in Table A).

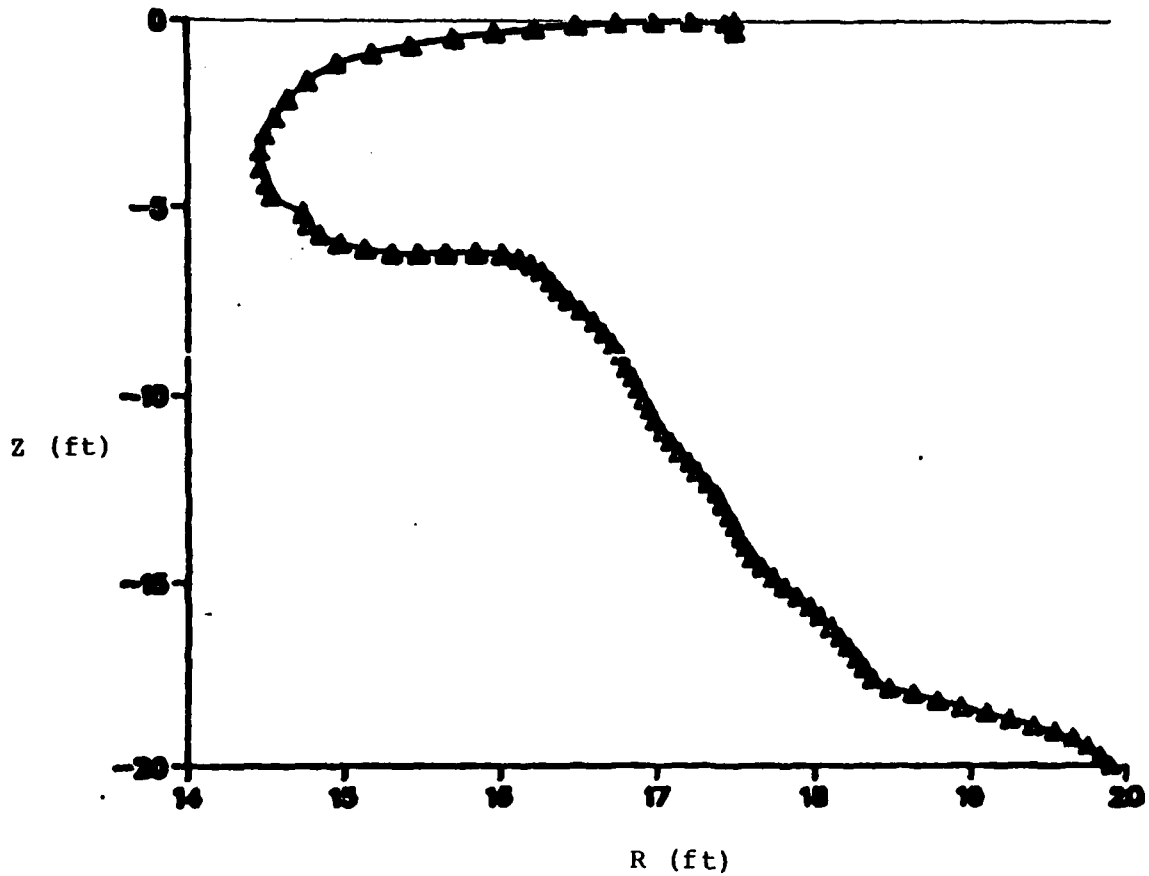

Figure 6.2.a Vertical displacement, z, as a function of the radius, R, for the vortex-line emanating from the tip point of the trailing edge at timestep #21 (for case defined in Table A.)

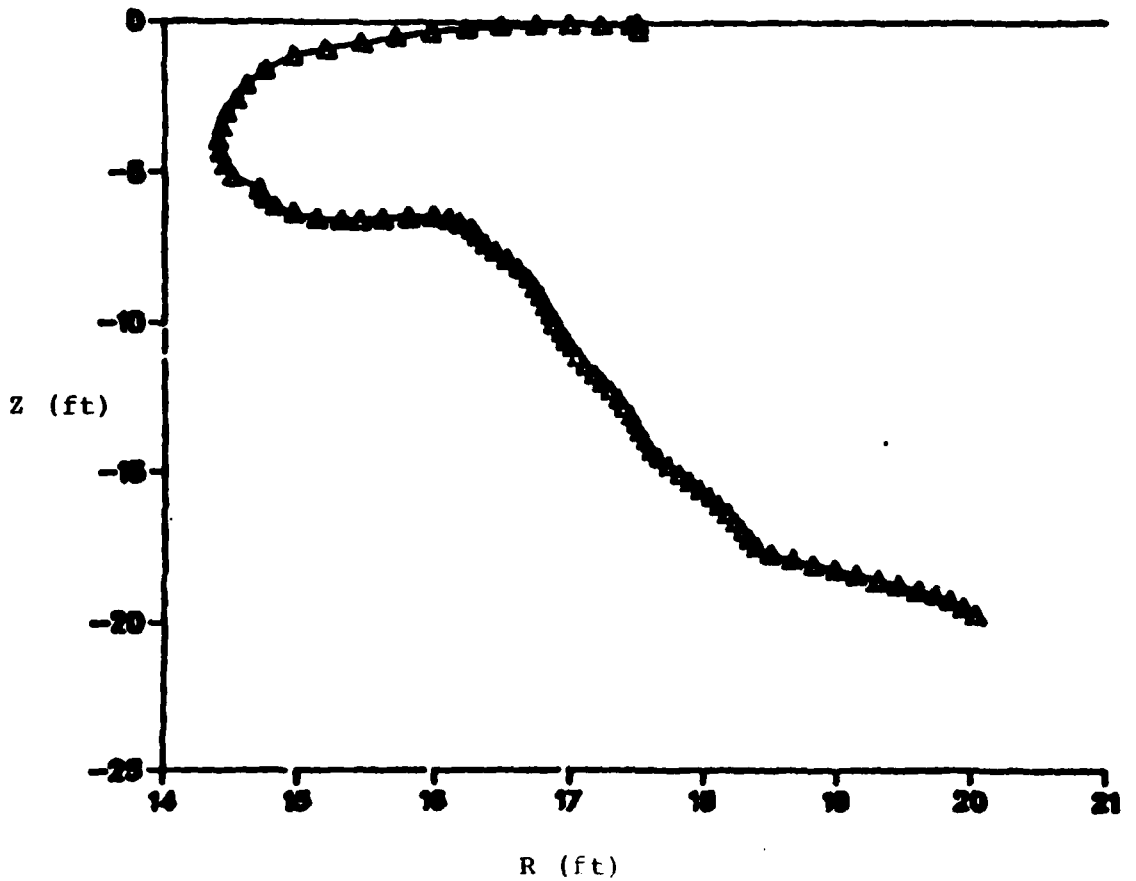

Figure 6.2.b Vertical displacement, z, as a function of the radius, R, for the vortex-line emanating from the tip point of the trailing edge at timestep #22 (for case defined in Table A.)

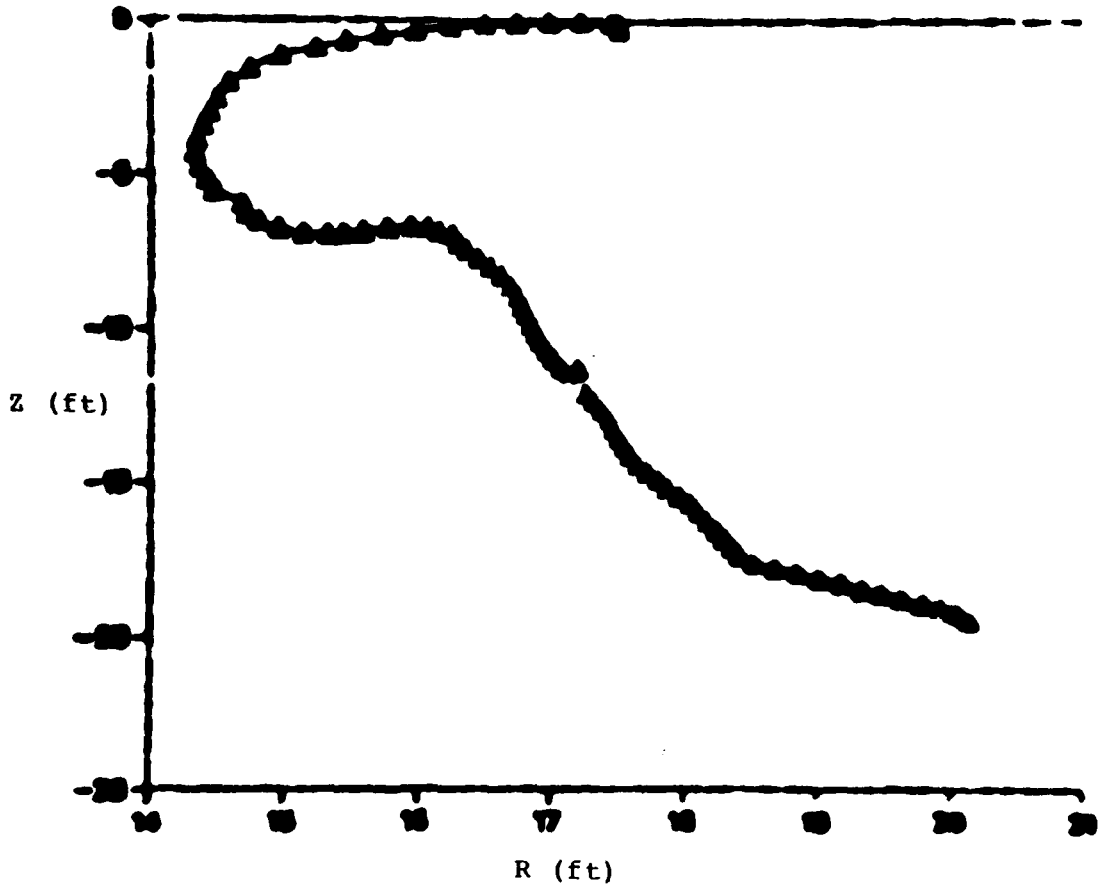

Figure 6.2.e Vertical displacement, z, as a function of the radius, R, for the vortex-line emanating from the tip point of the trailing edge at timestep #23 (for case defined in Table A.)

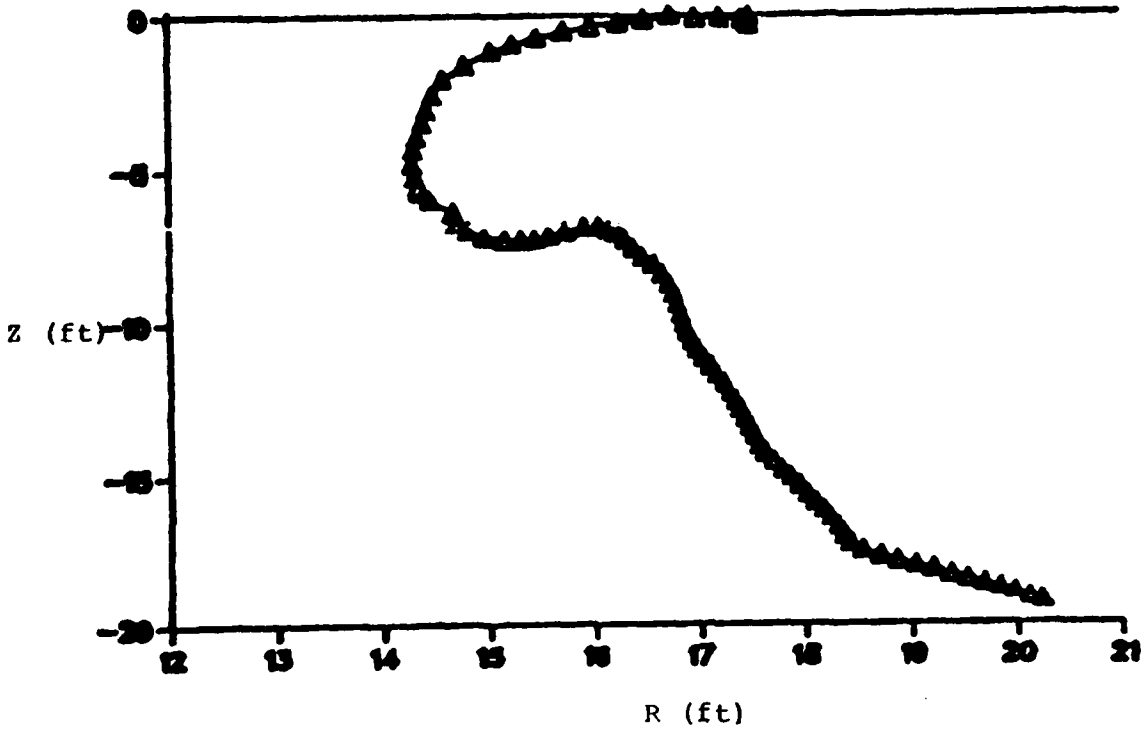

Figure 6.2.d Vertical displacement, z, as a function of the radius, R, for the vortex-line emanating from the tip point of the trailing edge at timestep #25 (for case defined in Table A.)

As mentioned in Section 5.8, the reason no far-wake model was introduced is because such a model does not exist for arbitrary motion (although the far-wake model introduced in Ref. 40 and 41 for the hover case could have been used here in order to improve these specific results).

In spite of the fact that the wake geometry does not seem to have reached convergence, the lift distribution appears to be converged: no appreciable changes occur between time steps 40 and 50. This is shown in Figures 6.3.a and 6.3.b for the five- and seven-spiral models respectively: the converged five- and seven-spiral results are compared in Figure 6.4. We believe that the explanation for this seemingly inconsistent behavior can be understood from the results shown in Figure 6.5 which shows the vertical displacement of the last vortex line as a function of the azimuth angle at the last time step considered here (that is, at time step 50): the three lines correspond to the three-, five-, and seven-spiral models respectively. It may be seen that the first two spirals are very close for all three cases (whereas the first three spirals are in good agreement for the five- and seven-spiral models). Since the first one or two spirals have the strongest impact on the section lift distribution, it is no surprise that the five- and seven-spiral models are in good agreement on the section-lift distribution.

Finally, the results obtained with the seven-spiral wake are compared against existing data in Figures 6.6, 6.7, and 6.8. Figure 6.6 shows a cross section of the wake (first two spirals only) at 90° behind the trailing edge. Also shown in Figure 6.6 are the location of the tip vortex and of the vortex sheet as predicted by Landgrebe's generalized wake model. Note that Landgrebe's model comes from the experimental data and therefore the tip vortex is not necessarily the location of the last vortex, but rather the 'center of mass' of the rolled-up portion of the vortex sheet. Taking this into account, we do consider this comparison to be very satisfactory especially if one considers the low number of elements used to describe the blade and its wake: much stronger roll-up is expected if a higher number of elements is used. (It may be worth noting that Landgrebe model is only an approximate interpolation of the experimental data.) Similar good agreements are shown in Figure 6.7 in which the radial location of the last vortex as a function of the azimuth Θ is compared to the radial location of the tip vortex in Landgrebe's model.

Finally, Figure 6.8 shows a comparison of our results with those of Rao and Schatzle (Ref. 7). As mentioned in Section 6.1, their results for a four-bladed rotor are in excellent agreement with the experimental results of Bartsch (Ref. 37). Again, we consider that the agreement is satisfactory if one considers the low number of elements used in the analysis and that Rao and Schatzle results are obtained with a prescribed wake. (It may be worth noting that our results are in excellent agreement with their results for classical-wake analysis, see Ref. 32.)

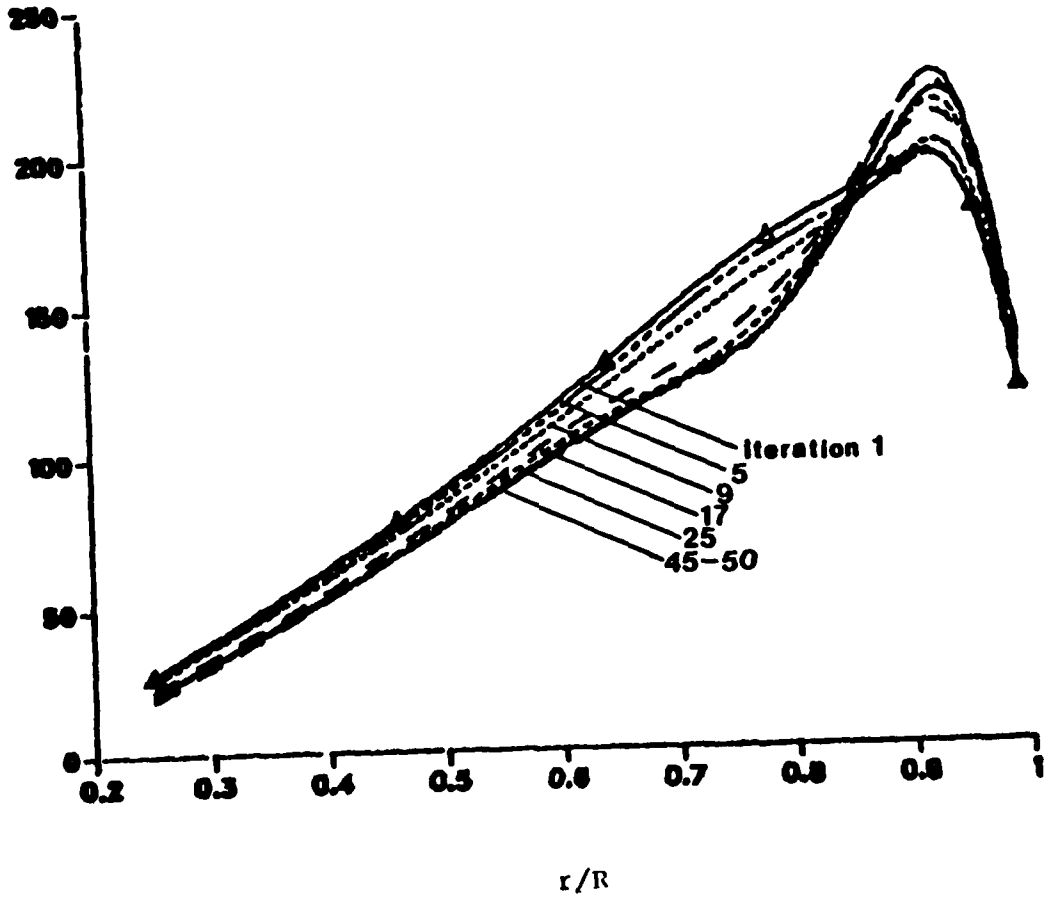

Figure 6.3.a. Convergence analysis: spanwise sectional lift distribution, (lb/ft), as a function of radial distance, r/R, for five spiral wake (for case defined in Table A).

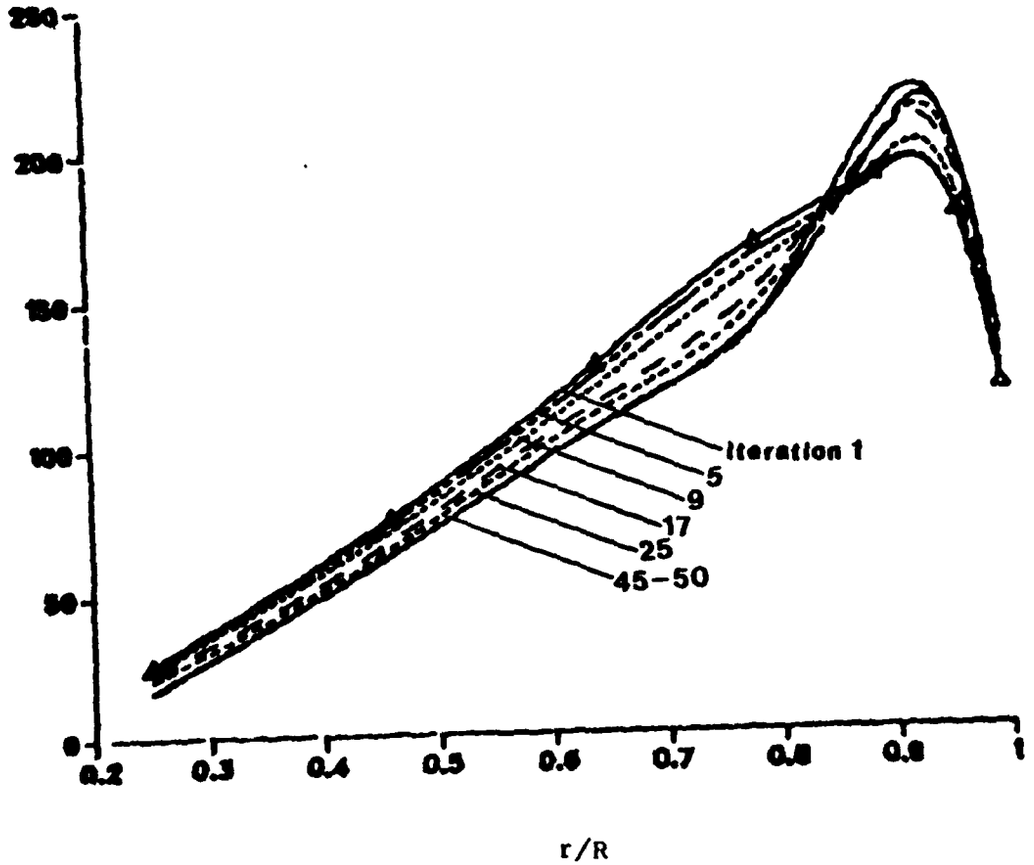

Figure 6.3.b. Convergence analysis: spanwise sectional lift distribution, (lb/ft), as a function of radial distance, r/R, for seven spiral wake (for case defined in Table A).

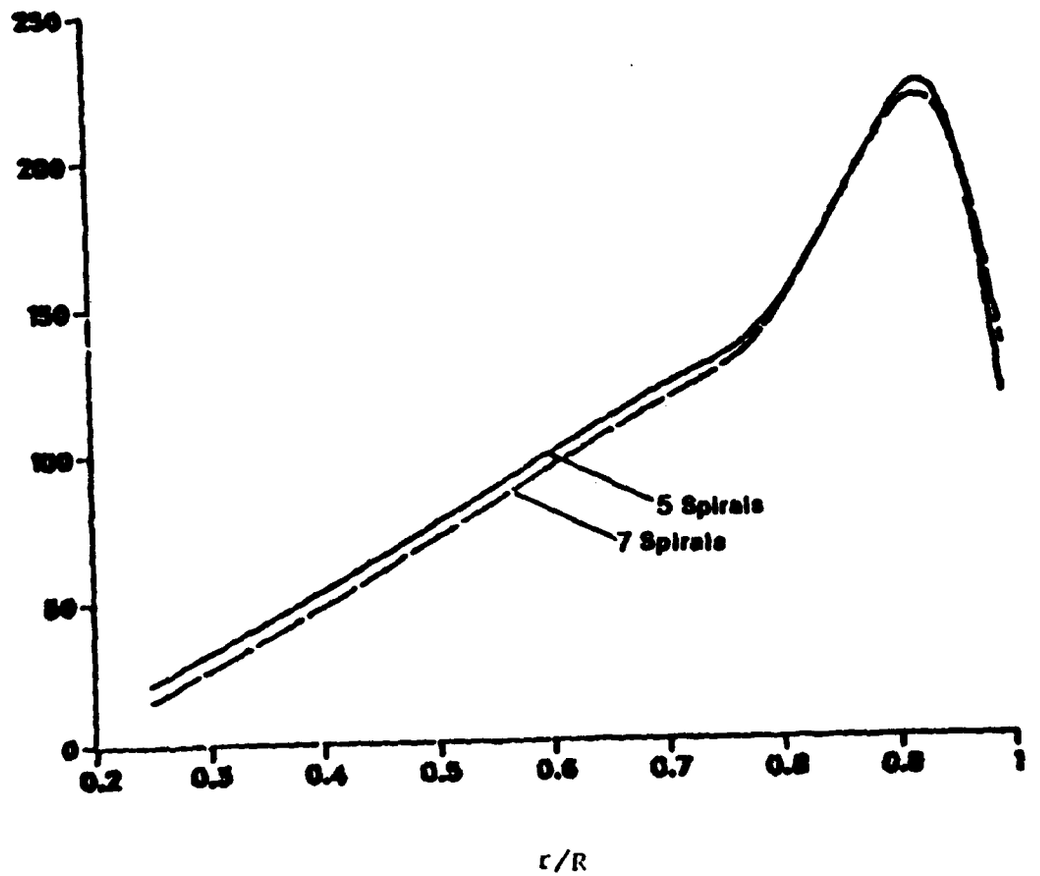

Figure 6.4 Effect of the number of spirals on the lift distribution: spanwise sectional lift distribution, (lb/ft), as a function of radial distance, r/R, for different numbers of wake spirals (timestep 50).

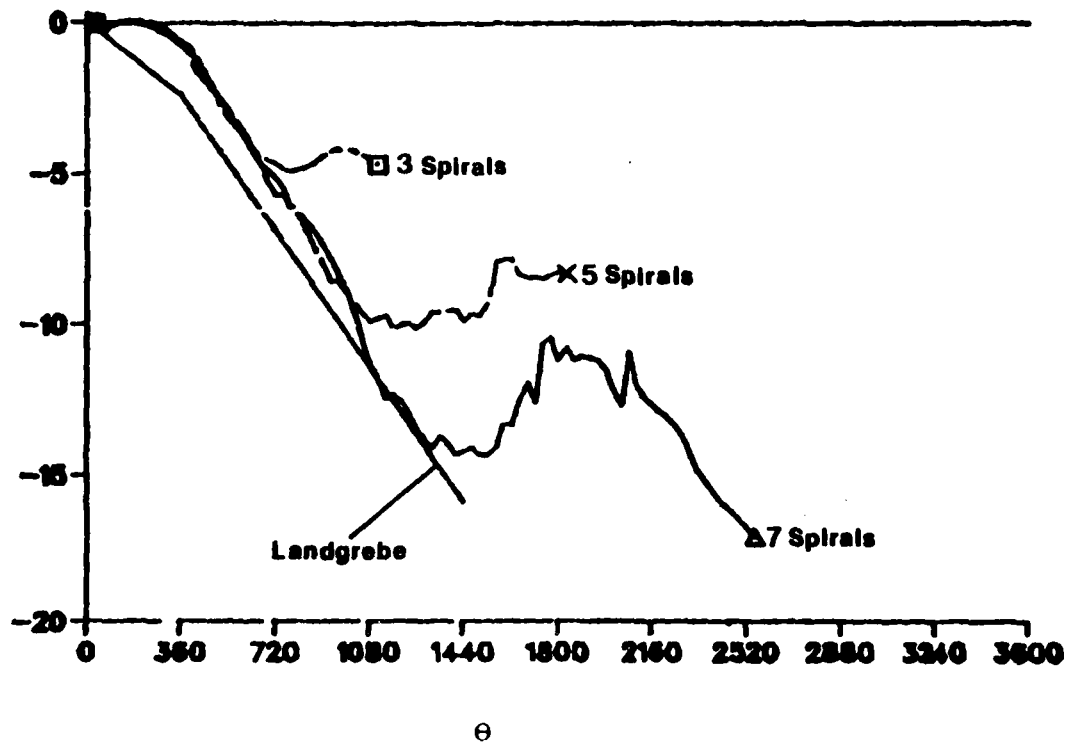

Figure 6.5. Effect of the number of spirals on the wake geometry: vertical displacement, Z, as a function of azimuth angle, θ, for different numbers of wake spirals (time step 50).

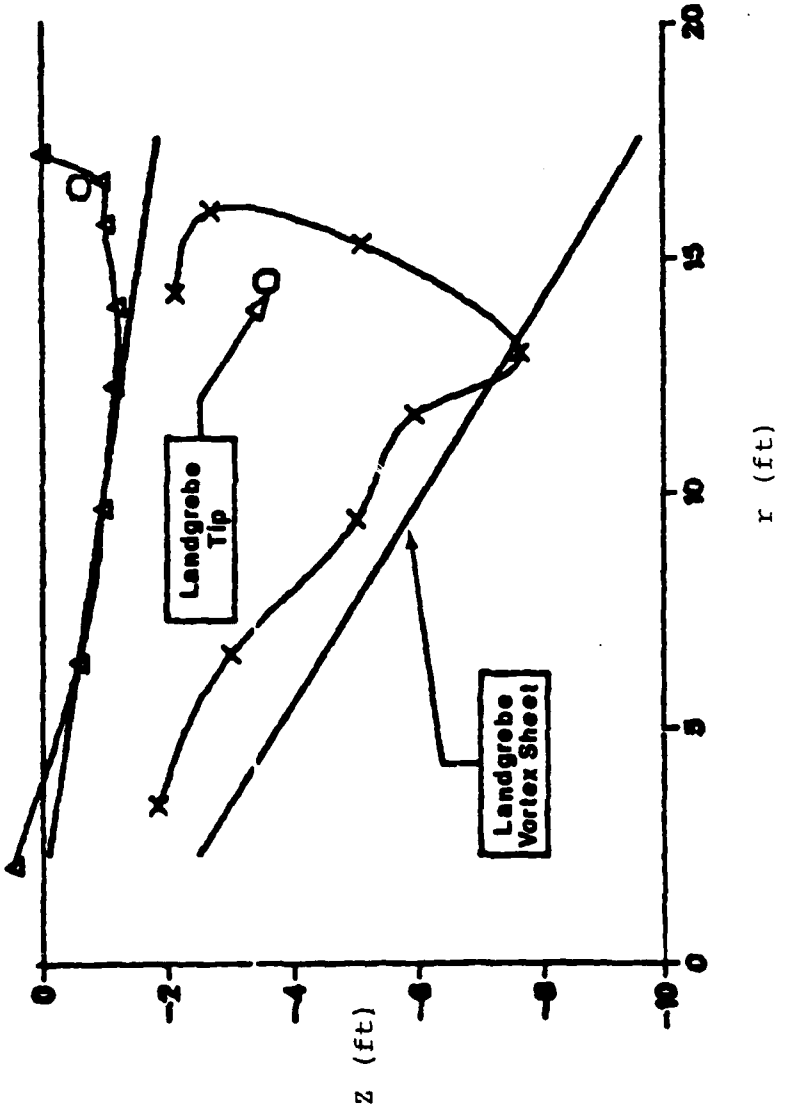

Figure 6.6. Wake cross-section compared with Landgrebe -Wake cross-section at 90 degrees behind T.E.

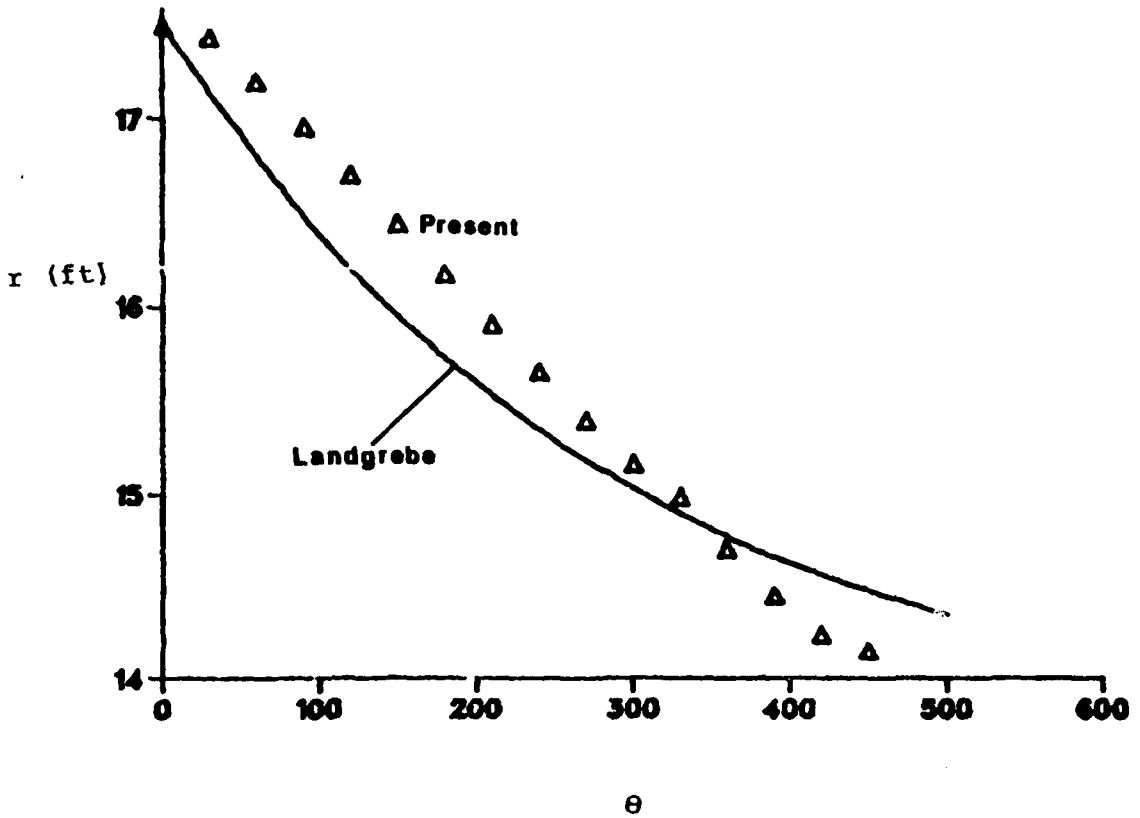

Figure 6.7. Radial coordinate, r, as a function of the azimuth angle, θ, for the vortex-line emanating from the tip point of the trailing edge at timestep 50 (for case defined in Table A), compared to Landgrebe analytical model.

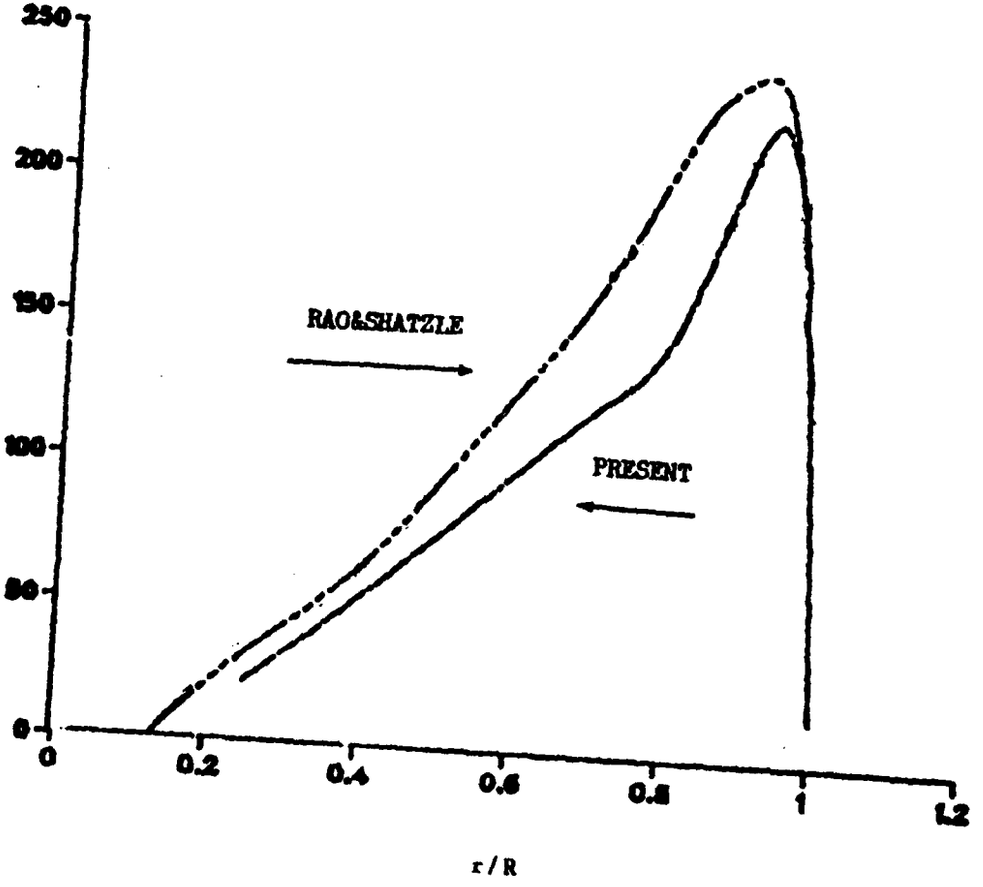

Figure 6.8. Comparison of present results with those of Rao and Shatzle.

6.4. Comments: Numerical Stability

From the numerical results presented in this Section one may conclude that the algorithm is capable of reproducing the correct trend in wake rollup and pressure distribution. The discrepancy between our results and the existing ones may be due to either the physical approximation (i.e., inviscid flow) or numerical approximation. An analysis of convergence is needed in order to discriminate between the two. (The irregular behaviour at $\theta = 60^{\circ}$ is probably due to the trailing edge condition discussed in Section 5.3 and deserves further attention).

The main accomplishment however, is that the numerical results indicate that the algorithm appears to be free of numerical instabilities, even though no ad-hoc assumption (such as prescribed radial contraction) has been used.

More precisely we believe that the instability in the last few spirals on the wake is due to the truncation of the wake and should not be thought of as a numerical instability in the classical sense: in such a case the vortex line would depart from a smooth-behavior spiral with a disturbance that oscillates and grows in space and time such as that reported by Summa (Ref. 6). All of our results are very smooth: an illustrative example of such smooth behavior is presented in Figure 6.9, which shows the geometry of the vortex-line emanating from the tip point of the trailing edge for all the spirals (for the five-spiral case) at time step $n = 45$.

We believe that this is the first time that such an accomplishment has been reported.

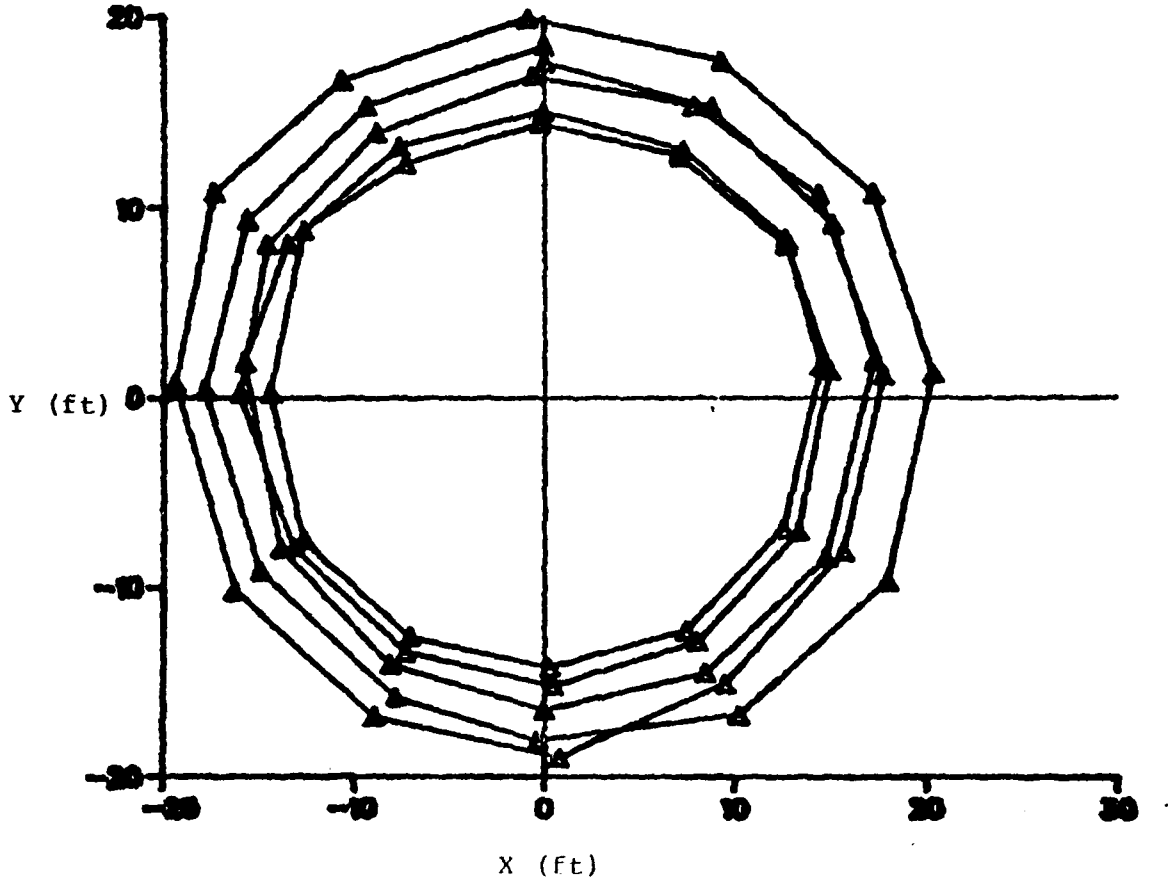

Figure 6.9 Geometry of the vortex-line emanating from the tip point of the trailing edge for all the spirals (for the five-spiral case) at time step, n=45 (for case defined in Table A).

SECTION 7

CONCLUDING REMARKS

A general formulation for the aerodynamic analysis of the unsteady incompressible potential flow around a helicopter rotor has been presented (the extension to compressible flows is outlined in Appendix A). New theoretical results incorporated in the formulation include a thorough discussion of the wake dynamics (Section 2) and of the wake generation (Section 4), both examined from very basic principles. In particular the trailing edge condition is examined in detail. It is shown that Kutta condition (that the vorticity distribution does not go to infinity at the trailing edge), necessary to insure uniqueness of the solution for two dimensional flows, is not needed for three dimensional flows (in simply connected regions). On the other hand Joukowski hypothesis (that concentrated vortices, if formed, are immediately shed off the trailing edge) is used in the discussion of the wake generation. The numerical algorithm is also presented: it is shows how the time-discretization of the problem yields a series of 'sudden starts' with the consequence that discrete vortices are generated (and shed) at the trailing edge.

Numerical results are then introduced. The main conclusions which may be drawn from these results are that

1. the algorithm appears to be numerically stable
2. seven spiral wakes are needed to obtain 'good behavior' for the first two or three spirals
3. the finite-core assumption (artificial viscosity) does not seem to affect the results
4. the wake-geometry results are in good agreement with the empirical analytical model of Landgrebe (Ref. 33)
5. the section lift distribution is in good agreement with the results of Rao and Schatzle (Ref. 7)

The most important new development is that to our knowledge this is the first time that results have been obtained without the need for an empirical input to avoid numerical instability.

Although the validation has been obtained only for a rotor in hover, the formulation is quite general (the main limitations being irrotationability and incompressibility) and applicable, in particular, to a rotor in forward flight.

Additional work is recommended in the following areas:

1. Convergence analysis: it is expected that a stronger roll-up would be obtained by using a larger number of elements in the radial direction (this in turn would affect the section-lift distribution).

2. Wake truncation: it is recommended that some intermediate- and far-wake model be introduced for the purpose of reducing the number of wake spirals (and hence the CPU time). However, as mentioned in Section 5.7, such models should be based on first principles rather than on empirical data, if the objective of the methodology is to use it for the calculation of generalized wakes.

3. Validation: continue the validation of the formulation by applying it to additional hover cases and then to forward flight cases (it is hoped that comprehensive experimental results for forward-flight become available in the near future).

REFERENCES

1. Landgrebe, A.J., Moffitt, R.C., and Clark, D.R., 'Aerodynamic Technology for Advanced Rotorcraft, Part I,' Journal of American Helicopter Society, Vol. 22, No. 2, April 1977, pp. 21-27.

2. Landgrebe, A.J., Moffitt, R.C., and Clark, D.R., 'Aerodynamic Technology for Advanced Rotorcraft, Part II,' Journal of American Helicopter Society, Vol. 22, No. 3, July 1977, pp. 2-9.

3. Friedmann, P., and Yuan, C., 'Effects of Modified Aerodynamic Strip Theories on Rotor Blade Aeroelastic Stability,' AIAA Journal Vol. 15, No. 7, July 1977, pp. 932-940.

4. Van Holten, Th., 'On the Validity of Lifting Line Concepts in Rotor Analysis,' Vertica, 1977, Vol. 1, pp. 239-254.

5. Johansson, B.C.A., 'Compressible Flow about Helicopter Rotors,' Vertica, 1978, Vol. 2, pp. 1-9.

6. Summa, J.M., 'Potential Flow about Impulsively Started Rotors,' Journal of Aircraft, Vol. 13, No. 4, April 1976, pp. 317-319.

7. Rao, B.M., and Schatzle, P.R., 'Analysis of Unsteady Airloads of Helicopter Rotors in Hover,' AIAA Paper 77-159, AIAA 15th Aerospace Sciences Meeting, Los Angeles, California, January 1977.

8. Suciu, E.O., Preuss, R.D., and Morino, L., 'Potential Aerodynamic Analyses of Horizontal-Axis Windmills,' AIAA Paper No. 77-132, January 24-26, 1977.

9. Dat, R., 'Representation d'une ligne portante animee d'un mouvement vibratoire par une ligne de doublets d'accelerations,' La Reserche Aerospatiale, No. 133, Nov.-Dec. 1969. English translation NASA TT.F12952 (1970).

10. Dat, R., 'La theorie de la surface portante appliquee a l'aile fixe et a l'helice,' La Reserche Aerospatiale, No. 1973-4. English translation ESRO-TT.90 (1974).

11. Costes, J.J., 'Calcul des forces aerodynamiques instationnaires sur les pales d'un rotor d'helicoptere,' La Reserche Aerospatiale, No. 1972-2. English Translation NASA-TT.F15039 (1973).

12. Costes, J.J., 'Application of the Lifting Line Concept to Helicopter Computation,' presented at the 'Fourth European Rotorcraft and Power Lifted Aircraft Forum,' Stresa, Italy, September 13-15, 1978.

13. Hess, J.L., and Smith, A.M.O., 'Calculation of Nonlifting Potential Flow about Arbitrary Three Dimensional Bodies,' Report No. ES 40622, Douglas Aircraft Company. Long Beach, Calif., 1962.

14. Rubbert, P.E., and Saaris, G.R., 'Review and Evaluation of Three-Dimensional Lifting Potential Flow Analysis Method for Arbitrary Configurations,' AIAA Paper No. 72-188, Jan. 1972.

15. Hess, J.L., 'Calculation of Potential Flow about Arbitrary Three-Dimensional Lifting Bodies,' Report No. MDC J5679-01, Douglas Aircraft Company, Long Beach, Calif., 1972.

16. Labrujere, T.G., Loeve, W., and Sloof, J.W., 'An Approximate Method for the Calculation of the Pressure Distribution of Wing-Body Combinations at Subcritical Speeds,' AGARD Specialist Meeting on Aerodynamic Interference, Silver Spring, Maryland, September 1970, AGARD Conference Proceedings No. 71.

17. Woodward, F.A., 'Analysis and Design of Wing-Body Combinations at Subsonic and Supersonic Speeds,' Journal of Aircraft, Vol. 5, No. 6, Nov.-Dec. 1968, pp. 528-534.

18. Fox, C.H., Jr., and Breedlove, W.J., Jr., 'Application of an Improved Unified Subsonic-Supersonic Potential Flow Method for the Aerodynamic Analysis of Aircraft Configurations,' AIAA Paper No. 74-186, Jan.-Feb. 1974.

19. Albano, E., and Rodden, W.P., 'A Double Lattice Method for Calculating Lift Distributions on Oscillating Surfaces in Subsonic Flows,' AIAA Journal, Vol. 7, No. 2, February 1969, pp. 279-285.

20. Giesing, J.P., Kalman, T.P., and Rodden, W.P., 'Subsonic Steady and Oscillatory Aerodynamics for Multiple Interfering Wings and Bodies,' Journal of Aircraft, Vol. 9, No. 10, October 1972, pp. 693-702.

21. Morino, L., 'Unsteady Compressible Potential Flow Around Lifting Bodies Having Arbitrary Shapes and Motions,' Boston University, College of Engineering, TR-72-01, June 1972.

22. Morino, L., 'Unsteady Compressible Potential Flow Around Lifting Bodies: General Theory,' AIAA 11th Aerospace Sciences Meeting, Washington, D.C., AIAA Paper No. 73-196, January 1973.

23. Morino, L., 'A General Theory Of Unsteady Compressible Potential Aerodynamics,' NASA CR-2464, December 1974.

24. Morino, L., and Kuo, C.C., 'Subsonic Potential Aerodynamics for Complex Configurations: A General Theory,' AIAA J., Vol. 12, No. 2, February 1974, pp. 191-197.

25. Morino, L., Chen, L.T., and Suciu, E.O., 'Steady and Oscillatory Subsonic and Supersonic Aerodynamics Around Complex Configurations,' AIAA J., Vol. 13, No. 3, March 1975, pp. 368-374.

26. Morino, L., and Chen, L.T., 'Indicial Compressible Potential Aerodynamics Around Complex Aircraft Configurations,' NASA Conference on Aerodynamic Analysis Requiring Advanced Computers, NASA Langley Research Center, Hampton, Virginia, March 4-6, 1975.

27. Morino, L., and Tseng, K., 'Steady, Oscillatory and Unsteady, Subsonic and Supersonic Aerodynamics (SOUSSA) for Complex Aircraft Configurations,' AGARD Symposium on Unsteady Aerodynamics, Ottawa, Canada, September 26-28, 1977.

28. Morino, L., and Tseng, K., 'Time-Domain Green's Function Method for Three-Dimensional Nonlinear Subsonic Flows,' AIAA Paper No. 78-1204, AIAA 11th Fluid and Plasma Dynamics Conference, Seattle, Washington, July 1978.

29. Dvorak, F.A., Maskew, B., and Woodward, F.A., 'Investigation of Three-Dimensional Flow Separation on Fuselage Configurations,' Analytical Methods, Inc., USAAMRDL TechnicalReport 77-4, Eustis Directorate, U.S. Army Air Mobility Research and Development Laboratory, Fort Eustis, Virginia, March 1977.

30. Clark, D.R.,'The Use of Analytic Tools in the Design and Development of Rotorcraft,' presented at the 'Fourth European Rotorcraft and Powered Lift Aircraft Forum,' Stresa, Italy, September 13-15, 1978.

31. Morino, L., and Soohoo, P., 'Green's Function Method for Compressible Unsteady Potential Aerodynamic Analysis of Rotor-Fuselage Interaction,' presented at the 'Fourth European Rotorcraft and Powered Lift Aircraft Forum,' Stresa, Italy, September 13-15, 1978.

32. Soohoo, P., Noll, R.B., Morino, L., and Ham, N.D., 'Green's Function Method for the Computational Aerodynamic Analysis of Complex Helicopter Configurations,' AIAA 17th Aerospace Sciences Meeting, Ne Orleans, La., AIAA Paper No. 79-0347, January 15-17, 1979.

33. Landgrebe, A.J., 'An Analytical Method for Predicting Rotor Wake Geometry,' Journal of the American Helicopter Society, Vol. 14, No. 4, October 1969, pp. 20-32.

34. Landgrebe, A.J., 'An Analytical and Experimental Investigation of Helicopter Rotor Hover Performance and Wake Geometry Characteristics,' USAAMRDL Technical Report 71-24, Eustis Directorate, U.S. Army Air Mobility Research and

Development Laboratory, Fort Eustis, Va., June 1971, AD 728835.

35. Crews, S.T., Hohenemser, K.H., and Ormiston, R.A., 'An Unsteady Wake Model for a Hingeless Rotor,' Journal of Aircraft, Vol. 10, No. 12, December 1973, pp. 758-760.

36. Kocurek, J.D., 'A Lifting Surface Performance Analysis with Circulation Coupled Wake for Advanced Configuration Hovering Rotors', Ph.D. Dissertation, Graduate College, Texas A+M University, May 1978.

37. Bartsch, E.A., 'In-Flight Measurement and Correlation with Theory of Blade Airloads and Responses on the XH-51A Compound Helicopter Rotor-Volume I: Measurement and Data Reduction of Airloads and Structural Loads,' USAAVLABS Technical Report 68-22A, U.S. Army Aviation Material Laboratories, Fort Eustis, Va., May 1968, AD 674193.

38. Scully, M.P., 'Computation of Helicopter Rotor Wake Geometry and it's Influence on Rotor Harmonic Airloads', MIT ASRL-TR-176-1, March 1971.

39. Pouradier, J.M., and Horowitz, E., 'Aerodynamic Study of a Hovering rotor', Sixth European Rotorcraft and Powered Lift Aircraft Forum, Paper No. 26, Bristol, England, September 1980.

40. Summa, J.M., and Clark, D.R., 'A Lifting-Surface Method for Hover/Climb Airloads,' 35th Annual Forum of American Helicopter Society, Washington, D.C., May 1979.

41. Summa, J.M., 'Advanced Rotor Analysis Method for the Aerodynamics of Vortex/Blade Interactions in Hover,' Eighth European Rotorcraft and Powered Lift Aircraft Forum, Paper No. 2.8, Aix-en Province, France, August 31-September 3, 1982.

42. Miller, R.H., 'Application of Fast Free Wake Analysis Techniques to Rotors,' Eighth European Rotorcraft Forum, Aix-en-Provence, France, August 31 through September 3, 1982.

43. Loewy, R.G., 'A Two-Dimensional Approximation to the Unsteady Aerodynamics of Rotary Wings,' Journal of the Aeronautical Sciences, Vol. 24, 1957, pp. 81-92, 144.

44. Hammond, C.E., and Pierce, G.C., 'A Compressible Unsteady Aerodynamic Theory for Helicopter Rotors,' AGARD Specialists Meeting on the Aerodynamics of Rotary Wings, Marseille, France, September 1972.

45. Jones, W.P., and Rao, B.M., 'Compressibility Effects on Oscillating Rotor Blades in Hovering Flight,' AIAA Journal Vol. 8, February 7, 1970, pp. 321-329.

46. Jones, W.P., 'The Influence of the Wake on the Flutter and Vibration of Rotor Blades,' The Aeronautical Quarterly, Vol. IX, August 1958, pp. 258-286.

47. Isaacs, R., 'Airfoil Theory for Rotary Wing Aircraft,' Journal of Aeronautical Sciences, Vol. 12, January 1945, pp. 113-117.

48. Isaacs, R., 'Airfoil Theory for Rotary Wing Aircraft,' Journal of Aeronautical Sciences,Vol. 13, April 1946, pp. 218-220.

49. Greenberg, J.M., 'Airfoil in Sinusoidal Motion in a Pulsating Stream,' NACA TN 1326, 1947.

50. Rao, B.M., and Jones, W.P., 'Application to Rotary Wings of Simplified Aerodynamic Lifting Surface Theory for Unsteady Compressible Flow,' Proceedings of the AHS/NASA-AMES Specialist's Meeting on Rotorcraft Dynamics, February 1974.

51. Caradonna, F.X., and Isom, M.P., 'Subsonic and Transonic Potential Flow over Helicopter Rotor Blades,' AIAA Journal, Vol. 10, No. 12, December 1972.

52. Caradonna, F.X., and Isom, M.P., 'Numerical Calculation of Unsteady Transonic Potential Flow over Helicopter Rotor Blades,' AIAA J., Vol. 14, NO. 4, April 1976.

53. Caradonna, F.X., and Phillippe, J.J., 'The Flow over Helicopter Blade Tip in the Transonic Regime,' Vertical, 1978, Vol. 2, pp. 43-60.

54. Caradonna, F.X., 'The Transonic Flow on a Helicopter Rotor,' Ph.D. Thesis, Stanford University, March 1978.

55. Morino, L., Foundations of Computational Aerodynamics, Part I, Inviscid Flows, in preparation.

56. Lamb, H., Hydrodynamics, 6th ed., Cambridge University Press, 1932.

57. Batchelor, G.K., An Introduction to Fluid Dynamics, Cambridge University Press, 1967.

58. Serrin, J., 'Mathematical Principle of Classical Fluid Mechanics' in Encyclopedia of Physics Ed. S. Fluegge, Vol. VII/1, Fluid Dynamics I, Springer Verlag, 1959.

59. Kutta, M.W., 'Auftriebskraefte in stroemenden Fluessigkeiten,' Illustrierte Aeronautische Mitteilungen, 6 (1902), 133-135,'Ueber eine mit den Grundlagen des Flugproblems in Beziehung stehende zweidimensionale Stroemung,' Sitzungsberichte der Bayerischen Akademie der

Wissenschaften, mathematisch- physikalische Klasse (1910), 1-58, 'Ueber ebene Zirkulationsstroemungen nebst Flugtechnischen Anwendungen,' ibid. (1911), 65-125.

60. Joukowski, N., 'On the Adjunct Vortices' (in Russian), Obshchestvo liubitelei estestvoznaniia, antropologii i etnografee, Moskva, Izviestiia, 112, Transactions of the Physical Section, 13 (1907), 12-25, 'De la chute dans l'air de corps legers de forme allongee, animes d'un mouvement rotatoire,' Bulletin de l'Institut Aerodynamique de Koutchino, 1 (1912), 51-65, 'Ueber die Kontouren der Tragflaechen der Drachenflieger,' Zeitschrift fuer Flugtechnik und Motorluftschiffahrt, 1 (1910), 281-284, 3 (1912), 81-86, Aerodynamique (Paris, 1916 and 1931).

61. Von Karman, Th., Aerodynamics, McGraw Hill, 1963.

62. Mangler, K.W. and Smith, J.H.B., 'Behaviour of the Vortex Sheet at the Trailing Edge of a Lifting Wing,' Journal of the Royal Aeronautical Society, Vol. 74, Nov. 1970, pp. 906-908.

63. Deutsch, David J., 'An Integral Equation for the Solution of the Nonlinear Wave Equation,' Ph.D. Dissertation, Boston University, College of Engineering, in preparation.

64. Sipcic, S.R., Ph.D. Dissertation, University of Belgrade, Yugoslavia, in preparation.

65. Ffowcs-Williams, J.E., and Hawkins, D.C., 'Sound Generation by Turbulence and Surface in Arbitrary Motion,' Philosophical Transactions of the Royal Society of London, Series A, Vol. 264, May 8, 1969, pp. 321-342.

APPENDIX A

FORMULATION FOR COMPRESSIBLE FLOWS

The integral formulation of Section 3 is extended here to the case of compressible flows. The frame of reference is assumed to have arbitrary motion. The surface is assumed to be moving with respect to the frame of reference in order to accommodate structural deformations as well as wake roll-up. However, for the sake of simplicity, such motion is assumed to be small. The general case is considered in Refs. 63 and 64. The formulation is an extension of that introduced in Ref. 65 for acoustics.

Equivalent Problems

The equation for the velocity potential in a frame of reference connected with the undisturbed air is given by

$$\nabla^2\varphi - \frac{1}{a_\infty^2}\frac{\partial^2\varphi}{\partial\tau^2} = \chi \qquad \text{A.1}$$

where χ contains all nonlinear terms. The boundary conditions represent the zero flow at infinity

$$\varphi = 0 \qquad \text{at } \infty \qquad \text{A.2}$$

and the no-flow-through condition on the surface boundary

$$\frac{\partial\varphi}{\partial n} = \bar{v}_b \cdot \bar{n} \qquad \text{on } \sigma_b \qquad \text{A.3}$$

In addition,

$$\frac{D_w}{D\tau}\Delta\varphi = 0 \qquad \text{on wake} \qquad \text{A.4}$$

In order to simplify the derivation of the Green's theorem for a frame of reference having arbitrary motion, it is convenient to extend the problem to the whole space by introducing the function $\hat{\varphi} = E\varphi$ where, for a surface σ surrounding both body and wake

$$\begin{aligned} E &= 1 \quad \text{inside } \sigma \\ &= 0 \quad \text{outside } \sigma \end{aligned} \qquad \text{A.5}$$

so that

$$\begin{aligned} \hat{\varphi} &= \varphi \quad \text{inside } \sigma \\ &= 0 \quad \text{outside } \sigma \end{aligned} \qquad \text{A.6}$$

Note that $\hat{\varphi}$ is defined in the whole space and satisfies the equation

$$\nabla^2\hat{\varphi} - \frac{1}{a_\infty^2}\frac{\partial^2\hat{\varphi}}{\partial\tau^2} = E\chi + \bar{\nabla}\varphi\cdot\bar{\nabla}E + \bar{\nabla}\cdot(\varphi\bar{\nabla}E)$$

$$- \frac{1}{a_\infty^2}(2\frac{\partial\varphi}{\partial\tau}\frac{\partial E}{\partial\tau} + \frac{\partial^2 E}{\partial\tau^2}) \qquad \text{A.7}$$

The presence of the $\bar{\nabla}E$ and $\partial E/\partial\tau$ terms introduce source layers which act only on the surface σ (which is not to be considered as a boundary of the domain of validity of the equation which is the infinite space). The only boundary is at infinity where we specify $\hat{\varphi} = 0$. By denoting the right hand of Equation A.7 by $\hat{\chi}$, Eq. A.7 may be rewritten as

$$\nabla^2\hat{\varphi} - \frac{1}{a_\infty^2}\frac{\partial^2\hat{\varphi}}{\partial\tau^2} = \hat{\chi} \qquad \text{A.8}$$

whereas, according to Eq. A.2, the boundary condition at infinity, is

$$\hat{\varphi} = 0 \qquad \text{at } \infty \qquad \text{A.9}$$

Equation A.8 subject to boundary condition A.9 is equivalent to Equation A.1 to A.4 in the sense that if a function satisfies Eqs. A.8 and A.9, it also satisfies Eqs. A.1 to A.4. The solution to Equations A.8 and A.9 is

$$\hat{\varphi}(\bar{\xi}_*,\tau_*) = \int_{-\infty}^{\infty}\iiint\hat{\chi}\,G\,d\bar{\xi}d\tau \qquad \text{A.10}$$

where

$$G(\bar{\xi},\tau) = -\frac{\delta(\tau_*-\tau-\theta)}{4\pi\rho} \qquad \text{A.11}$$

(with $\rho = |\bar{\xi}-\bar{\xi}_*|$ and $\theta = \rho/a_\infty$) is the well known Green's Function for the wave operator.

Transformation to the Moving Frame of Reference

Here we introduce a coordinate system $(\bar{x},t)$ moving in rigid-body motion (e.g., connected to the rotor if the rotor moves with rigid body motion). We make use of a transformation from

AD-A129 710 FREE WAKE AERODYNAMIC ANALYSIS OF HELICOPTER ROTORS(U) 2/2
BOSTON UNIV MA CENTER FOR COMPUTATIONAL AND APPLIED
DYNAMICS.. L MORINO ET AL. 26 MAY 83 CCAD-TR-83-01
UNCLASSIFIED ARO-16294.2-EG DAAG29-80-C-0016 F/G 20/4 NL

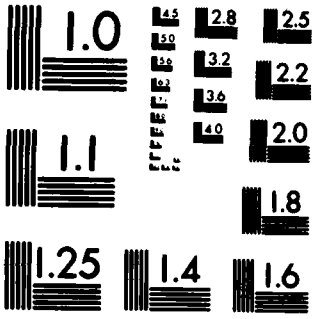

MICROCOPY RESOLUTION TEST CHART
NATIONAL BUREAU OF STANDARDS-1963-A

the fixed frame of reference $(\bar{\xi},\tau)$ to the moving frame of reference $(\bar{x},t)$

$$\frac{d\bar{\xi}}{dt} = \bar{V}(\bar{x},t) \qquad \text{A.12}$$

$$\bar{\xi}(\bar{x},0) = \bar{x} \qquad \text{A.13}$$

Then

$$\bar{\xi}(\bar{x},t) = \bar{x} + \int_0^t \bar{V}(\bar{x},t_1)dt_1 \qquad \text{A.14}$$

$$\tau = t \qquad \text{A.15}$$

From Equation (6) we have

$$\hat{\varphi}(\bar{x}_*,t_*) = \iiint_{-\infty}^{\infty} \frac{\hat{\chi}(x,t)\ \delta(t-t_*+\theta(\bar{x},t))}{4\pi\rho(\bar{x},t)}\ d\bar{x}\ dt \qquad \text{A.16}$$

where

$$\rho(\bar{x},t) = |\bar{\xi}(\bar{x},t) - \bar{\xi}(\bar{x}_*,t_*)| \qquad \text{A.17}$$

(Since the velocity $\bar{V}$ corresponds to rigid body motion, the transformation is a length preserving and hence the Jacobian is equal to one.) Recalling a result from theory of distributions

$$\int_{-\infty}^{\infty} f(t)\ \delta\ [g(t)]\ dt = \sum_i [f/|g'|]_{t=t_i} \qquad \text{A.18}$$

(where t_i are the roots of $g(t) = 0$) and integrating with respect to the time variable, one obtains

$$4\pi\hat{\varphi}(\bar{x}_*,t_*) = \sum_i \iiint_{-\infty}^{\infty} [\hat{\chi}(\bar{x},t_i)/r_{ii}(x,t_i)]\ d\bar{x} \qquad \text{A.19}$$

where $r_{ii}(x,t_i) = \rho(x,t_i)\ |g'(t_i)|$, whereas the values of t_i are the solutions of

$$g(t) = 0 \qquad \text{A.20}$$

where

$$g(t) = t_* - t - |\bar{\xi}(\bar{x},t) - \bar{\xi}(\bar{x}_*,t_*)|/a_\infty \qquad \text{A.21}$$

We note that the Eq. A.19 is the desired integral representation for the velocity potential in the frame of reference moving with the body.

Integral Equation for Non-Lifting Rigid Rotor

Note that if $\chi = 0$ (i.e., if the nonlinear terms in the differential equation for the velocity potential, Eq. A.1, are negligible) then the right hand side of Eq. A.7, $\hat{\chi}$, is equal to zero except on the surface σ (since E is constant both outside and inside σ). Hence, if $\chi = 0$, the right hand side of Eq. A.19 can be rewritten in the form of the surface integrals.

For the sake of clarity, consider first the case of a non-lifting rotor in rigid body motion. Let the coordinate system ξ coincide with the Cartesian coordinates of a Cartesian frame of reference rigidly connected with the rotor. In this frame of reference

$$\frac{\partial E}{\partial t} = 0 \qquad \text{A.22}$$

In addition, assume that the rotor speed is always subsonic so that Eq. A.20 has only one root, t=T.

Note that, for any function f

$$\iiint f\bar{\nabla}E \, dV = \oiint f \, \bar{n} \, d\sigma \qquad \text{A.23}$$

and

$$\iiint G \, \bar{\nabla}\cdot(f\bar{\nabla}E) \, dV = \bar{V}_* \cdot \iiint Gf\bar{\nabla}E \, dV$$
$$= \bar{V}_* \cdot \oiint_\sigma Gf\bar{n} \, d\sigma \qquad \text{A.24}$$

Performing the calculations, one obtains (see Ref. 63 for details)

$$-4\pi E_* \varphi_* = \oiint_\sigma [\frac{1}{r_{II}} \frac{\partial \varphi}{\partial n}]_T \, d\sigma$$
$$+ \bar{V}_* \cdot \oiint_\sigma [\frac{1}{r_{II}} \varphi \, \bar{n}]_T \, d\sigma + \frac{1}{a_\infty} \oiint_\sigma [\frac{1}{r_{II}} \frac{\partial \varphi}{\partial \tau} V_s]_T \, d\sigma$$
$$+ \frac{1}{a_\infty} \frac{\partial}{\partial \tau} \oiint_\sigma [\frac{1}{r_{II}} \varphi \, V_s]_T \, d\sigma \qquad \text{A.25}$$

In Eq. A.25, $[\ ]_T$ indicates evaluation at retarded time t=T (such that $g(t) = t - t_* + |\bar{\xi}(\bar{x},t) - \bar{\xi}(\bar{x}_*,t_*)|/a_\infty = 0$). Equation A.25 is the desired integral representation. In the limit, as P_* approaches the surface σ, one obtains an integral equation for (see Section 3). The numerical solution of such an equation is similar to that given in Section 5.

Rotor/Fuselage Configuration

Next consider the case of rotor/fuselage configuration in which both the rotor and the fuselage move in arbitrary but rigid-body motions. Also for simplicity, assume that the wake remains where it is generated: this is a reasonable assumption when (in a frame of reference connected with the undisturbed air) the velocity of the fluid is small compared to that of the rotor fuselage configurations (this assumption is removed in the analysis of Ref. 63). Hence the surface σ can be broken into three surfaces: the surface of the rotor, σ_r, the surface of the fuselage σ_f, and the surface of the wake, σ_w. For each of these surfaces there exists a frame of reference which is rigidly connected with the surface.

Next consider the volume on the right hand side of Eq. A.18 and consider three 'thin' volumes containing σ_r, σ_f and σ_w respectively (the portion of the integrand containing derivatives of E is equal to zero in the rest of the volume). Next assume that $\bar{x}$ in each volume coincides with the frame of reference connected with the corresponding surface. Following the same procedure outlined above (but locating each surface integral independently), one obtains an expansion similar to Eq. A.25 with each integral replaced with the sum of three integrals over σ_r, σ_f and σ_w respectively.

If the motion of the surfaces with respect to 'their frame of reference' is small, Eq. A.25 is still valid but such motion 'shows up' in the boundary conditions for $\partial\varphi/\partial n$. The case of completely arbitrary motion is discussed in Ref. 63 (including nonlinear terms and removing shocks): the derivation of the equations is very complicated but the final results are slightly more complex than the ones presented here.